AD-A014 231

TURBINE ENGINE CONTROL SYNTHESIS. VOLUME III.
EXPERIMENTAL ENGINE IDENTIFICATION AND MODELING

R. B. Beale, et al

Honeywell, Incorporated

Prepared for:

Air Force Aero Propulsion Laboratory

March 1975

NOTICE

When Government drawings, specifications, or other data are used for any purpose other than in connection with a definitely related Government procurement operation, the United States Government thereby incurs no responsibility nor any obligation whatsoever; and the fact that the Government may have formulated, furnished, or in any way supplied the said drawings, specifications, or other data, is not to be regarded by implication or otherwise as in any manner licensing the holder or any other person or corporation, or conveying any rights or permission to manufacture, use, or sell any patented invention that may in any way be related thereto.

This final report was submitted by Systems & Research Center, Honeywell Inc., under Contract F33615-72-C-2190. The effort was sponsored by the Air Force Aero-Propulsion Laboratory, Air Force Systems Command, Wright-Patterson AFB, Ohio under Project 3066, Task 306603, and Work Unit 30660363 with Charles E. Ryan, Jr, AFAPL/TBC as Project Engineer. Mr. C. R. Stone (Vol I & II) and Mr. R. B. Beale (Vol III) of Honeywell, Inc. were technically responsible for the work.

This report has been reviewed by the Information Office, (ASD/OIP) and is releasable to the National Technical Information Service (NTIS). At NTIS, it will be available to the general public, including foreign nations.

This technical report has been reviewed and is approved for publication.

C. E. Ryan

CHARLES E. RYAN JR, GS-14
Project Engineer

FOR THE COMMANDER

Charles E. Bentz

CHARLES E. BENTZ
Technical Area Manager, Controls

REPORT DOCUMENTATION PAGE		READ INSTRUCTIONS BEFORE COMPLETING FORM
1. REPORT NUMBER AFAPL-TR-75-14	2. GOVT ACCESSION NO.	3. RECIPIENT'S CATALOG NUMBER
4. TITLE (and Subtitle) TURBINE ENGINE CONTROL SYNTHESIS, Vol. III: Experimental Engine Identification and Modeling		5. TYPE OF REPORT & PERIOD COVERED Final Technical Report - 30 June 1972 - 15 March 1975
		6. PERFORMING ORG. REPORT NUMBER F0164-FR, Vol. III
7. AUTHOR(s) R. B. Beale and N. E. Miller		8. CONTRACT OR GRANT NUMBER(s) F33615-72-C-2190
9. PERFORMING ORGANIZATION NAME AND ADDRESS Honeywell Inc. Systems and Research Center Minneapolis, Minnesota 55413		10. PROGRAM ELEMENT, PROJECT, TASK AREA & WORK UNIT NUMBERS Proj. 3066 Task 306603 W.U. 30660363
11. CONTROLLING OFFICE NAME AND ADDRESS Air Force Aero-Propulsion Laboratory (TBC) Wright-Patterson Air Force Base, OH 45433		12. REPORT DATE March 1975
		13. NUMBER OF PAGES 163
14. MONITORING AGENCY NAME & ADDRESS(if different from Controlling Office)		15. SECURITY CLASS. (of this report) Unclassified
		15a. DECLASSIFICATION/DOWNGRADING SCHEDULE N/A

16. DISTRIBUTION STATEMENT (of this Report)

Approved for Public Release; distribution unlimited.

17. DISTRIBUTION STATEMENT (of the abstract entered in Block 20, if different from Report)

18. SUPPLEMENTARY NOTES

19. KEY WORDS (Continue on reverse side if necessary and identify by block number)

Optimal control	Identification
J85 jet engine	Engine test
Synthesis	Frequency response
Digital control	Transfer functions

20. ABSTRACT (Continue on reverse side if necessary and identify by block number)

This program develops a practical design procedure for turbine engine control systems based on multivariable control theory. Volume I of the report describes the synthesis and demonstration of a control system designed by the application of quadratic optimal control technology. Volume II contains the linear and nonlinear models, as well as the design algorithms used for control synthesis. This volume describes a practical procedure for experimentally obtaining high-fidelity linear engine models

DD FORM 1473 EDITION OF 1 NOV 65 IS OBSOLETE
1 JAN 73

20. Abstract (Continued)

from frequency response measurements. This procedure satisfies the modeling requirements for high-bandwidth control systems which are needed in the future for better regulation of surge margins and disturbances. A dynamic transfer matrix model of the GE-J85-13 engine is obtained at three engine operating speeds. The instrumentation is described for obtaining tape-recorded engine responses. Fourier filtering and servoanalysis techniques are demonstrated. An algorithm is described for identifying dynamic states and transfer functions from frequency responses.

FOREWORD

This final report was submitted by Systems and Research Center, Honeywell Inc., under Contract F33615-72-C-2190. The effort was sponsored by the Air Force Aero-Propulsion Laboratory, Air Force Systems Command, Wright-Patterson AFB, Ohio, under Project 3066, Task Area 306603, and Work Unit 30660363, with Charles E. Ryan, Jr., AFAPL/TBC, as Project Engineer. The Honeywell Systems and Research work was managed by Dr. E. E. Yore. Mr. C. R. Stone (Vols. I and II) and Mr. R. B. Beale (Vol. III) of Honeywell Inc. were technically responsible for the work.

The report is presented in three volumes. Volume I contains the main part of the report for the optimization design and wind tunnel test evaluation. Volume II contains detailed computer programs and background material for the optimization effort. Volume III presents experimental identification and modeling of the General Electric J85 engine.

R. B. Beale and N. E. Miller were principal investigators for the modeling and identification effort. R. Beale defined the procedure, set up the experimental apparatus, and obtained the experimental data. N. Miller aided in obtaining the data, reduced the data to Bode plots, performed the modeling and state identification analysis, and interpreted the results. B. Reed was responsible for developing the identification algorithm which is a key element in the procedure.

TABLE OF CONTENTS

LIST OF ILLUSTRATIONS

LIST OF SYMBOLS

u_f — Fuel flow command, lb/hr

u_A — Exhaust area command, in^2

u_{BLD} — Bleed command, percent full scale

u_{IGV} — Inlet guide vane command, percent full scale

W_f — Fuel flow, lb/hr

A_8 — Exhaust area, in^2

BLD — Bleed position, percent full scale

IGV — Inlet guide vane angle, percent full scale

N — Spool speed, rpm

P_3 — Compressor discharge pressure, psi

P_5 — Turbine discharge pressure, psi

$\Delta P/P_3$ — Compressor discharge Mach number sensor

T_5 — Turbine discharge temperature, °R

$G(j\omega)$ — Experimental frequency response data

$G_a(j\omega)$ — Frequency response of transfer function model

E — Integral squared difference between $G(j\omega)$ and $G_a(j\omega)$

ω — Frequency, rad/sec

j — Imaginary number, $\sqrt{-1}$

N_{max} — Maximum spool speed, rpm

ΔP_{fn} — Fuel nozzle pressure differential, psi

P_{fn} — Fuel nozzle pressure, psi

C_d — Fuel nozzle discharge coefficient

A_N — Fuel nozzle area, in^2

g_c — Gravitational constant, 32.17 ft/sec^2

ρ — Fuel density, lb/ft^3

$N_1(s)$ — Numerator dynamics associated with fuel valve

$D_1(s)$ — Denominator dynamics associated with fuel valve

$N_2(s)$ — Numerator dynamics associated with fuel line

$D_2(s)$ — Denominator dynamics associated with fuel line

$N_3(s)$ — Numerator dynamics associated with P_3 response

$D_3(s)$ — Denominator dynamics associated with P_3 response

$E(t)$, $E_1(t)$, $E_2(t)$ — Sensor output signals

ϕ, ϕ_1, ϕ_2 — Phase angles associated with sensor signals

N — Number of cycles (defined in Appendix A)

T — Time/cycle, sec (defined in Appendix A)

ω_1 — Test frequency, rad/sec

I — In-phase component of frequency response

Q — Quadrature component of frequency response

$G(j\omega_i)$ — Discrete experimental frequency response data

R — Real part of frequency response

I — Imaginary part of frequency response

A — Amplitude ratio

θ — Phase shift

s — Complex variable

$N_a(s)$ — Numerator of $G_a(s)$

$D_a(s)$ — Denominator of $G_a(s)$

x

LIST OF SYMBOLS (CONCLUDED)

$G_a(s)$ - Transfer function model

ϕ_i - Weighting coefficients (defined in Appendix B)

E_N - Real error

c_N - Real error tolerance

E_ϕ - Equation error

c_ϕ - Equation error tolerance

$T(s)$ - Transfer function

SECTION I
INTRODUCTION AND SUMMARY

MODELING AND IDENTIFICATION REQUIREMENTS

The regulation accuracy and speed of response of any control system is directly proportional to its bandwidth. The increasing demand for reliable engine controls with tighter surge margins requires higher-bandwidth control systems. Thus, there is a need to model engine dynamics out to higher frequencies than has been required in the past. It is not sufficient to provide large gain and phase margins to provide for model uncertainty. These margins reduce the bandwidth and therefore the regulation accuracy. Some performance will have to be sacrificed to allow for engine variations due to tolerances and wear. However, performance should not be sacrificed for inaccurate modeling practice.

This report presents a modeling and identification procedure which is simple and inexpensive. In addition, it provides both high-fidelity models and dynamic state identification which gives an indication of the physical phenomena which are occurring. The procedure has been used for many years. The accuracy of the technique has been considerably improved by the use of two-channel Fourier filtering and computerized state identification of engine frequency responses.

The optimal control system, which is described in Volumes I and II of this report, demonstrated improved regulation of the engine at steady state and during transients. This was accomplished by linear regulation of pressure and temperature boundaries as well as rotor speed. Each of these regulators used fuel control bandwidths higher than standard practice. In implementation of the optimal control system, the bandwidth had to be reduced to allow

margin for differences between the model and the engine. This provided the incentive to study the engine dynamics at slightly higher frequencies.

It is important to have a practical technique for accurately determining engine dynamics. If nominal engine dynamics were accurately known, as well as engine-to-engine variations in the dynamics, the proper amount of gain margin could be allowed for the variations. Then excess performance would not be sacrificed because of lack of knowledge of the nominal dynamics. These considerations will become more important when control systems are designed for disturbance insensitivity in the future. Disturbances such as augmentor lightoff and inlet instability will require higher bandwidth control systems.

The primary objective of this modeling program was to develop a modeling procedure which would be very practical. The procedure outlined in this report meets that objective. The procedure is inexpensive due to the small amount of engine running time required. Only 0.5 hour is required to oscillate each engine actuator over the frequency range. The nine engine responses were recorded on tape simultaneously. This was possible because of the tape synchronizing signals used by the servoanalyzer. The oscillations are very small, on the order of 2 percent of actuator deflection, so that the engine is not endangered during the test.

The accuracy of the results was improved in three ways. First, the actuator dynamics were separated from the engine dynamics with the two-channel capability of the analyzer. The Fourier filtering capability allowed analysis at low signal-to-noise levels and provided describing functions for nonlinear dynamics such as dead zone and hysteresis. Finally, the automation of the identification procedure provided very close matching of the models to the frequency responses.

The limitation of the procedure is that it is a linear analysis of a nonlinear process. Several operating points must be evaluated to determine the variations in the linear models. If the nonlinearities are dominant even in the

2

small perturbations, such as with hysteresis and saturation, their describing functions for sinusoidal inputs are not always useful. However, linear models are required for all types of control synthesis. Therefore, this procedure should be very useful even though nonlinear models are the ultimate objective.

Experimental data of engine dynamics are very limited for two reasons. First, engine test time is very expensive, so that only the highest priority tests are performed. Second, the dynamics are well known at low frequency, within the bandwidth of current control systems. Higher-bandwidth systems will increase the priority of dynamic tests in the future, at least until the dynamics become well known at slightly higher frequencies. The technique described in this report should prove to be very cost effective, since the engine test time can be reduced to a few hours. The primary impact this technique has on engine testing is the requirement for electrical readout on actuator positions and engine sensors.

The two-channel Fourier analyzer is a key item to making the procedure practical. This is because it can analyze the amplitude ratio and phase shift between any two signals in a very noisy environment. The computerized identification procedure, which determines the dynamic states and transfer functions from the frequency responses, is very useful for determining practical models of the engine dynamics. These models provide insight to the physics of the engine which can be used as guidelines in future analytical modeling efforts.

Frequency response analysis is limited to the study of small perturbations around a nominal operating point. This linear analysis is required for control system design, but is not a substitute for the nonlinear modeling of the engine. The frequency response analysis is also limited to perturbations around steady-state operating points, since the engine must remain at the nominal operating point for a few minutes at a time. The modeling of transient conditions must be accomplished by approximating transient loads

3

on the rotor. However, for control design purposes, frequency response measurements can be obtained from a hybrid simulation at any operating condition and compared with the engine responses at steady state to verify the results.

FORM OF THE MODEL

A dynamic model was obtained for the response of five engine variables to the four engine actuators. These 20 linear transfer functions were obtained at three operating points. The actuator transfer functions were separated from the engine dynamics. Thus, there were 64 transfer functions evaluated in all. Figures 1, 2, and 3* show these transfer functions combined into a dynamic transfer matrix for each operating point. It is clear from the matrix that there is considerable interaction between the control variables, since each actuator has an effect on most of the responses. However, the effect of the inlet guide vane (IGV) and bleed (BLD) variables is considerably less than the fuel flow (W_f) and exhaust area (A_8). This fact is obscured in the transfer function by the units chosen for the DC gain. Fuel flow is expressed in pounds per hour and exhaust area in square inches, while IGV and BLD are expressed in percent of full scale (i.e., P_3/BLD is psi/full-scale deflection).

A state space model of the engine can be obtained from the transfer matrix. The dynamic states are the poles of the transfer functions. The order of the state space model is the lowest-order denominator that can be factored out of the matrix (i.e., add up all the unique poles. If they appear more than once, they are counted only once). Before one could determine the lowest-order state space model, the roots would have to be analyzed to determine which ones are appearing in several responses. It is not always clear, as the

---

*To avoid interrupting the continuity of the text, all referenced figures and tables are gathered at the end of their respective section or appendix.

errors in the procedure cause states to appear at slightly different frequencies in different responses. Not all of the states have to be included for control design purposes. High-frequency terms can be left off. After truncating the terms, frequency response plots can be compared with the experimental data to ensure that accuracy is maintained out to the desired bandwidth of the control system.

RESULTS OF ENGINE RESPONSE MEASUREMENTS

Engine frequency responses reveal much information about engine dynamics in addition to that needed for modeling purposes. In the paragraphs that follow, some of the interesting facts picked out of the data are discussed. Much of this information would not be available were it not for the Fourier filtering capability of the instrumentation. This noise-rejection capability allowed accurate responses to be analyzed out in frequency to the limit of the actuator response. The fuel flow responses were measured out to 100 Hz. The geometry actuators proved to be much faster responding than originally modeled.

It should be noted that fuel flow dynamics cannot be separated from engine dynamics as desired. This is due to the fact that fuel flow is effected by pressure drop across the fuel nozzle. The dynamics of the combustor pressure appear in both the actuator and engine responses. This phenomenon is described in detail in Appendix A. This suggests a need for flow feedback in engine control systems.

The exhaust area actuator was much faster than expected. It responsed well out to 8 Hz. The hysteresis and dead zones added only 30 degrees of phase shift at low frequency. Of course, the nonlinearity in the actuator will cause it to respond differently at other amplitude levels. The amplitude level for This data was ±5 percent of full scale. This control variable has a large

5

effect on the engine response. Therefore, it should prove to be an important control in a multivariable system. There is considerably more phase shift in the combustor pressure response to exhaust area than there is to fuel flow, however. If the optimal control system were to be redesigned, the exhaust area would be added as a second dynamic control variable.

As mentioned above, the compressor bleeds and inlet guide vanes had little effect on the engine responses. As noted in the transfer matrix, some of the transfer functions are shown as zero. The small effect is obscured in the transfer functions because of the units chosen for these variables. The gain in the transfer functions appears high because it is in terms of output/full-scale deflection. If fuel flow and exhaust area were to be expressed in these units, the gain would be much higher. The combustor pressure, P_3, response to bleeds has very little phase shift, which means that the effect is immediate. However, the magnitude of the effect is small, presumably due to the small size of the bleed openings. Thus, the bleeds and inlet guide vanes are not very effective dynamic control variables for this engine.

One of the most interesting results of the frequency response tests is the second-order dynamic response of spool speed. This second state appearing in the spool speed response causes considerable phase shift at frequencies within the bandwidth range of most current engine control systems. The fuel flow response shows the two first-order lags. The first appears as expected at 3 radians per second and the second at 77 radians per second (at the high-speed operating point). The exhaust area response shows a second lag in spool speed also, but it moves out in frequency at low speed. The additional phase shift in spool speed response caused considerable difficulty when the high-bandwidth optimal controllers were run on the engine. Therefore, the engine tests were run with reduced gains to allow for additional gain and phase margin.

Another very interesting result revealed in the frequency responses is the unexpectedly large time delay in the engine pressure responses. This time delay ranges from 11 to 14 milliseconds. It causes very rapid phase shift at frequencies above 10 Hz. This is above the frequency range of speed control systems. However, pressure disturbance control systems in the future will have to consider this time delay.

The turbine outlet temperature, T_5, response provided accurate dynamic data out to 50 Hz, even though the thermocouple has very slow response. The added gain reduction and phase shift did not prevent temperature response models from being obtained. This implies that fast temperature control is possible with adequate lead compensation for the thermocouple. However, the signal noise, which was rejected by Fourier filtering, will limit the amount of lead that can be applied.

COMPARISON OF EXPERIMENTAL AND ANALYTICAL MODELS

One of the main objectives of this program was to compare the engine model, used for optimal control design, with experimental data. Engine frequency response data were plotted with frequency responses from the linearized NASA component model and the analog computer model at APL. These data are presented in Section II. The following paragraphs point out some of the interesting comparisons.

The fuel flow responses are of primary concern, as fuel flow is usually the only dynamic control variable. The fuel-metering actuator is modeled accurately. The spool speed response is modeled accurately at low frequency. As mentioned above, there is considerably more phase shift in the engine data above 2 Hz. The experimental model has a second first-order lag at about 8 Hz. This error in the model meant that the bandwidth of the optimal controller had to be reduced during the engine tests. This caused a corresponding decrease in regulation accuracy.

7

The pressure responses are accurate in the component model except for the large time delay. The analog model has considerable phase error in the $\Delta P/P$ and P_5 responses at low frequency. The temperature responses have considerable phase error above 7 Hz. In addition, the analog model temperature gain begins falling off rapidly at 0.3 Hz, which is about a decade slower than the engine data.

The exhaust area actuator is a decade faster than the models. The gain is flat out to 5 Hz, as compared with 0.5 Hz. This difference is very important in deciding whether to use the exhaust area as a dynamic control variable. The optimal controller did not use the exhaust area because it was assumed to be too slow. At 5 Hz, the exhaust area can be used effectively. If the optimal controller were redesigned, the exhaust area would be added as a second control variable. This would have a considerable effect on the controller performance.

The spool speed response to exhaust area has similar second-order dynamics as with fuel flow. The phase shift increases from that of the model above 3 Hz. The combustor pressure responses to exhaust area are well modeled. However, the turbine discharge pressure, P_5, varies considerably between the three models. P_5 responds faster and with greater amplitude on the engine than in the component model. The analog model is 1.5 decades slower.

The bleed and IGV actuators are much faster than the models. However, this is not an important factor, since these actuators are not very effective, dynamically. The models show these control variables to be even less effective. Spool speed response to bleed has more phase shift than the model above 0.1 Hz. The P_3 response to bleed is 1.5 decades slower in the models. The data shows very little phase shift in pressure response.

8

STATE IDENTIFICATION AND PHYSICAL INTERPRETATION

Dynamic engine models were identified from the engine frequency response data. This procedure proved to be very successful in that accurate pole and zero locations were identified that coincided well with engine physics. This is an established practice in the control field. However, the technique was improved by the accurate measurement techniques and computerized statistical identification. Therefore, the procedure promises to be a practical technique for future use. The identification algorithm is discussed in detail in Appendix B. The models are discussed in detail in Section III. The transfer functions are listed in Figures 1, 2, and 3, with some of them shortened for clarity.

An attempt was made to interpret the physical meaning of the dynamic states in Section III. Many of the interpretations are well known from comparison with existing models. But, the higher-frequency terms do not have obvious interpretations. The authors have made an attempt to classify these additional dynamics. However, this task is more appropriately accomplished by engine manufacturers who have more experience with engine physics. An objective of this program was to provide data to allow engine modelers to perfect their analytical procedures.

The significant differences between the engine and the component model are: (1) the additional first-order lag in the spool dynamics at 8 Hz; (2) the 0.011-second time delay in the pressure response; and (3) the location of the second-order pole in the exhaust actuator. The additional spool root could be associated with gas dynamics in the turbine or compressor. The time delay is assumed to be occurring in the fuel combustion. The dynamics of the exhaust actuator are understood fairly well.

9

Fuel Valve

$$1.0 \frac{\left[\left(\frac{S}{30.7}\right)^2 + \frac{2(0.107)S}{30.7} + 1\right]}{\left[\left(\frac{S}{34.2}\right)^2 + \frac{2(0.502)S}{34.2} + 1\right]}$$

u_{W_f} W_f

Exhaust Actuator

$$1.0 \frac{\left[\left(\frac{S}{50}\right)^2 + \frac{2(-0.284)S}{50} + 1\right]}{\left[\left(\frac{S}{27.2}\right)^2 + \frac{2(0.453)S}{27.2} + 1\right]}$$

u_{A_8} A_8

Inlet Guide Vane Actuator

u_{IGV} IGV

Bleed Actuator

$$1.0 \frac{\left[\frac{S}{107} - 1\right]}{\left[\frac{S}{31.3} + 1\right]}$$

u_{BLD} BLD

$$\frac{12.65\left[\frac{S}{148} - 1\right]}{\left[\frac{S}{0.714} + 1\right]\left[\frac{S}{42.8} + 1\right]}$$

$$\frac{0.0533\left[\frac{S}{6.37} + 1\right]\left[\left(\frac{S}{34.3}\right)^2 + \frac{2(0.017)S}{34.3} + 1\right]}{\left[\frac{S}{0.800} + 1\right]\left[\left(\frac{S}{34}\right)^2 + \frac{2(0.041)S}{34} + 1\right]}e^{-(0.015)S}$$

$$\frac{0.121E\text{-}3\left[\frac{S}{1.38} - 1\right]\left[\left(\frac{S}{36.2}\right)^2 + \right]}{\left[\frac{S}{0.716} + 1\right]\left[\left(\frac{S}{34.9}\right)^2 + 2\right]}$$

$$\frac{3.84}{\left[\frac{S}{0.698} + 1\right]}$$

$$\frac{+0.0601\left[\frac{S}{29.3} - 1\right]}{\left[\frac{S}{0.864} + 1\right]}$$

$$\frac{-0.455}{\left[1.\right]}$$

$$0 \qquad 0$$

$$\frac{-402\left[\frac{S}{3.34} - 1\right]}{\left[\frac{S}{0.936} + 1\right]}$$

$$\frac{-4.63\left[\frac{S}{4.47} + 1\right]}{\left[\frac{S}{1.06} + 1\right]\left[\frac{S}{80.1} + 1\right]}$$

Figure 1.   J85-13 Dynamic Tr
at 70 Percent Maxi

a

$$\frac{\left[\left(\frac{S}{36.2}\right)^2 + \frac{2(0.085)S}{36.2} + 1\right]\left[\frac{S}{54.6} - 1\right]e^{-(0.015)S}}{\left[\left(\frac{S}{34.9}\right)^2 + \frac{2(0.138)S}{34.9} + 1\right]\left[\frac{S}{58.4} + 1\right]} \qquad \frac{0.00667\left[\frac{S}{6.25} + 1\right]\left[\frac{S}{19.8} + 1\right]\left[\left(\frac{S}{50.7}\right)^2 + \frac{2(0.221)S}{50.7} + 1\right]e^{-(0.015)S}}{\left[\frac{S}{1.52} + 1\right]\left[\left(\frac{S}{43.7}\right)^2 + \frac{2(0.291)S}{43.7} + 1\right]\left[\left(\frac{S}{111}\right)^2 + \frac{2(0.734)S}{111} + 1\right]} \qquad \frac{-0.328\left[\frac{S}{0.450} - 1\right]\left[\frac{S}{122} - 1\right]}{\left[\frac{S}{0.395} + 1\right]\left[\frac{S}{2.98} + 1\right]\left[\frac{S}{94.4} + 1\right]}$$

N

P₃ → P_3

$$\frac{-0.455E{-}4\left[\frac{S}{4.76} - 1\right]}{\left[\frac{S}{1.98} + 1\right]} \qquad \frac{-0.0175\left[\frac{S}{0.719} + 1\right]\left[\frac{S}{24.5} + 1\right]}{\left[\frac{S}{2.27} + 1\right]\left[\frac{S}{33.2} + 1\right]} \qquad \frac{-0.954\left[\frac{S}{8.75} + 1\right]}{\left[\frac{S}{0.361} + 1\right]\left[\frac{S}{3.67} + 1\right]}$$

$\Delta P/P_3$

P_5

$$0 \qquad\qquad 0 \qquad\qquad 0$$

T_5

$$0 \qquad\qquad 0 \qquad\qquad \frac{83.4\left[\frac{S}{4.4} - 1\right]}{\left[\frac{S}{0.351} + 1\right]}$$

...ic Transfer Matrix -- Operating Point
Maximum Speed

b

Fuel Valve

u_{W_f} →

$$\frac{1.0\left[\left(\frac{S}{42.3}\right)^2 + \frac{2(0.061)S}{42.3} + 1\right]}{\left[\left(\frac{S}{44.9}\right)^2 + \frac{2(0.206)S}{44.9} + 1\right]}$$

→ W_f

$$\frac{6.36\left[\frac{S}{82.3} - 1\right]}{\left[\frac{S}{1.17} + 1\right]\left[\frac{S}{60.1} + 1\right]}$$

$$\frac{0.0514\left[\frac{S}{7.59} + 1\right]\left[\left(\frac{S}{39.8}\right)^2 + \frac{2(0.121)S}{39.8} + 1\right]e^{-(0.014)S}}{\left[\frac{S}{1.39} + 1\right]\left[\left(\frac{S}{38}\right)^2 + \frac{2(0.162)S}{38} + 1\right]}$$

$$\frac{0.408E\text{-}4\left[\left(\frac{S}{13.3}\right)^2 + \frac{2(-0.786)S}{13.3} + 1\right]\left[\frac{S}{60.6}\right]}{\left[\frac{S}{1.49} + 1\right]\left[\frac{S}{31.2} + 1\right]\left[\left(\frac{S}{63.6}\right)^2 + 2\right]}$$

Exhaust Actuator

u_{A_8} →

$$\frac{1.0\left[\left(\frac{S}{56.9}\right)^2 + \frac{2(-0.271)S}{56.9} + 1\right]}{\left[\left(\frac{S}{32.4}\right)^2 + \frac{2(0.402)S}{32.4} + 1\right]}$$

→ A_8

$$\frac{2.99}{\left[\frac{S}{2.68} + 1\right]}$$

$$\frac{+0.0512\left[\frac{S}{13.4} + 1\right]\left[\frac{S}{41.3} - 1\right]}{\left[\frac{S}{2.59} + 1\right]\left[\frac{S}{26.9} + 1\right]}$$

$$\frac{-0.471E\text{-}4\left[\frac{S}{7.19} - \right]}{\left[\frac{S}{3.74} + 1\right]}$$

Inlet Guide Vane Actuator

u_{IGV} →

$$\frac{1.0\left[\frac{S}{173} - 1\right]}{\left[\frac{S}{15.1} + 1\right]}$$

→ IGV

$$\frac{457\left[\frac{S}{38.6} - 1\right]}{\left[\frac{S}{1.81} + 1\right]}$$

$$\frac{0.280\left[\frac{S}{0.079} - 1\right]\left[\frac{S}{29.6} + 1\right]\left[\frac{S}{48.1} - 1\right]}{\left[\frac{S}{2.01} + 1\right]\left[\frac{S}{17.8} + 1\right]\left[\frac{S}{1570} + 1\right]}$$

0

Bleed Actuator

u_{BLD} →

$$\frac{1.0\left[\frac{S}{327} - 1\right]}{\left[\frac{S}{34.9} + 1\right]\left[\frac{S}{107} + 1\right]}$$

→ BLD

$$\frac{-505\left[\frac{S}{15.6} - 1\right]}{\left[\frac{S}{1.14} + 1\right]}$$

$$\frac{-5.85\left[\frac{S}{5.74} + 1\right]\left[\frac{S}{81.6} + 1\right]}{\left[\frac{S}{1.98} + 1\right]\left[\frac{S}{40.1} + 1\right]}$$

0

Figure 2. J85-13 Dynamic Tran
at 85 Percent Maximu

G

$$\frac{\left[\frac{S}{60.6}\right]^2 + \frac{2(0.166)S}{60.6} + 1}{\left[\frac{S}{63.6}\right]^2 + \frac{2(0.188)S}{63.6} + 1}\, e^{-(0.014)S}$$

$$\frac{0.00714\left[\frac{S}{14}+1\right]\left[\frac{S}{17.3}+1\right]\left[\left(\frac{S}{50.9}\right)^2 + \frac{2(0.139)S}{50.4}+1\right]}{\left[\frac{S}{3.13}+1\right]\left[\left(\frac{S}{44.7}\right)^2 + \frac{2(0.234)S}{44.7}+1\right]\left[\frac{S}{81.7}+1\right]\left[\frac{S}{130}+1\right]}\, e^{-(0.014)S}$$

$$\frac{0.187\left[\frac{S}{0.074}+1\right]\left[\frac{S}{170}+1\right]\left[\left(\frac{S}{241}\right)^2 + \frac{2(-0.279)S}{241}+1\right]}{\left[\frac{S}{0.749}+1\right]\left[\frac{S}{4.31}+1\right]\left[\frac{S}{214}+1\right]\left[\frac{S}{360}+1\right]}$$

N

$$\frac{\text{E-4}\left[\frac{S}{7.19}-1\right]}{\left[\frac{S}{74}+1\right]}$$

$$\frac{-0.0363\left[\frac{S}{1.46}+1\right]}{\left[\frac{S}{1.42}+1\right]}$$

$$\frac{-1.78\left[\frac{S}{13.4}+1\right]}{\left[\frac{S}{1.01}+1\right]\left[\frac{S}{8.14}+1\right]}$$

P_3

$\Delta P/P_3$

P_5

0

0

$$\frac{-18.3\left[\frac{S}{0.576}-1\right]\left[\frac{S}{6.61}-1\right]\left[\frac{S}{10.2}+1\right]}{\left[\frac{S}{0.390}+1\right]\left[\frac{S}{4.59}+1\right]\left[\frac{S}{17.9}+1\right]}$$

T_5

0

0

$$\frac{60.3\left[\frac{S}{16.5}+1\right]\left[\frac{S}{26.7}-1\right]}{\left[\frac{S}{1.15}+1\right]\left[\frac{S}{159}+1\right]}$$

c Transfer Matrix -- Operating Point
Maximum Speed

13

b

Fuel Valve

u_{W_f}

$$1.0 \frac{\left[\left(\frac{S}{49.8}\right)^2 + \frac{2(0.049)S}{43.8} + 1\right]}{\left[\left(\frac{S}{48.4}\right)^2 + \frac{2(0.242)S}{49.4} + 1\right]}$$

W_f

$$2.86 \frac{\left[\frac{S}{192} - 1\right]}{\left[\frac{S}{2.86} + 1\right]\left[\frac{S}{76.7} + 1\right]\left[\frac{S}{260} + 1\right]}$$

$$0.0308 \frac{\left[\frac{S}{10.8} + 1\right]\left[\left(\frac{S}{50.1}\right)^2 + \frac{2(0.013)S}{50.1} + 1\right]e^{-(0.011)S}}{\left[\frac{S}{2.83} + 1\right]\left[\left(\frac{S}{49.6}\right)^2 + \frac{2(0.021)S}{49.6} + 1\right]}$$

$$0.835E\text{-}5 \frac{\left[\frac{S}{4.32} - 1\right]\left[\frac{S}{41.1} - 1\right]\left[\left(\frac{S}{51.0}\right)^2 + \right.}{\left[\frac{S}{3.5} + 1\right]\left[\left(\frac{S}{49.7}\right)^2 + \frac{2(0.0044)S}{49.7} + 1\right]}$$

Exhaust Actuator

u_{A_8}

$$1.0 \frac{\left[\left(\frac{S}{59.7}\right)^2 + \frac{2(-0.307)S}{59.7} + 1\right]}{\left[\left(\frac{S}{38.2}\right)^2 + \frac{2(0.433)S}{38.2} + 1\right]}$$

A_8

$$\frac{11.0}{\left[\frac{S}{3.38} + 1\right]\left[\frac{S}{53.9} + 1\right]}$$

$$\frac{+0.0445}{\left[\frac{S}{3.41} + 1\right]\left[\frac{S}{45.8} + 1\right]}$$

$$-0.116E\text{-}3 \frac{\left[\frac{S}{30} - 1\right]}{\left[\frac{S}{4.90} + 1\right]}$$

Inlet Guide Vane Actuator

u_{IGV}

$$1.0 \frac{\left[\frac{S}{189} - 1\right]}{\left[\frac{S}{19.4} + 1\right]}$$

IGV

$$631 \frac{\left[\frac{S}{22.3} - 1\right]\left[\frac{S}{27} + 1\right]}{\left[\frac{S}{2.70} + 1\right]\left[\frac{S}{19} + 1\right]}$$

$$0.886 \frac{\left[\frac{S}{0.775} - 1\right]\left[\frac{S}{51.4} - 1\right]}{\left[\frac{S}{3.26} + 1\right]\left[\frac{S}{400} + 1\right]}$$

0

Bleed Actuator

u_{BLD}

$$1.0 \frac{\left[\frac{S}{372} - 1\right]}{\left[\frac{S}{35.8} + 1\right]\left[\frac{S}{139} + 1\right]}$$

BLD

$$134 \frac{\left[\frac{S}{5.27} - 1\right]}{\left[\frac{S}{1.53} + 1\right]}$$

$$-4.54 \frac{\left[\frac{S}{12} + 1\right]\left[\frac{S}{77.1} - 1\right]}{\left[\frac{S}{1.96} + 1\right]\left[\frac{S}{76.3} + 1\right]}$$

0
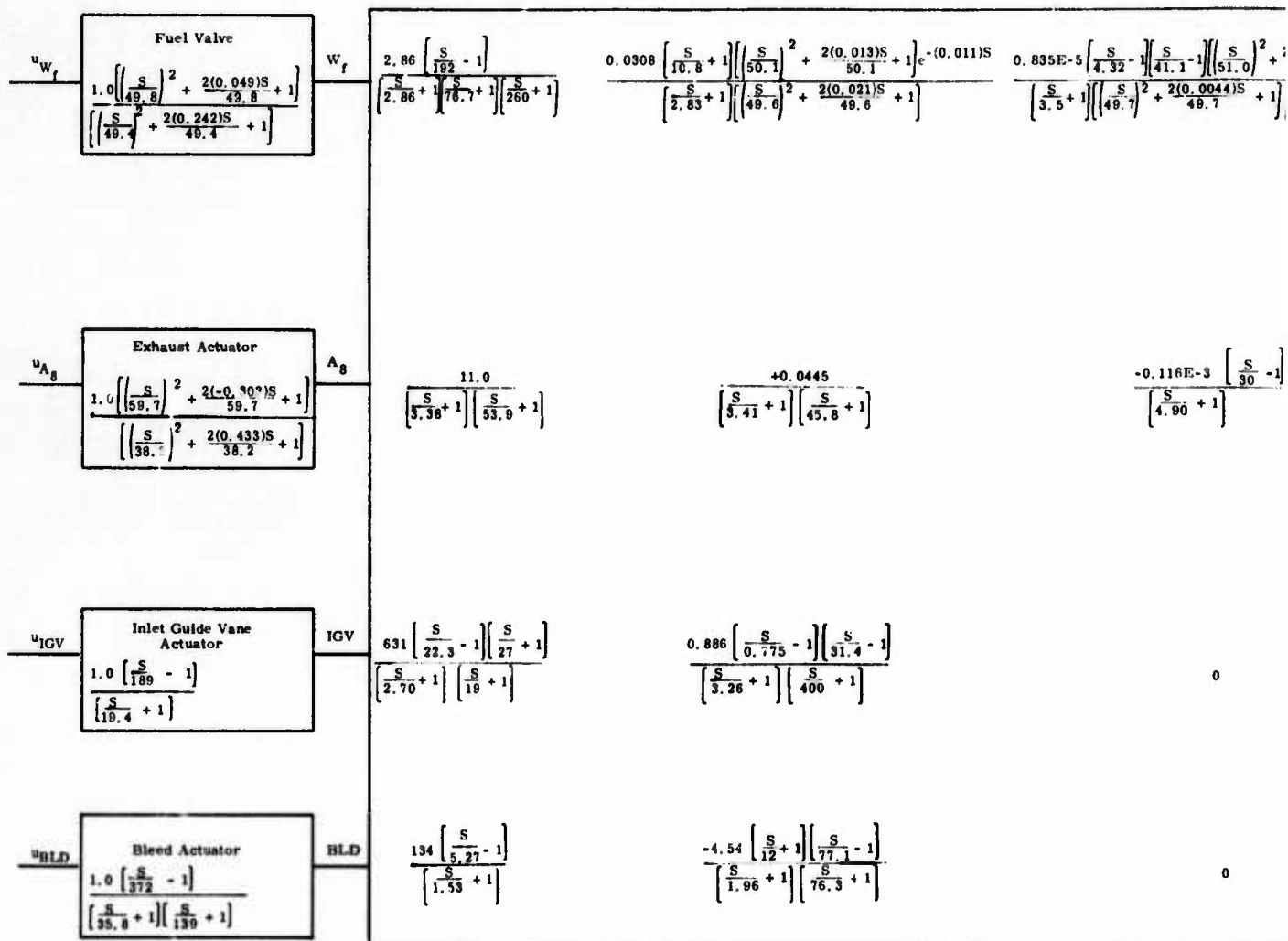
Figure 3. J85-13 Dynamic Tr
at 95 Percent Maxi

a

$$\frac{\left[\left(\frac{S}{51.0}\right)^2 + \frac{2(0.0045)S}{51.0} + 1\right] e^{-(0.011)S}}{\left[\frac{044)S}{.7} + 1\right]\left[\frac{S}{60.4} + 1\right]}$$

$$\frac{0.00833\left[\left(\frac{S}{25.2}\right)^2 + \frac{2(0.953)S}{25.2} + 1\right]\left[\left(\frac{S}{53}\right)^2 + \frac{2(0.219)S}{53} + 1\right] e^{-(0.011)S}}{\left[\frac{S}{8.82} + 1\right]\left[\left(\frac{S}{45.7}\right)^2 + \frac{2(0.268)S}{45.7} + 1\right]\left[\left(\frac{S}{123}\right)^2 + \frac{2(0.866)S}{123} + 1\right]}$$

$$\frac{0.294\left[\left(\frac{S}{253}\right)^2 + \frac{2(-0.773)S}{253} + 1\right]}{\left[\frac{S}{6.19} + 1\right]\left[\frac{S}{160} + 1\right]}$$

PZ

P₃

$$\frac{\left[\frac{S}{30} - 1\right]}{1}$$

$$\frac{-0.100\left[\frac{S}{0.591} + 1\right]}{\left[\frac{S}{5.28} + 1\right]\left[\frac{S}{97.2} + 1\right]}$$

$$\frac{-5.10\left[\frac{S}{42.4} + 1\right]}{\left[\frac{S}{1.42} + 1\right]\left[\frac{S}{13} + 1\right]}$$

ΔP/P₃

P₅

0

0

$$\frac{-20.5\left[\frac{S}{1.93} - 1\right]\left[\frac{S}{17.1} - 1\right]\left[\frac{S}{36.9} + 1\right]}{\left[\frac{S}{1.90} + 1\right]\left[\frac{S}{7.08} + 1\right]\left[\frac{S}{58.5} + 1\right]}$$

T₅

0

0

$$\frac{19.1\left[\frac{S}{11.3} + 1\right]\left[\frac{S}{13} - 1\right]}{\left[\frac{S}{1.88} + 1\right]\left[\frac{S}{416} + 1\right]}$$

ic Transfer Matrix -- Operating Point
Maximum Speed

15

b

SECTION II
FREQUENCY RESPONSE DATA-COMPARISON OF ENGINE, ANALOG MODEL, AND LINEARIZED NASA COMPONENT MODEL

INTRODUCTION

Frequency response data experimentally obtained from a J85 engine in a test cell at APL are presented in this section and compared with similar data obtained from two analytic models, the linearized NASA component model and the APL analog model. The Bode plots presented show that both analytic models adequately represent the low-frequency dynamics of the J85 engine below 2 Hz. However, significant high-frequency effects above 2 Hz associated with gas dynamics identified from the engine responses are not included in either analytic model. Details of the engine-analytic model comparison are discussed in the following paragraphs.

A BAFCO servoanalyzer was used to obtain the J85 frequency response plots. This instrument is designed to perform frequency response analysis of complicated servomechanisms such as the J85 engine through the implementation of Fourier analysis. Since it is a two-channel analyzer, it can measure the dynamics between any two outputs; hence, it is not restricted to input-output pairs. This feature allows separation of actuator dynamics from engine dynamics. Operation of the analyzer is shown in diagram form in Figure 4 and briefly discussed here. A complete description of the analyzer is included in Appendix A.

The analyzer produces a sinusoidal voltage signal with time-dependent frequency (i.e., the frequency varies logarithmically with time) which is used to drive one of the engine actuators. Responses from two engine sensors are fed back into the analyzer which contains the necessary electronics to compute the amplitude ratio and phase shift between the two sensor signals.

17

This information is recorded as a function of frequency by two x - y plotters, thereby producing the Bode frequency response plot of sensor 2 with respect to sensor 1. These input and output variables are described schematically in Figure 4.

The BAFCO servoanalyzer was used in this manner to obtain frequency responses of various engine parameters with respect to the four engine controls: fuel flow, exhaust area, compressor bleed, and inlet guide vane. Four frequency sweeps, one for each control variable, were performed at each of three operating points: engine speed (N/N_{max}) = 70 percent, 85 percent, and 95 percent. Representative data obtained from these tests are presented in Figures 5 through 29. Complete documentation of the data is included in References 1 through 3. The frequency responses included in these figures are discussed in the subsections that follow, in the following order:

	Ref. Figure	Response	N/N_{max}
Actuator responses	5	Fuel flow/fuel command	95%
	6	Exhaust area/exhaust command	95%
	7	Compressor bleed/bleed command	95%
	8	Inlet guide vane/inlet guide vane command	95%
Engine responses to fuel flow	9	Spool speed/fuel flow	95%
	10	Spool speed/fuel flow	85%
	11	Spool speed/fuel flow	70%
	12	Compressor discharge pressure/ fuel flow	95%
	13	Compressor discharge pressure/ fuel flow	85%
	14	Compressor discharge pressure/ fuel flow	70%
	15	Turbine discharge pressure/fuel flow	95%

18

	Ref. Figure	Response	N/N_{max}
Engine responses to fuel flow (continued)	16	Turbine discharge pressure/ fuel flow	85%
	17	Turbine discharge pressure/ fuel flow	70%
	18	Mach number sensor/fuel flow	95%
	19	Turbine discharge temperature/ fuel flow	95%
Engine responses to exhaust area	20	Spool speed/exhaust area	95%
	21	Compressor discharge pressure/ exhaust area	95%
	22	Turbine discharge pressure/ exhaust area	95%
	23	Turbine discharge temperature/ exhaust area	95%
Engine responses to compressor bleed	24	Spool speed/compressor bleed	95%
	25	Compressor discharge pressure/ compressor bleed	95%
	26	Turbine discharge temperature/ compressor bleed	95%
Engine responses to inlet guide vane	27	Spool speed/inlet guide vane	95%
	28	Compressor discharge pressure/ inlet guide vane	95%
	29	Turbine discharge temperature/ inlet guide vane	95%

Actuator inputs and sensor measurements represented in these data are identified below. A more complete description of the actuators and sensors is included in Appendix A.

Actuator Input Description

1) Fuel flow command, u_f = Request to fuel valve.

2) Exhaust area command, u_A = Request to exhaust nozzle actuator

3) Compressor bleed command, u_{BLD} = Request to compressor bleed actuator.

4) Inlet guide vane command, u_{IGV} = Request to inlet guide vane actuator.

Sensor Output Description

1) Fuel flow, w_f = Fuel flow into combustion chamber. This signal was recorded as the pressure differential across the fuel nozzle, i.e., fuel nozzle pressure minus compressor discharge pressure, and corrected to actual fuel flow in lb/hr with a steady-state calibration.

2) Exhaust area, A_8 = Effective cross-sectional area of exhaust nozzle. This signal was recorded as the feedback voltage (calibrated in inches squared) from a mechanical potentiometer positioned on the nozzle drive mechanism.

3) Compressor Bleed, BLD = Effective area of compressor bleeds. The scale is nondimensionalized in the sense that 1 corresponds to fully open bleeds and 0 corresponds to fully closed bleeds. A potentiometer located on the actuator mechanism was used to record this signal.

4) Inlet Guide Vane, IGV = Incidence angle of inlet guide vanes. The nondimensional scale is constructed with 0.0

20

corresponding to the high-speed position of the inlet guide vanes and 1.0 corresponding to low-speed position. A potentiometer which measures actuator movement was used to record this signal.

5) Spool Speed, N = Angular frequency of rotor shaft. A sensor which measures elapsed time per revolution of the rotor was used to obtain this signal. The sensor does not contain any dynamics in the frequency range tested.

6) Compressor Discharge Pressure, P_3 = Static pressure at the compressor discharge. This signal was measured with a static pressure tap embedded in the wall of the engine slightly behind the compressor outlet guide vanes.

7) Turbine Discharge Pressure, P_5 = Total pressure at turbine discharge. The P_5 sensor consists of a system of five total pressure probes spread around the engine and in back of the turbine discharge. A single signal is obtained by averaging the outputs of the five probes.

8) Mach Number Sensor, $\frac{\Delta P}{P_3}$ = Total minus static pressure divided by total pressure at compressor discharge. This signal was obtained from a special sensor built by Bendix. All subtraction and division necessary to obtain the $\Delta P/P_3$ signal is performed in the sensor which is located behind the compressor discharge.

9) Turbine Discharge Temperature, T_5 = Temperature at turbine discharge. The T_5 sensor is composed of 19 individual thermocouples coupled in parallel. The thermocouples are spaced around the engine a few inches behind the turbine discharge.

21

Also included in Figures 5 through 29 are frequency response measurements obtained from the two analytic models, the linearized NASA component model and the APL analog model. The linearized NASA component model is the analytic model which was used to synthesize optimal controllers for the engine. State variables associated with the model are identified in Figure 30. A complete description of the model is included in Reference 4. The APL analog model is described in Reference 5.

A digital computer program was used to obtain frequency response data from the linearized NASA component model. The program computes the amplitude ratio and phase shift between an input-output pair.

The BAFCO servoanalyzer was used to obtain frequency response measurements from the APL analog model. Inlet guide vane and compressor bleed data are not presented for the analog model, since the model does not contain representations of these two controls.

Steady-state data defining the three operating points examined for this project are presented in Tables 1, 2, and 3. Corresponding data obtained from the linearized NASA component model and the APL analog model are also listed.

ACTUATOR RESPONSES

Bode frequency response plots for the four engine actuators (fuel valve, exhaust nozzle, compressor bleed, and inlet guide vane) are presented in Figures 5 through 8. Also presented in these figures are frequency responses of the actuator models included in the two analytic models, the linearized NASA component model and the APL analog model. Comparison of the results supports two observations: (1) the fuel valve actuator is accurately represented in the analytic models, and (2) the engine geometry actuators exhibit higher bandwidth than their counterparts in the analytic models.

22

The frequency response of the fuel valve actuator at 95 percent of maximum spool speed is presented in Figure 5. Both the linearized NASA component model and the APL analog model fuel valves are accurate representations of the engine fuel valve in the low-frequency region, i.e., the frequency responses agree up to about 4.0 Hz. There are significant differences above 4.0 Hz. These include experimental fuel valve dynamics, centered at 7.0 Hz, and high-frequency phase rolloff. These results are also valid at the other two operating points, 70 percent and 85 percent of maximum spool speed.

The frequency responses of the engine exhaust area actuator and the analytic models are presented in Figure 6. They show the engine actuator to be of higher bandwidth and to have a different phase response than the two analytic models. The principal differences are: (1) the component model gain rolls-off much sooner and faster than the engine actuator gain, and (2) the engine actuator has -30 degrees phase shift at low frequency, whereas the component model has little or no phase shift. A nonlinear hysterisis effect in the engine exhaust actuator is responsible for the -30 degrees of phase shift at low frequency. Since the component model is a linear model, this nonlinear effect is not duplicated in the component model response.

The nonlinear hysterisis effect of the engine actuator is included in the analog model, but the effect is too pronounced: the analog actuator model has about 20 degrees more phase shift than the engine actuator. This discrepancy could be minimized by reducing the deadband uncertainty in the nozzle actuator simulation in the analog model.

Frequency responses of the compressor bleed actuator and inlet guide vane actuator are contrasted with those of the linearized NASA component model in Figures 7 and 8. Representations for the analog model are not included in these figures, since compressor bleed and inlet guide vane effects are not included in the analog model.

23

The main difference between the frequency responses of the engine compressor bleed and inlet guide vane actuators and the frequency responses of the component model actuators is that the engine actuators are of considerably higher bandwidth than the component model actuators. This incompatibility also accounts for the observed differences in phase response.

ENGINE RESPONSE TO FUEL FLOW

Frequency response plots of spool speed, N, compressor discharge pressure, P_3, turbine discharge pressure, P_5, compressor Mach number, $\Delta P/P_3$, and turbine discharge temperature, T_5, for oscillations in fuel flow are presented in Figures 9 through 19. Comparison of these engine responses with similar responses obtained from the linearized NASA component model and the APL analog model leads to the following conclusions:

1) The spool speed and turbine discharge temperature frequency
    responses of the engine agree very well with the responses of
    the two analytic models up to 2.0 Hz. This is above the normal bandwidth for speed control loops of 1.0 Hz.

2) The pressure and Mach number responses of the engine agree
    very well with the responses of the analytic models up to
    10.0 Hz except for the turbine discharge pressure response of
    the analog model.

3) High-frequency dynamics present in the engine responses,
    primarily caused by time delay, are not represented in the
    analytic models.

4) The phase shift of the turbine discharge pressure response of
    the analog model does not agree with either the engine or component model results.

These conclusions are discussed in the following paragraphs.

Spool speed frequency responses are presented for three operating points, 70 percent, 85 percent, and 95 percent maximum spool speed, in Figures 9, 10, and 11. Examination of these responses shows that both the component model and the analog model contain good approximations to the fuel flow effects of the engine in the low-frequency region, up to 2.0 Hz. Above 2.0 Hz the phase response of the engine differs considerably from the phase response of the two models: the engine phase shift is much greater than that of either model. This behavior indicates that the engine contains significant high-frequency spool dynamics which are not included in either analytic model.

Compressor discharge pressure, P_3, responses at the three operating points, are presented in Figures 12, 13, and 14. Agreement between the engine data and the responses of the component model and analog model is exhibited out to about 10 Hz. The principal differences between the engine data and the analytic models are: (1) the engine data contains a time delay of about 10 to 15 milliseconds which is not represented in the analytic models, and (2) the frequency responses indicate that the engine contains significant dynamics in the 5.0 to 8.0-Hz frequency range which are not included in the analytic models.

Turbine discharge pressure, P_5, frequency responses presented in Figures 15, 16, and 17, substantiate most of the conclusions drawn from the compressor discharge pressure responses. Agreement between the engine data and the component model is observed out to about 10 Hz. These engine responses also show the time delay of about 10 to 15 milliseconds and the pressure dynamics in the 5.0 to 8.0-Hz frequency range which were noted in the compressor discharge pressure responses. However, one significant difference between the P_3 responses and the P_5 responses should be noted: the analog simulation of P_3 agrees very well with engine data, but the analog simulation of P_5 does not agree with the corresponding engine data. The

phase shift response of the analog P_5 response is incorrect throughout the frequency range. Correction of this incompatibility would enhance the usefulness of the analog model.

The engine Mach number sensor, $\Delta P/P_3$, frequency response at 95 percent maximum spool speed is presented in Figure 18 and compared with the frequency response of the analog model simulation. No data are presented for the component model because it does not include a model of the sensor. The principal difference between the responses, shown in the figure, is that the analog response has less phase shift than the engine response. Similar results were obtained at the other two operating points, 70 percent and 85 percent maximum spool speed.

Turbine discharge temperature, T_5, frequency responses of the engine and the two analytic models at 95 percent maximum spool speed are presented in Figure 19. The results show agreement between the engine response and the responses of the two models out to about 2.0 Hz. Beyond 2.0 Hz the phase shift of the engine response is much greater than the phase shift of the models, indicating that the engine contains some high-frequency dynamics which are not identified in the models. This observation substantiates the conclusions drawn from the spool speed responses discussed previously.

ENGINE RESPONSE TO EXHAUST AREA

Bode plots of spool speed, N, compressor discharge pressure, P_3, turbine discharge pressure, P_5, and turbine discharge temperature, T_5, for oscillations in exhaust area, A_8, are presented in Figures 20 through 23. Comparison of the engine responses shown in these figures with corresponding responses obtained from the linearized NASA component model and the APL analog model suggests the following conclusions:

1) DC gain levels do not agree very well between the engine responses and the two analytic models. This discrepancy is simply a calibration problem.

2) Except for differences in DC gain levels, the spool speed responses and turbine discharge temperature responses of the two analytic models agree fairly well with the corresponding engine responses in the frequency range below 2.0 Hz.

3) The compressor discharge pressure, P_3, response of the engine is accurately simulated by the two analytic models.

4) Neither the analog model nor the component model accurately represents the engine turbine discharge pressure, P_5, response.

These conclusions are discussed in the following paragraphs.

The spool speed response of the engine at 95 percent maximum spool speed is compared with the corresponding responses of the two analytic models in Figure 20. Except for differences in DC gain level, the model responses are seen to agree with the engine frequency response in the frequency range below 2.0 Hz. Beyond 2.0 Hz the engine phase shift drops considerably below the phase responses of the two models, indicating that the engine contains some high-frequency dynamics which are not included in the models.

Most of the mismatch in DC gain levels can be attributed to the exhaust area calibration incompatibility between the engine and the models. The two exhaust nozzle simulations and the engine exhaust area sensor all have different nozzle area calibrations. A method for correcting the nozzle area calibrations of the two models to agree with the engine calibration was not identified because engine nozzle area could not be measured directly. Different DC gain levels are characteristic of all of the exhaust actuator frequency data.

27

Compressor discharge pressure, P_3, response of the engine and the two models at 95 percent maximum spool speed are shown in Figure 21. These responses also show the DC gain mismatch discussed above. Other than that, the frequency responses of the two analytic models closely approximate the frequency response of the engine. This result is also valid for the frequency responses at the other operating points, 70 percent and 85 percent maximum spool speed.

The turbine discharge pressure, P_5, frequency responses are presented in Figure 22. They show that the P_5 simulations included in the models are not as accurate as the P_3 simulations. The gain and phase of the component model P_5 response have the same basic shape as the corresponding gain and phase of the engine response, but the component model gain is about 10 decibels lower and the component model phase response shows about 30 degrees more phase shift. Neither the gain nor phase of the analog model P_5 response matches the engine response.

The turbine discharge temperature, T_5, response of the engine is compared with the corresponding responses of the two analytic models in Figure 23. These responses show that the component model approximates the engine response well, especially in the frequency range below 2.0 Hz. The analog model also reasonably approximates the engine response; however, the analog model gain response is quite low and the phase response shows more phase shift than the engine.

ENGINE RESPONSES TO COMPRESSOR BLEED

Sample Bode frequency response plots of spool speed, compressor discharge pressure, and turbine discharge temperature for oscillations in compressor bleed are presented in Figures 24, 25, and 26. The plots include frequency data representing the engine and the linearized NASA component model; the

analog model is not represented, since the simulation does not contain compressor bleed effects. Comparison of the engine frequency responses with the component model responses supports the following conclusions:

1) The shape of the gain responses of the component model agrees with the shape of the corresponding engine responses. However, there are some significant differences in DC gain levels.

2) Phase responses of the component model do not accurately represent the engine phase responses. The engine frequency responses exhibit more phase shift than the component model responses throughout most of the frequency range.

Individual Bode plots are discussed in the following paragraphs.

The spool speed, N, frequency response of the engine at 95 percent maximum spool speed is compared with the corresponding frequency response of the component model in Figure 24. Agreement between the engine and component model gain responses is very good, within 3 decibels, but the engine phase response shows much more phase shift at high frequencies than the component model phase response, indicating that the engine contains high-frequency dynamics which are not included in the linear model.

Engine and component model frequency responses of P_3 and T_5 at 95 percent maximum spool speed are presented in Figures 25 and 26. Both plots show the engine to have 30 degrees more phase shift at low frequency than the component model. Gain responses of the engine and component model are similar in shape, but the DC gain levels are off by more than 6 decibels. Frequency responses of these variables obtained at the other two operating points, 70 percent and 85 percent maximum spool speed, further substantiate these observations.

29

ENGINE RESPONSES TO INLET GUIDE VANES

Frequency response plots of spool speed, compressor discharge pressure, and turbine discharge temperature for oscillation of the inlet guide vanes are presented in Figures 27, 28, and 29. Engine frequency response data and linearized NASA component model frequency response data are compared in the plots at one operating point, 95 percent maximum spool speed. Analog model data are not included, since the analog simulation does not contain inlet guide vane effects. Comparison of the engine and component model frequency responses supports the following conclusions:

1) The spool speed and P_3 responses of the component model are approximate representations of the engine frequency responses. The shape of the gain curves agree, and the phase responses agree within 30 degrees in the frequency range below 2.0 Hz.

2) The T_5 response of the component model is a poor representation of the corresponding engine response. The gain responses differ significantly in shape and the phase responses differ by as much as 140 degrees in the frequency range tested.

These conclusions are explained in the following paragraphs.

Engine and component model spool speed frequency responses are presented in Figure 27. These data show agreement typically within 3 decibels in the gain responses, but the phase shift of the engine above 0.5 Hz is significantly greater than the phase shift of the component model. The greater phase shift of the engine data indicates that the engine contains high-frequency dynamics which are not represented in the component model. As previously noted, a similar conclusion was made concerning the spool speed responses to oscillations in exhaust area and compressor bleeds.

The P_3 responses presented in Figure 28 show that, except for a different DC gain level and a constant phase error of about 20 degrees, the component model is a good enough approximation for design purposes to the engine frequency response, considering the nonlinearity of the actuator.

The frequency response data of Figure 29 show that inlet guide vane effect on T_5 is not correctly simulated in the component model. Neither the gain nor phase responses of the component model agree with the corresponding responses of the engine.

$$E_1(t) = E_1 \, SIN \, (\omega_1 t + \phi_1)$$
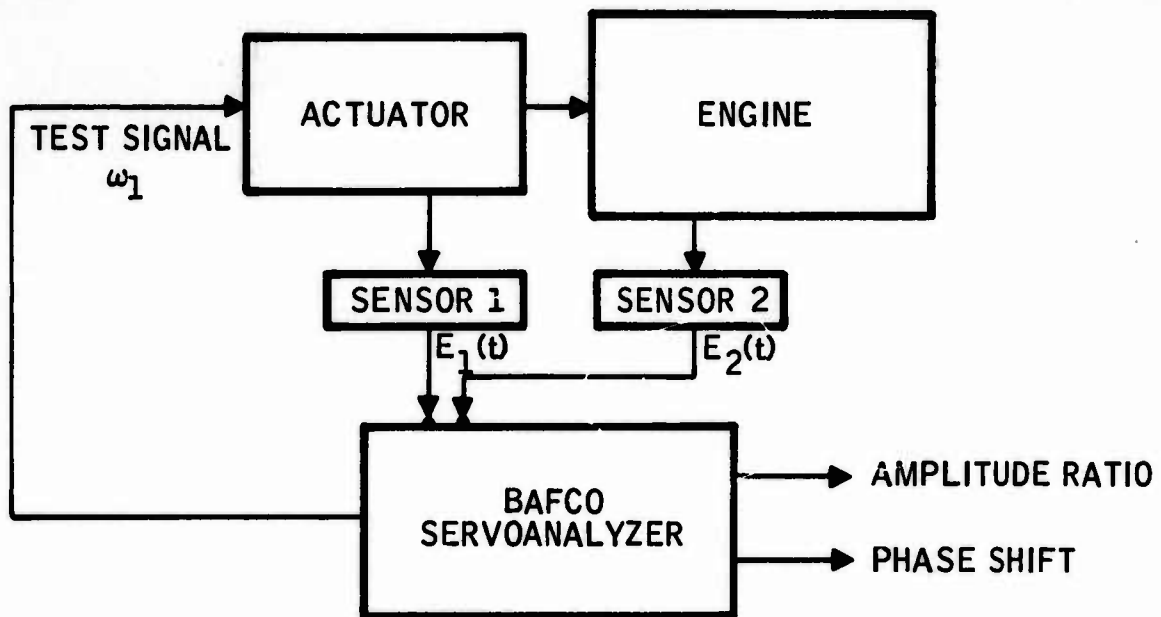
$$E_2(t) = E_2 \, SIN \, (\omega_1 t + \phi_2)$$

$$\text{AMPLITUDE RATIO} = \left| \frac{E_2}{E_1} \right|$$

$$\text{PHASE SHIFT} = \angle \phi_2 - \phi_1$$

Figure 4. Frequency Response Analysis
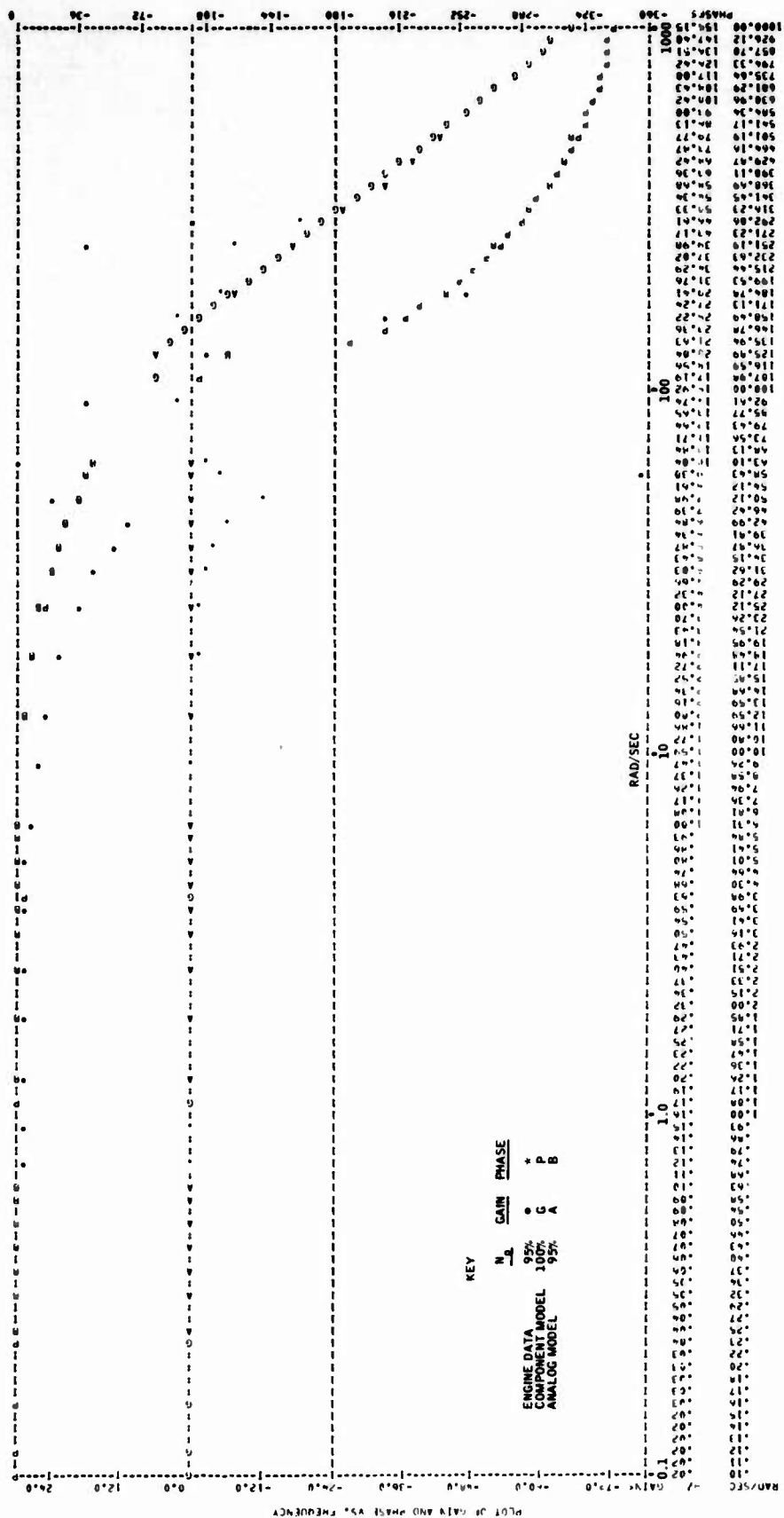
Figure 5. Fuel Flow/Fuel Command, W_f/u_f

33
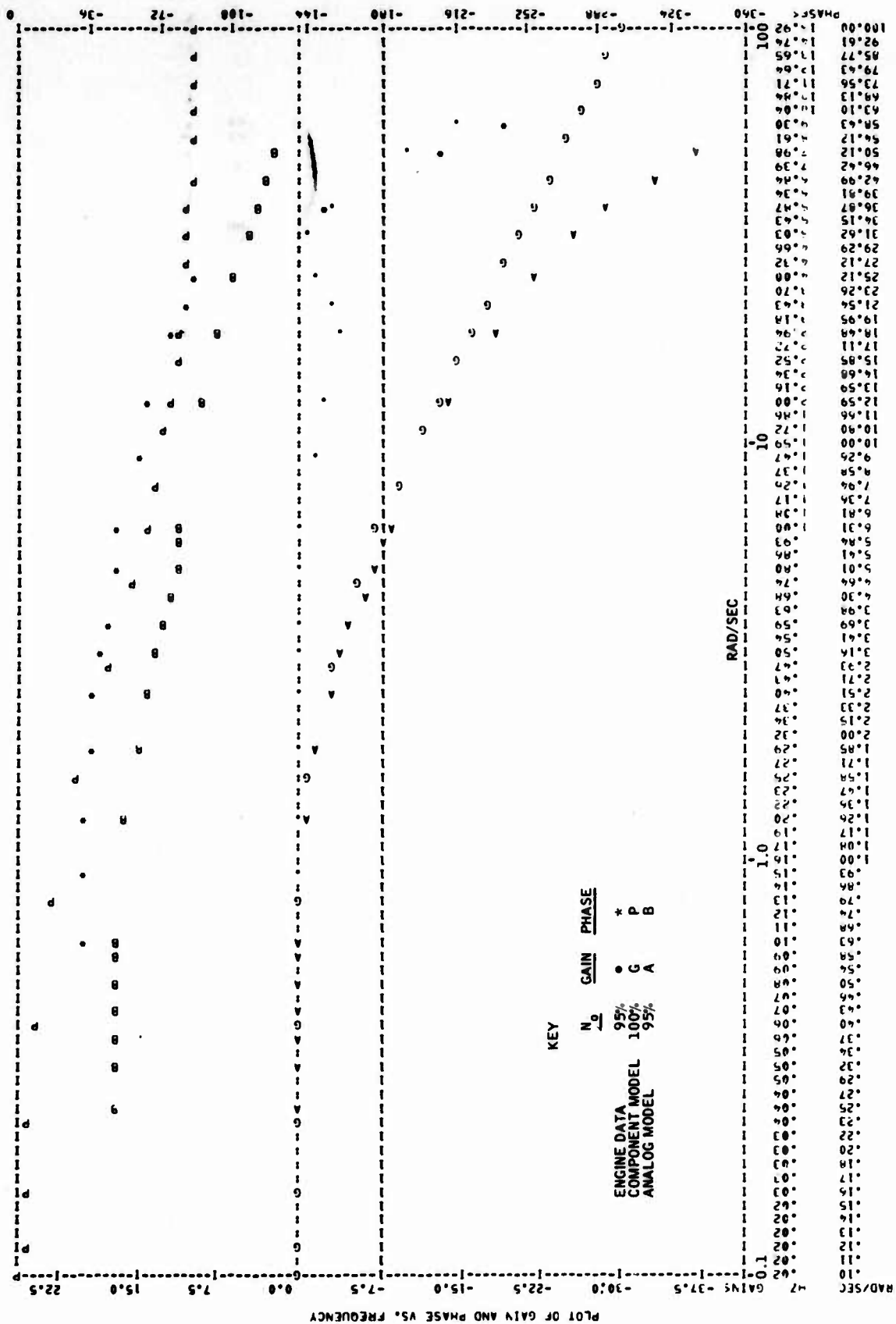
Figure 6. Exhaust Area/Exhaust Command, $A_8 u_A$
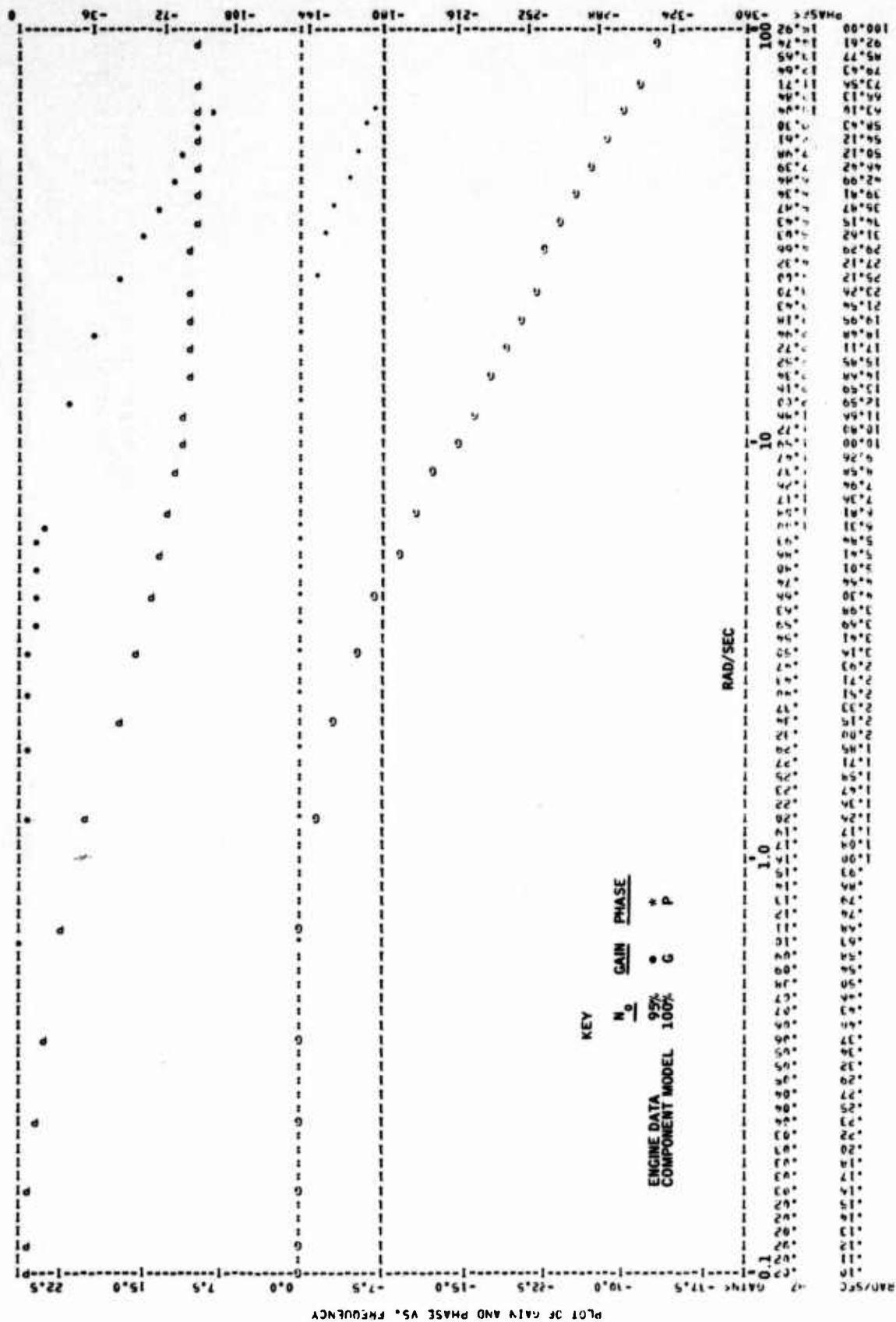
Figure 7. Compressor Bleed/Bleed Command, BLD/U_{BLD}

35
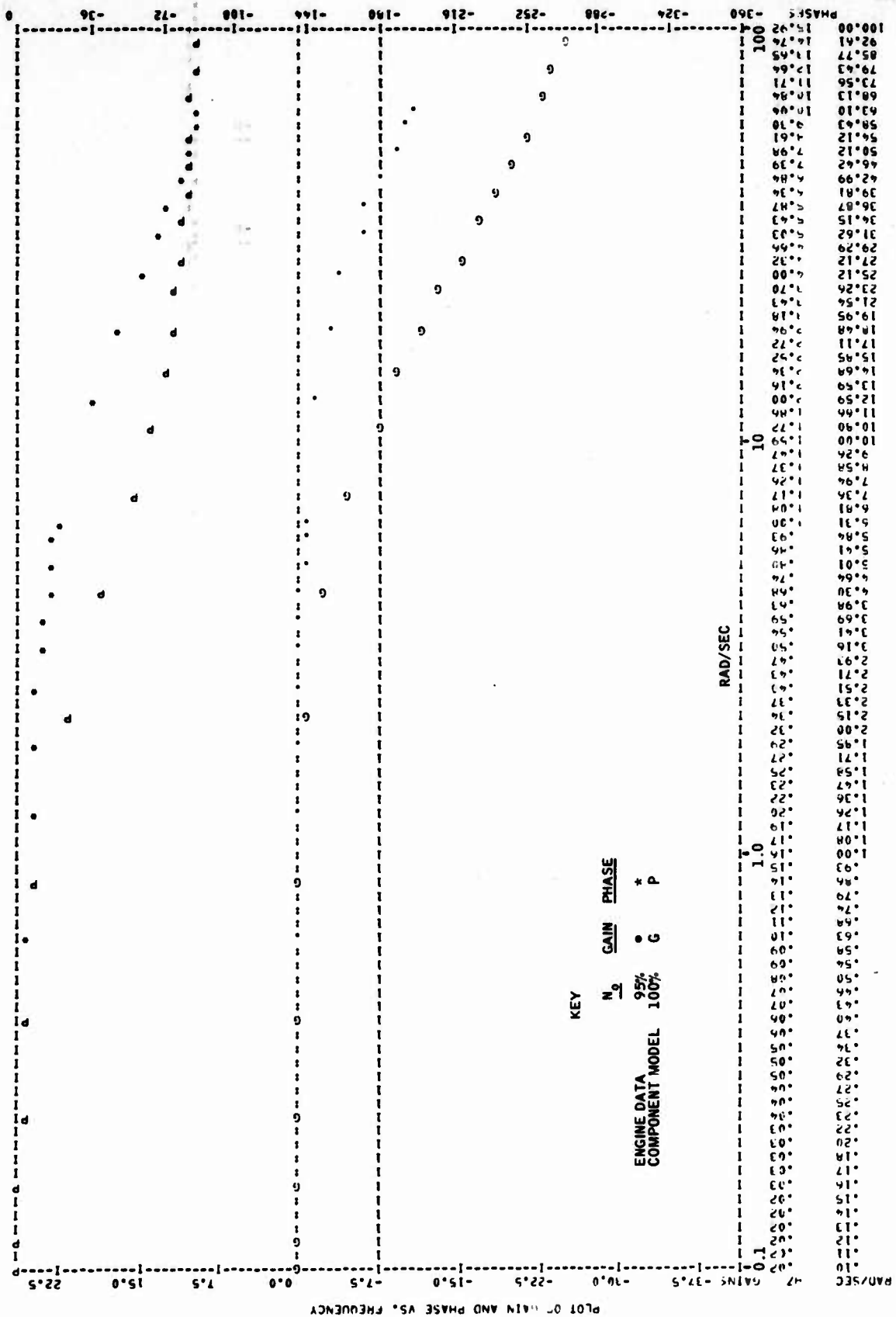
Figure 8. Inlet Guide Vane/Inlet Guide Vane Command, IGV/u_{IGV}

PLOT OF GAIN AND PHASE VS. FREQUENCY
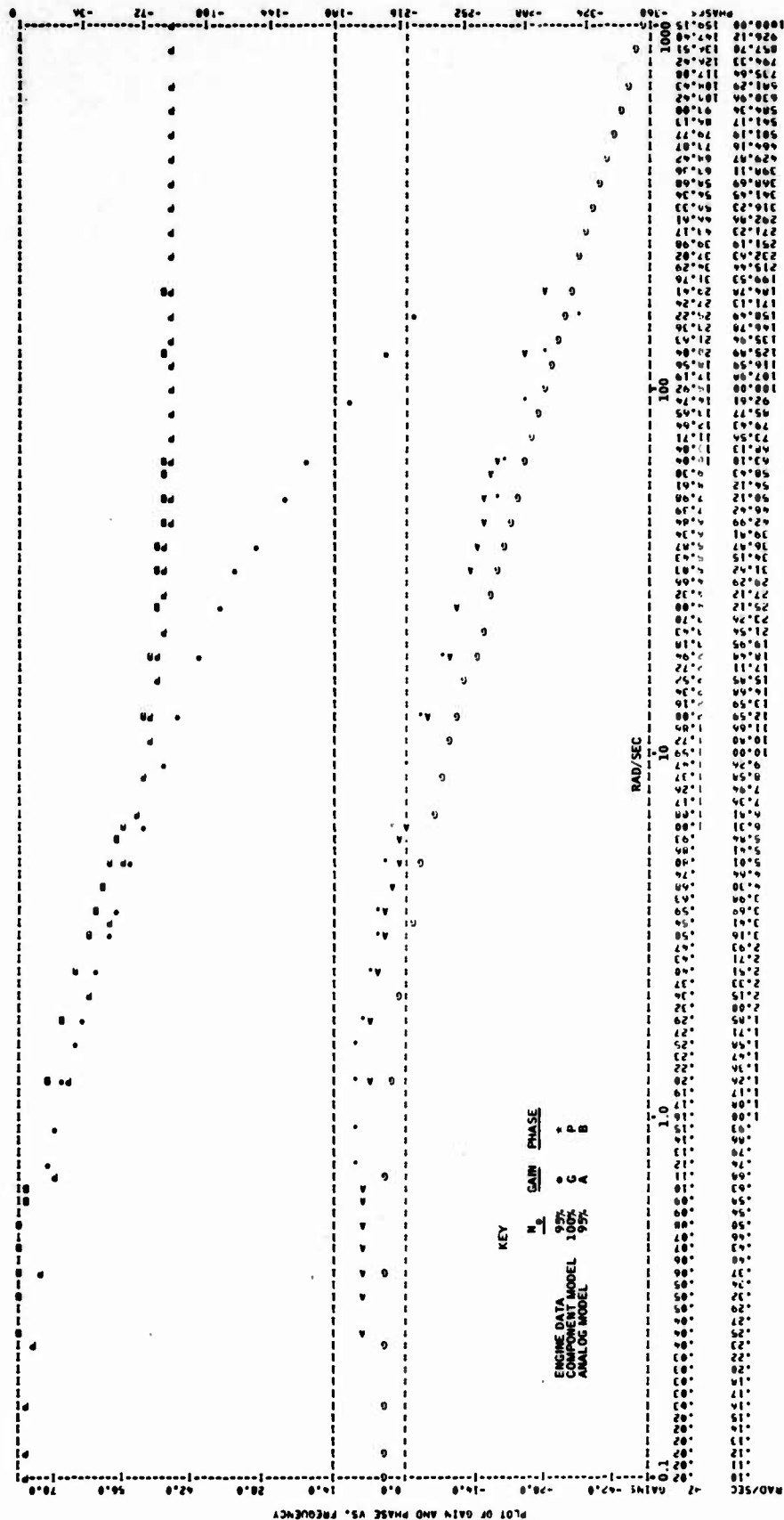
Figure 9. Spool Speed/Fuel Flow, N/W_f--95 and 100 Percent Maximum Speed

37
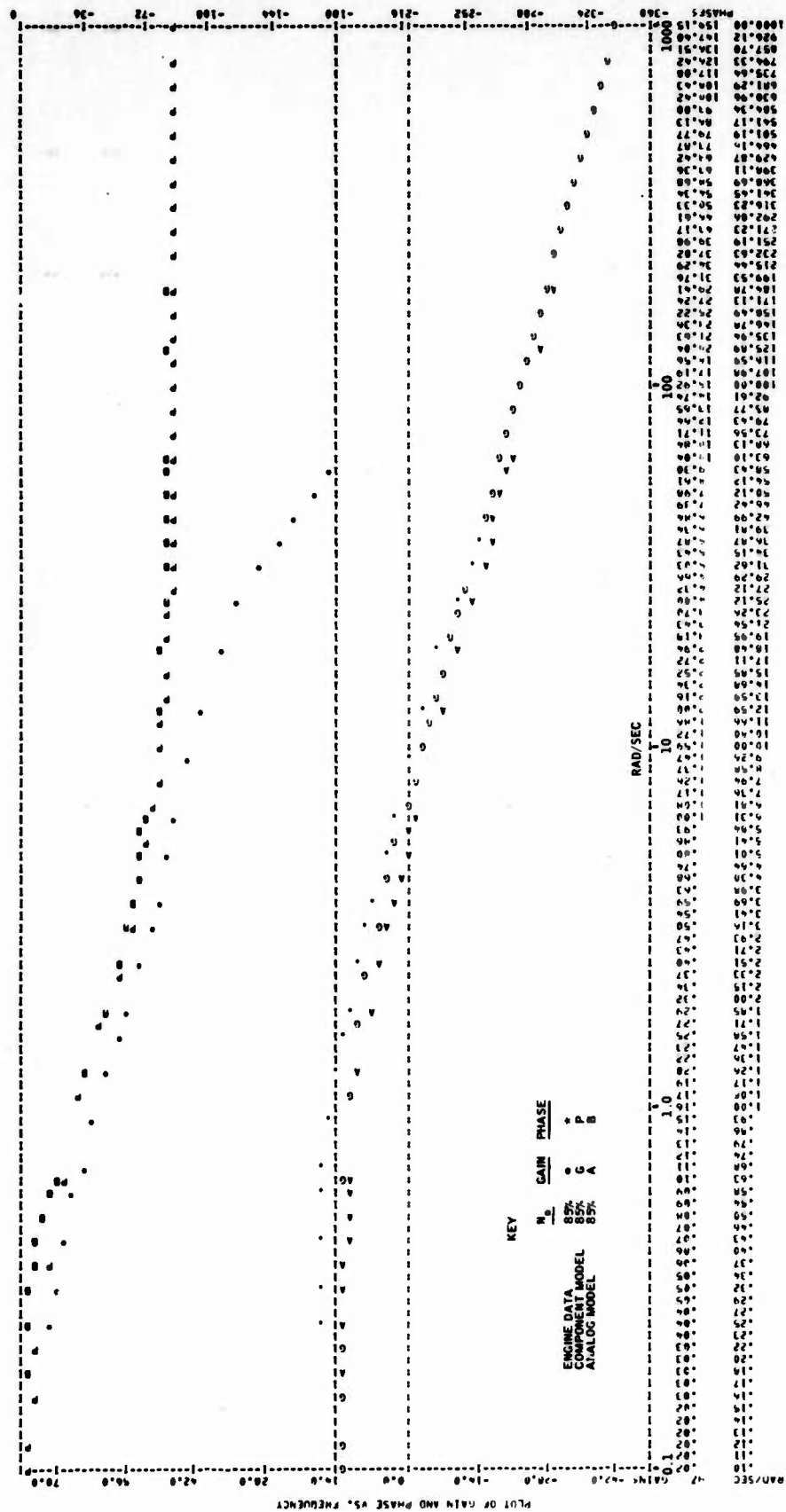
Figure 10. Spool Speed/Fuel Flow, N/W_f --85 Percent Maximum Speed

38

Figure 11. Spool Speed/Fuel Flow, N/W_f--70 Percent Maximum Speed
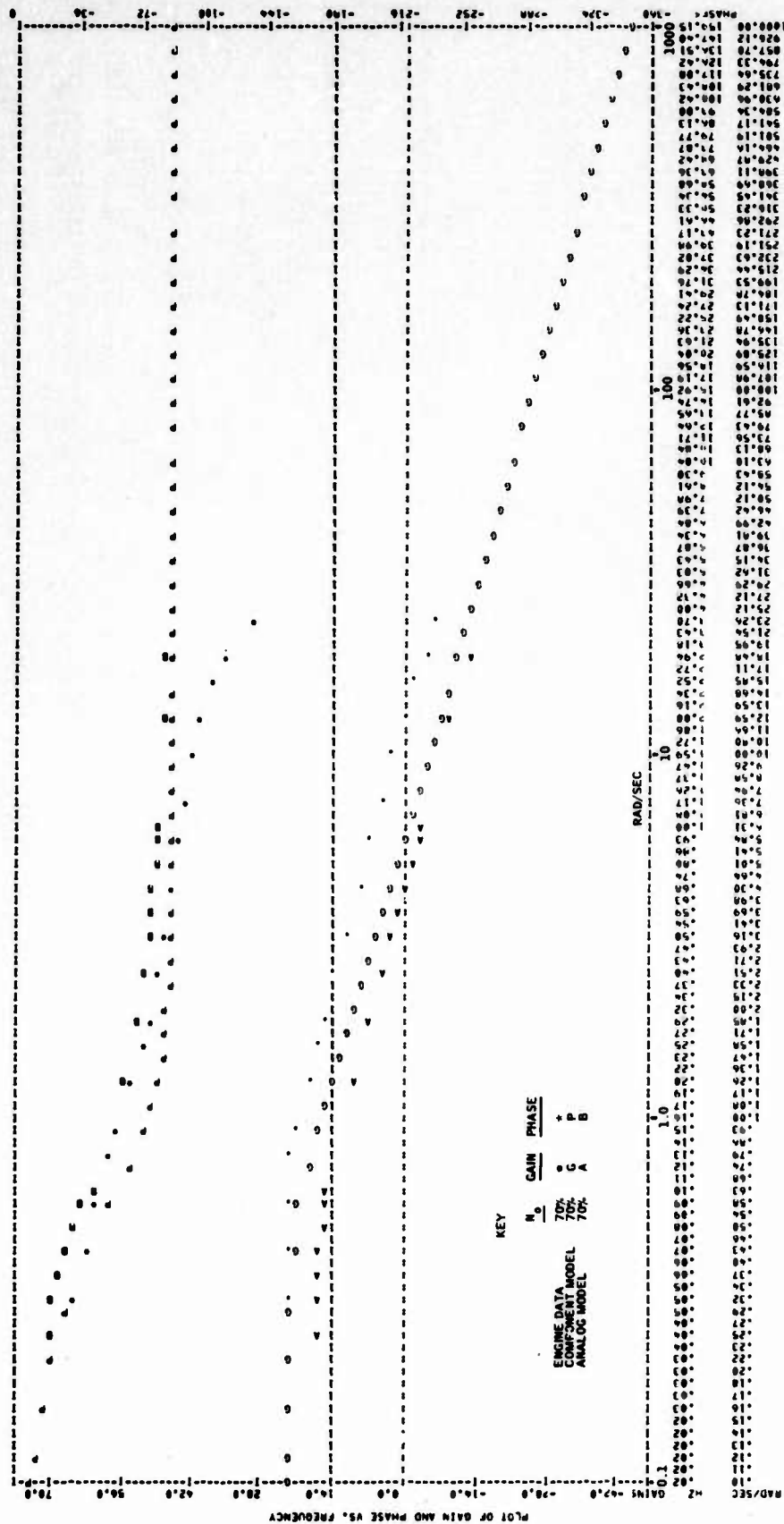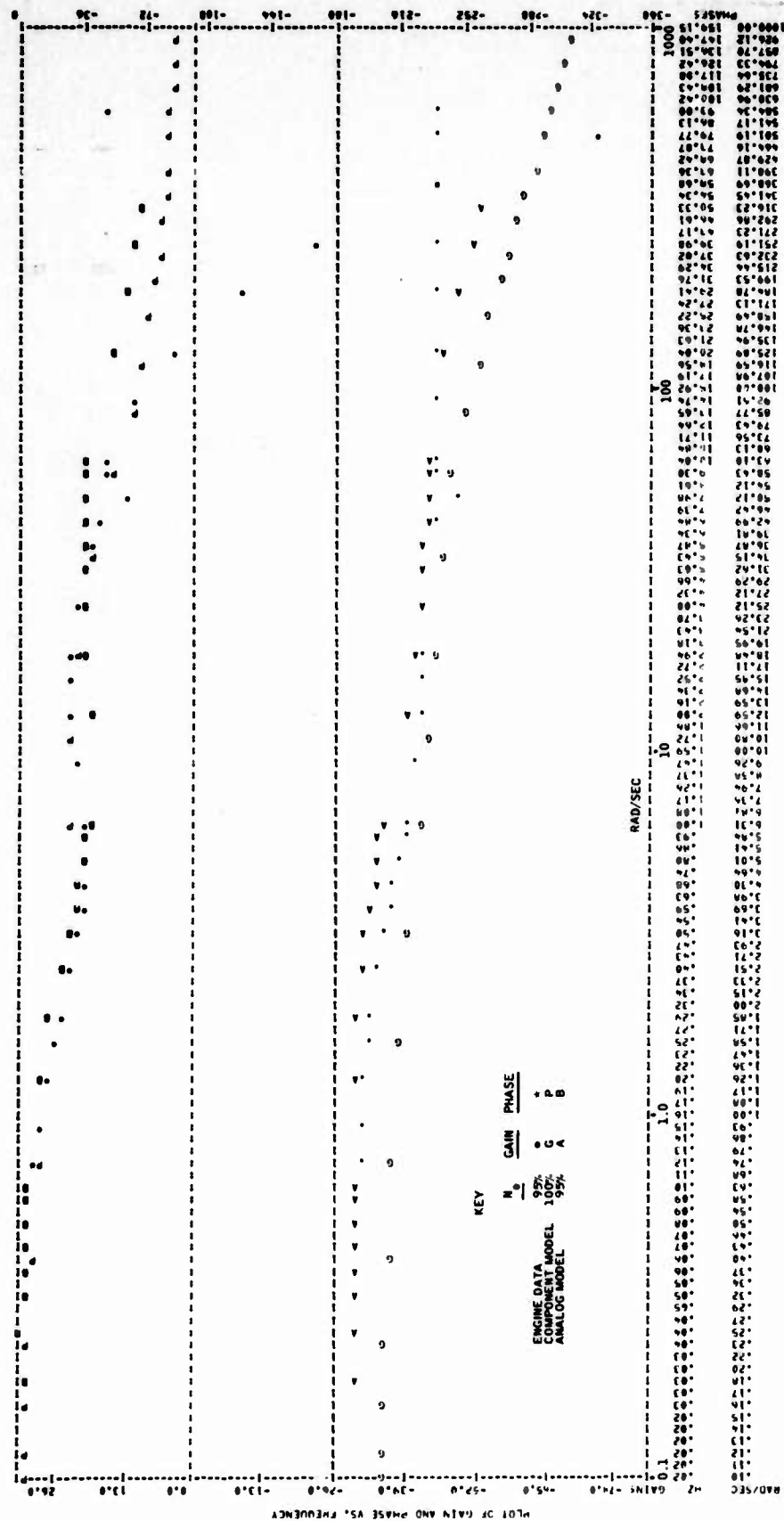
Figure 12. Compressor Discharge Pressure/Fuel Flow, P_3/W_f -- 95 and 100 Percent Maximum Speed

40

Figure 13. Compressor Discharge Pressure/Fuel Flow, P_3/W_f -- 85 Percent Maximum Speed

41
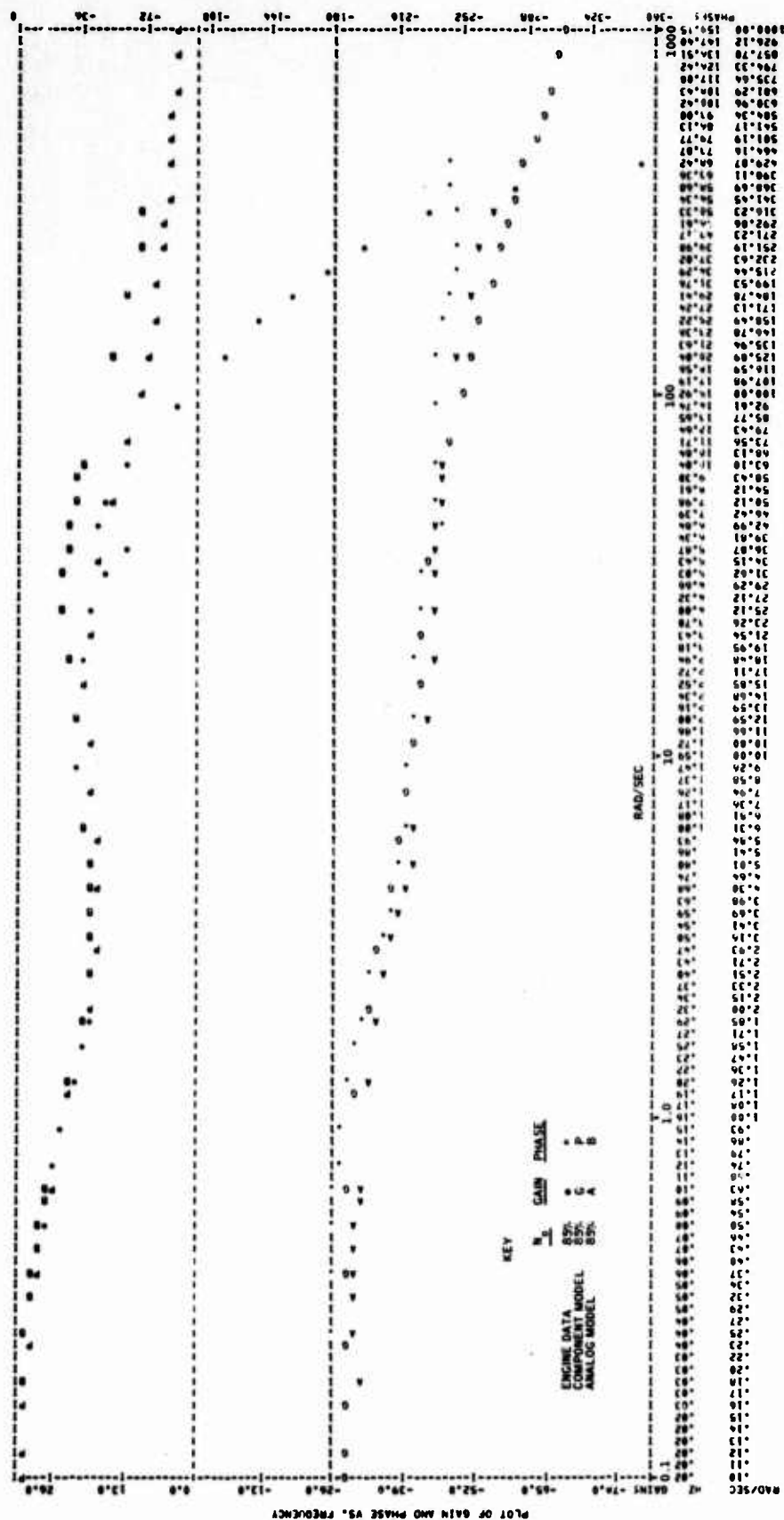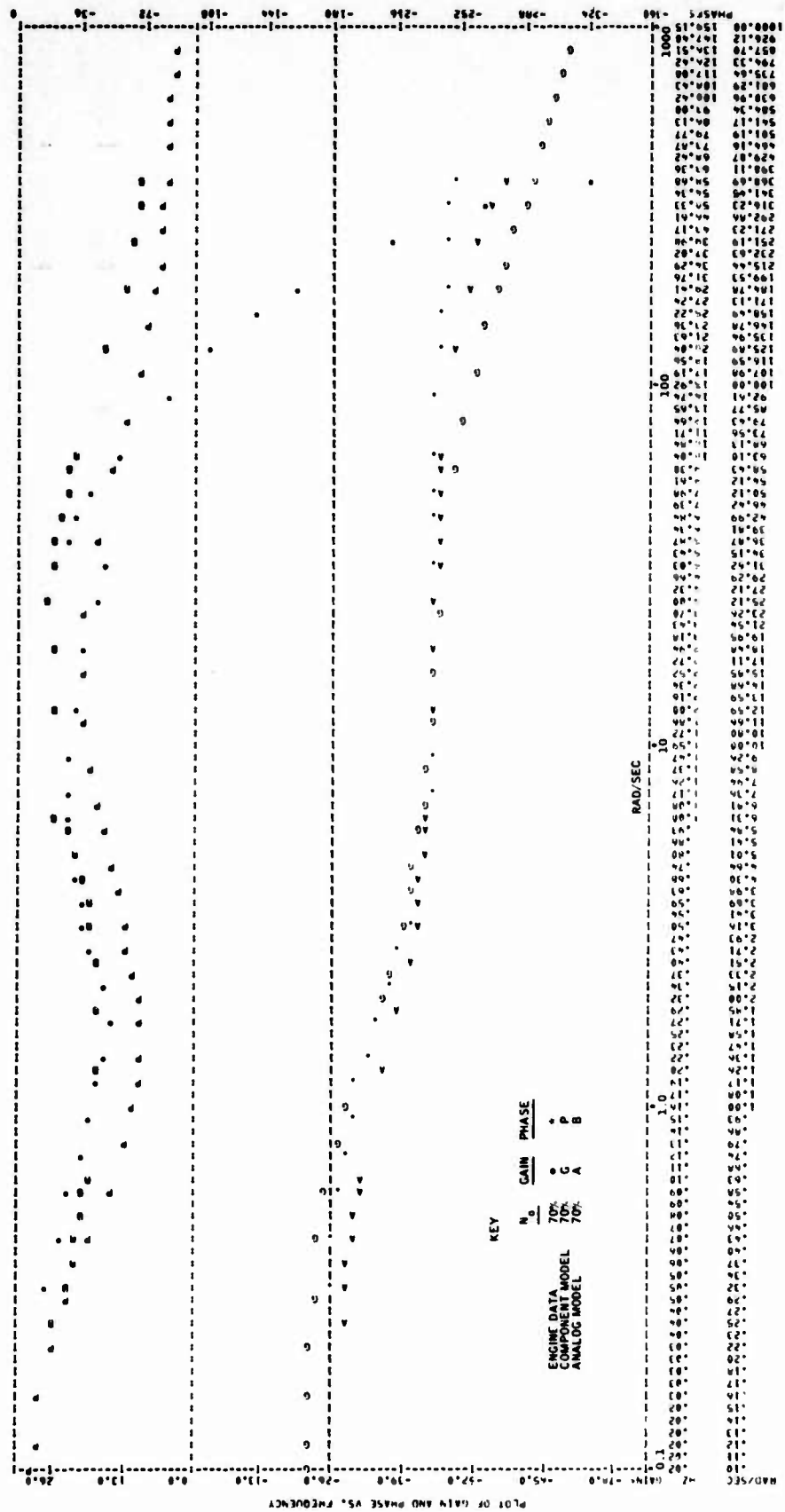
Figure 14. Compressor Discharge Pressure/Fuel Flow, P_3/W_f -- 70 Percent Maximum Speed

42
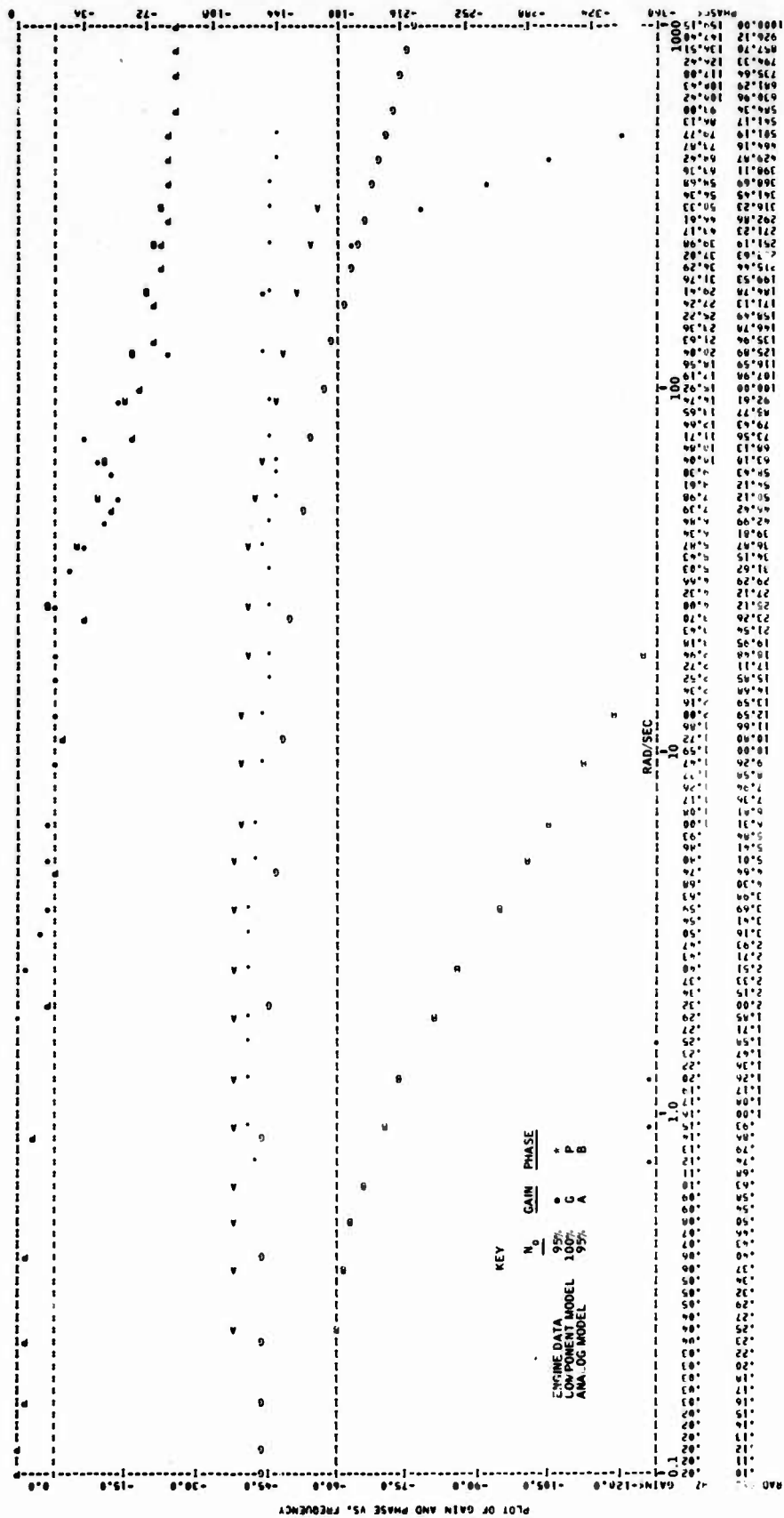
Figure 15. Turbine Discharge Pressure/Fuel Flow, P_5/W_f -- 95 and 100 Percent Maximum Speed

43

Figure 16. Turbine Discharge Pressure/Fuel Flow, P_5/W_f-- 85 Percent Maximum Speed

44
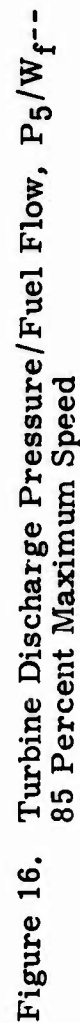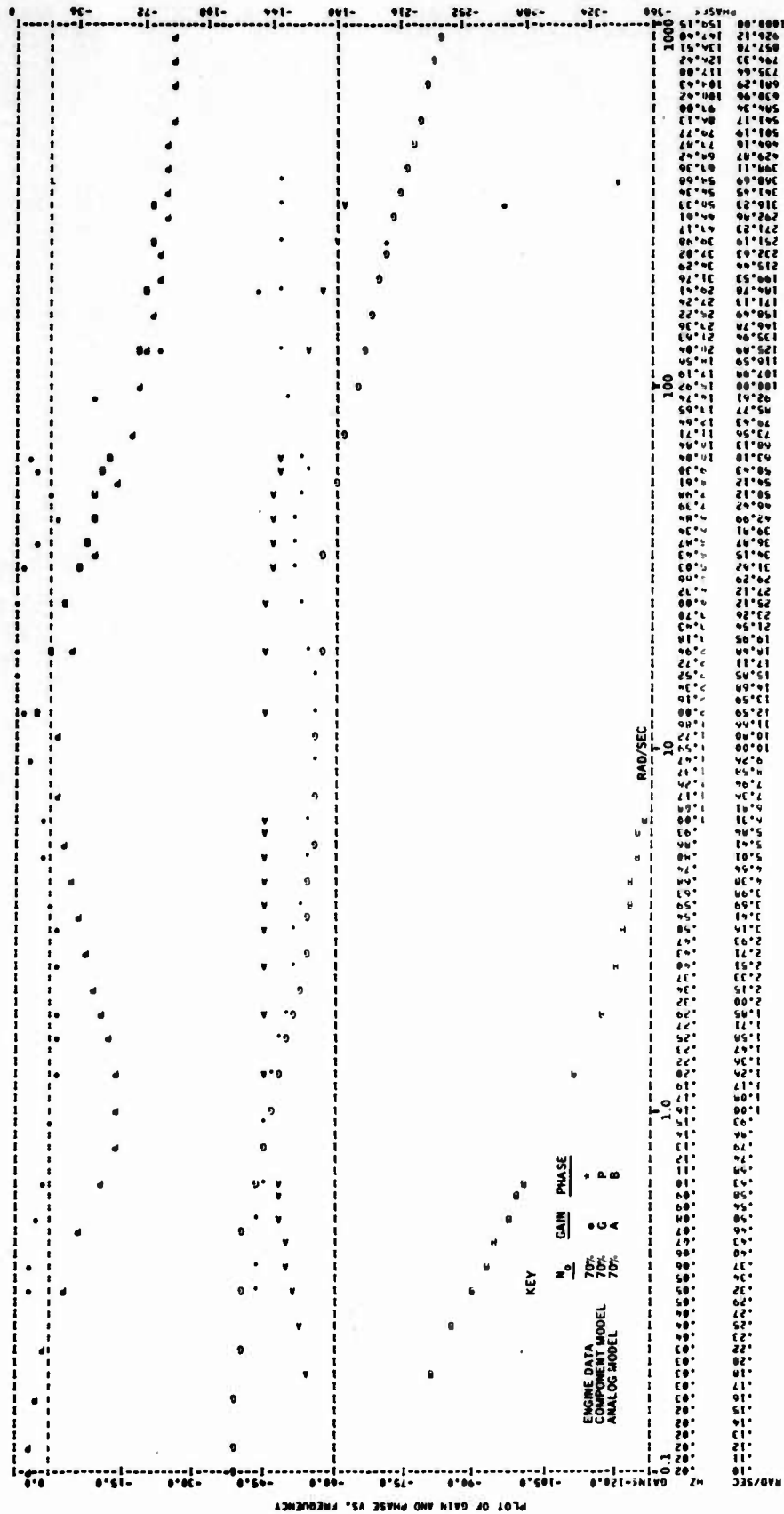
Figure 17. Turbine Discharge Pressure/Fuel Flow, P_5/W_f—
70 Percent Maximum Speed

45
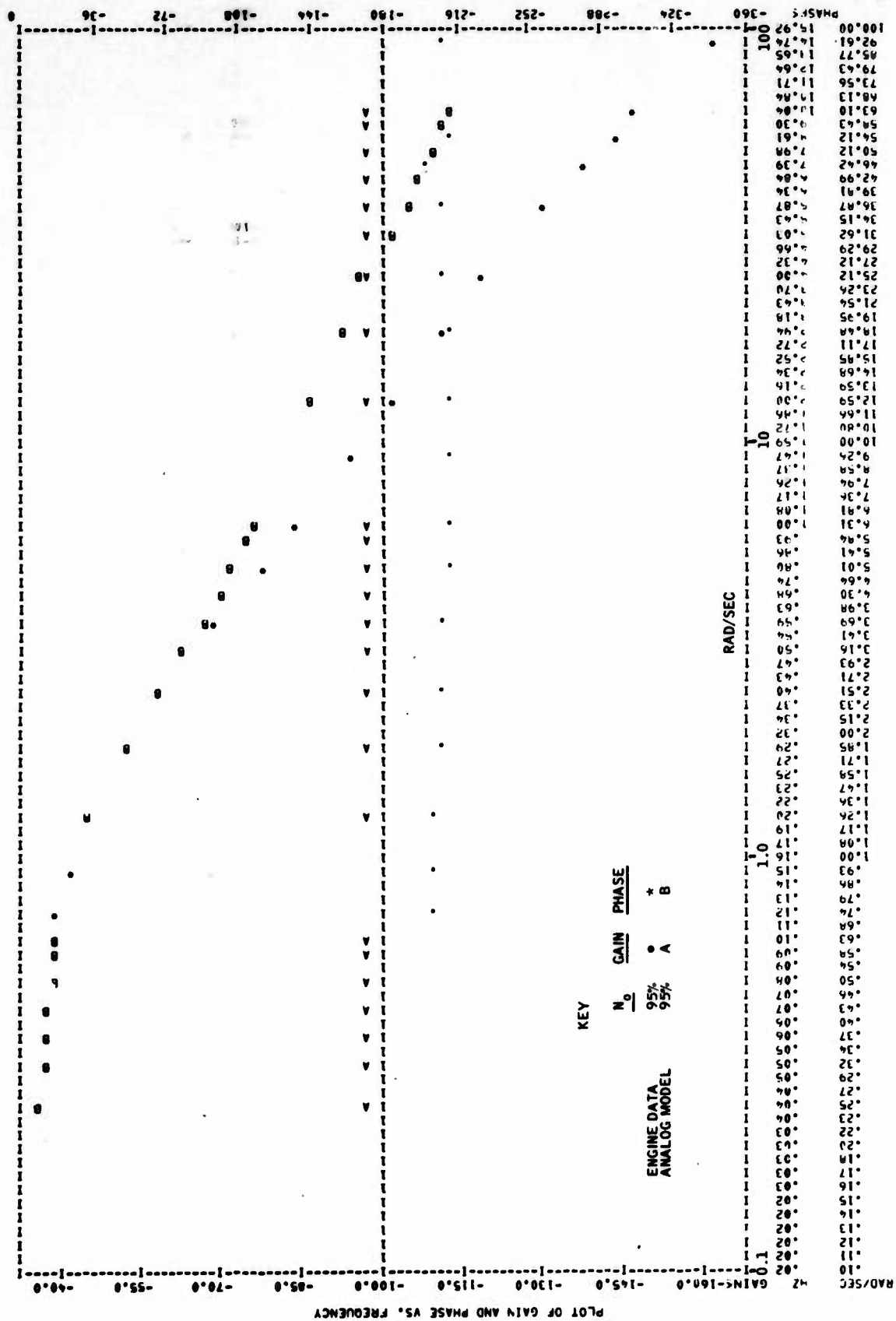
Figure 18. Mach Number Sensor/Fuel Flow, $\frac{\Delta P}{P_3}/W_f$
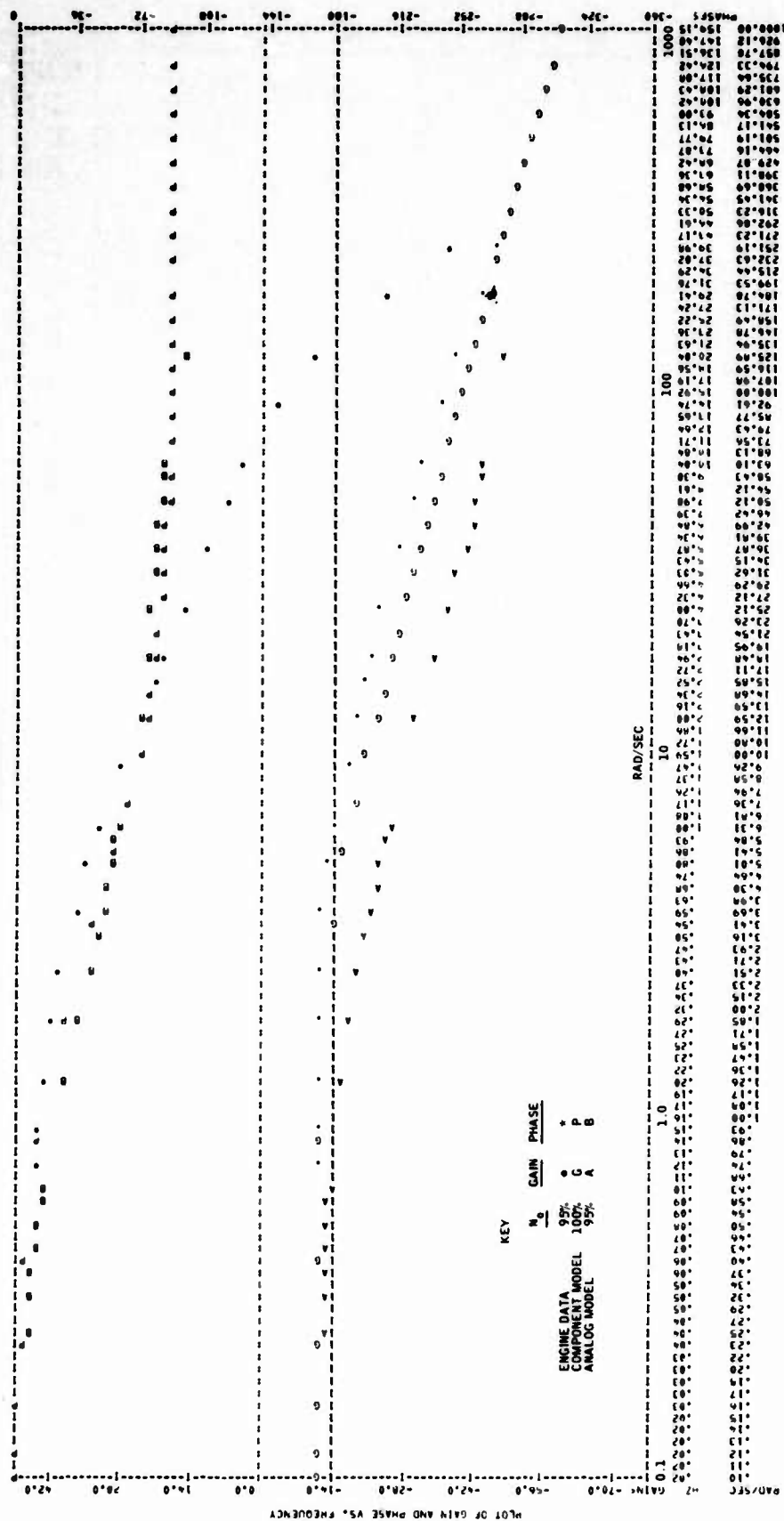
Figure 19.   Turbine Discharge Temperature/Fuel Flow, T_5/W_f
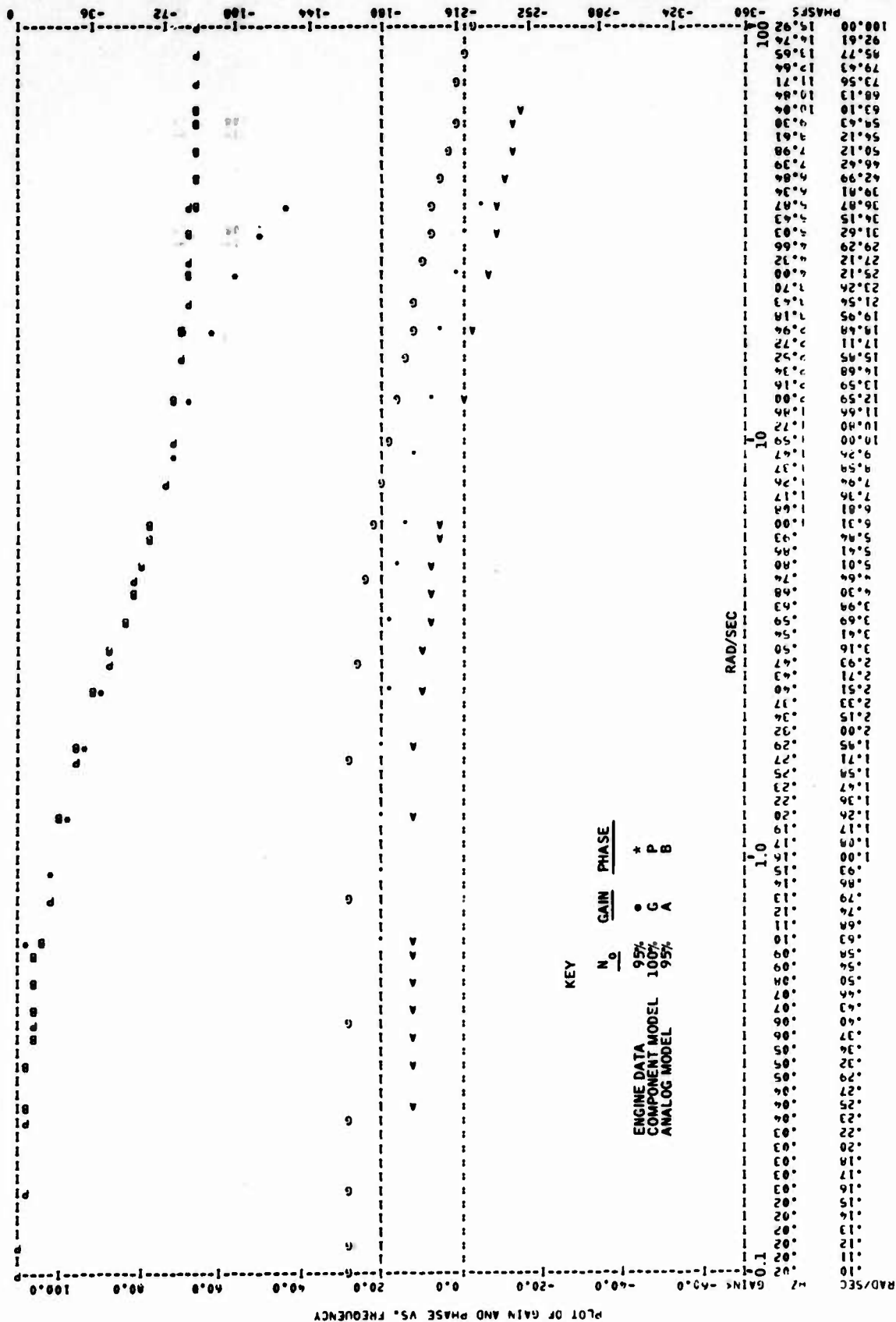
Figure 20. Spool Speed/Exhaust Area, N/A_8
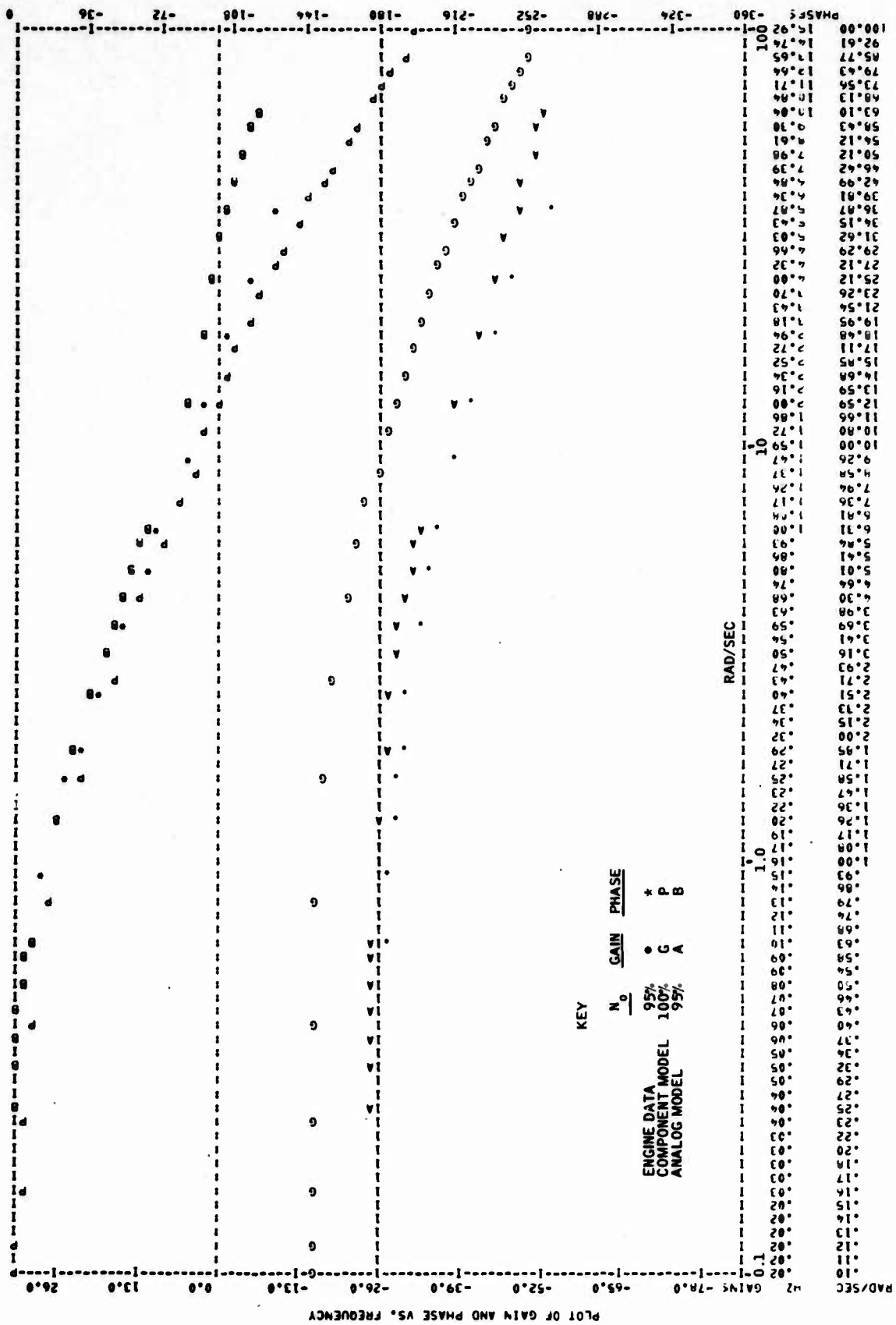
Figure 21. Compressor Discharge Pressure/Exhaust Area, P_3/A_8
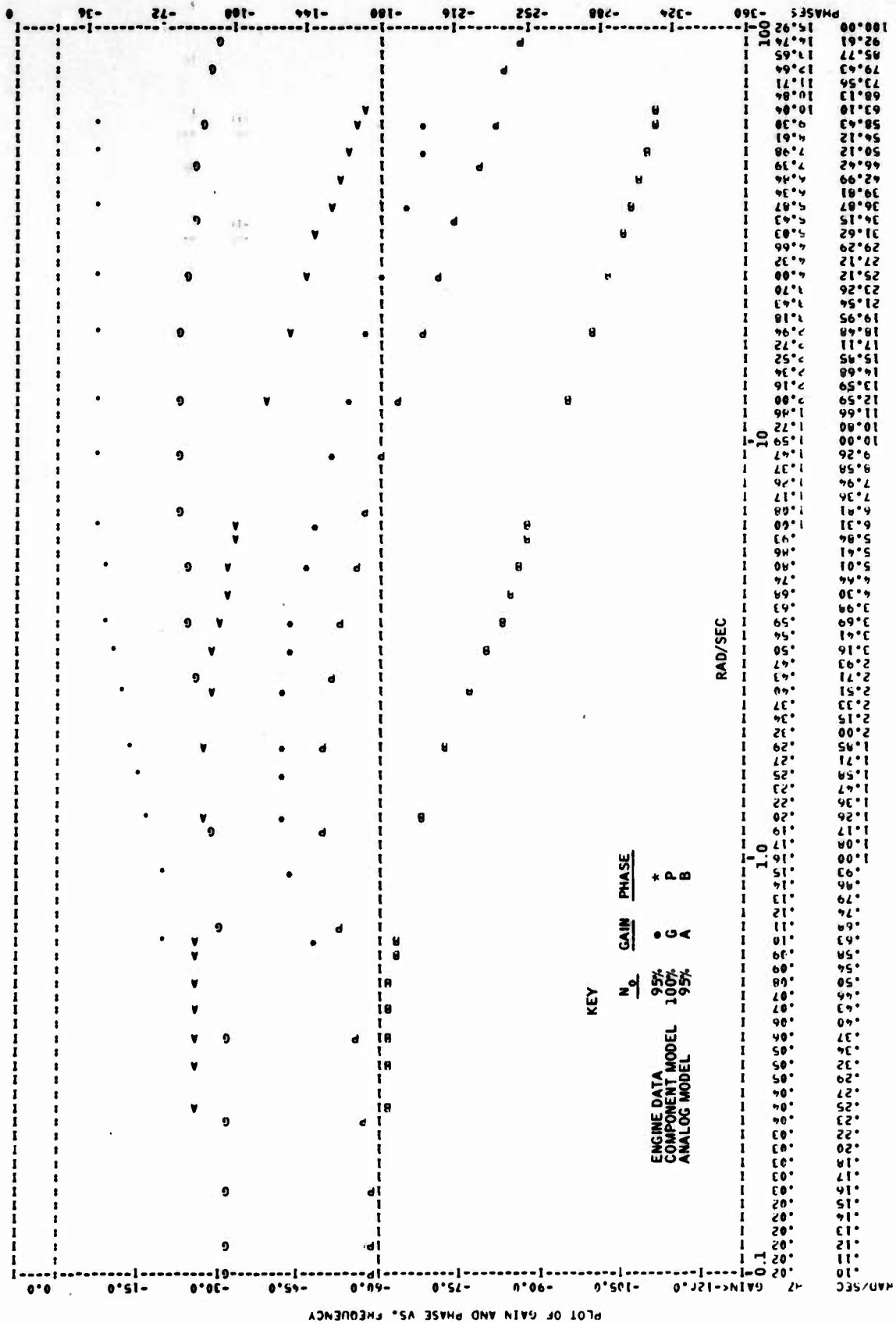
Figure 22. Turbine Discharge Pressure/Exhaust Area, P_5/A_8
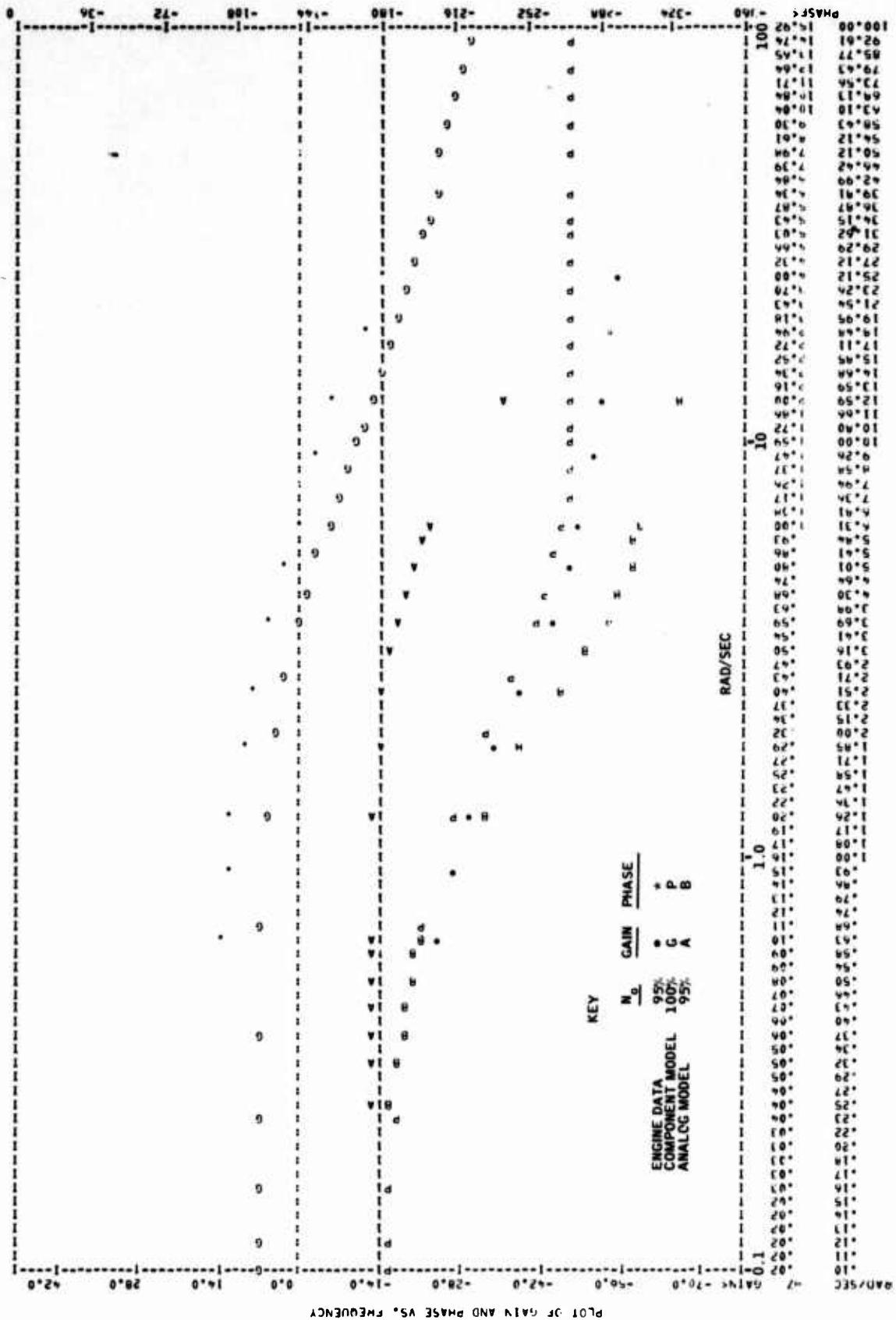
Figure 23. Turbine Discharge Temperature/Exhaust Area, T_5/A_8

PLOT OF GAIN AND PHASE VS. FREQUENCY
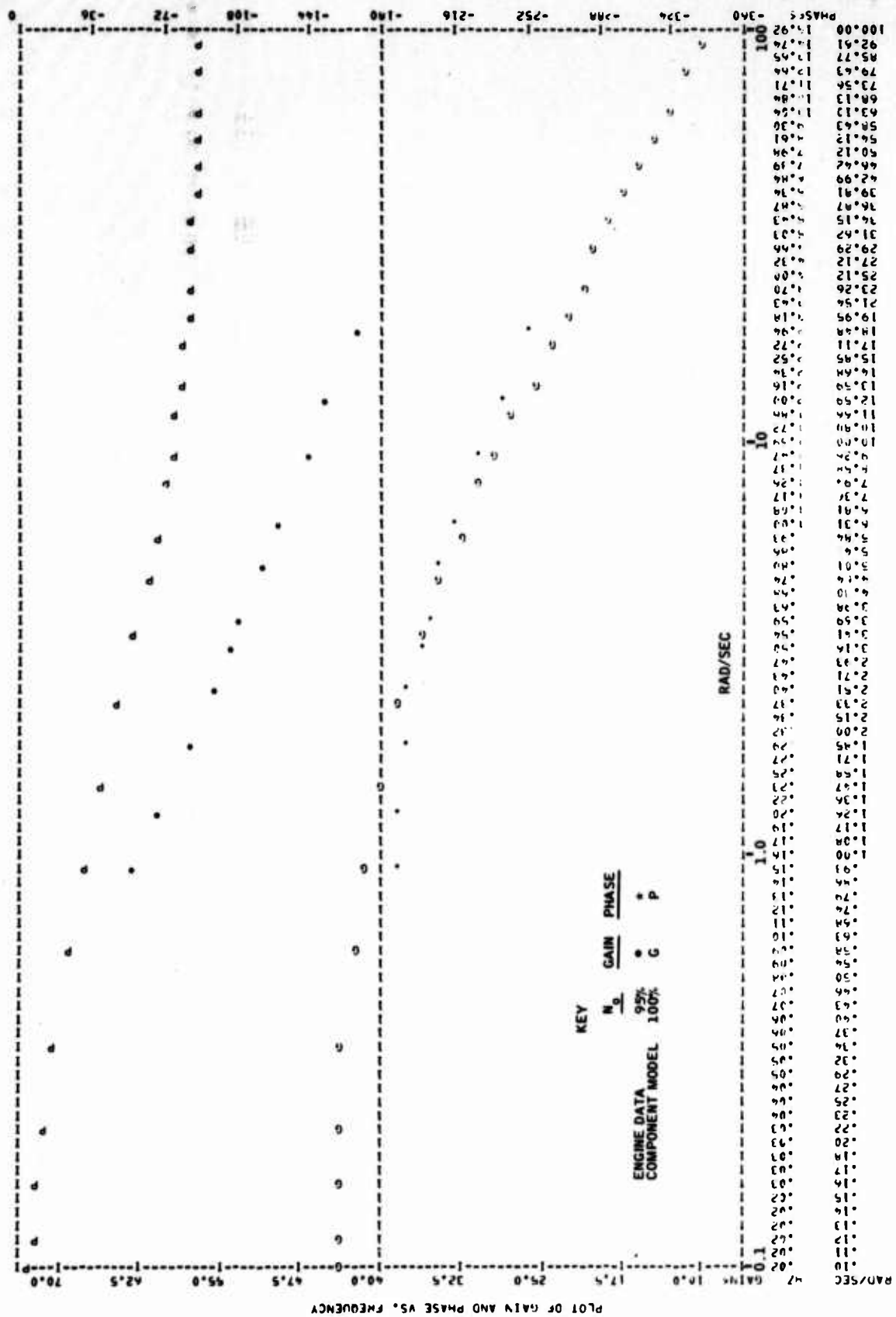
Figure 24. Spool Speed/Compressor Bleed, N/BLD
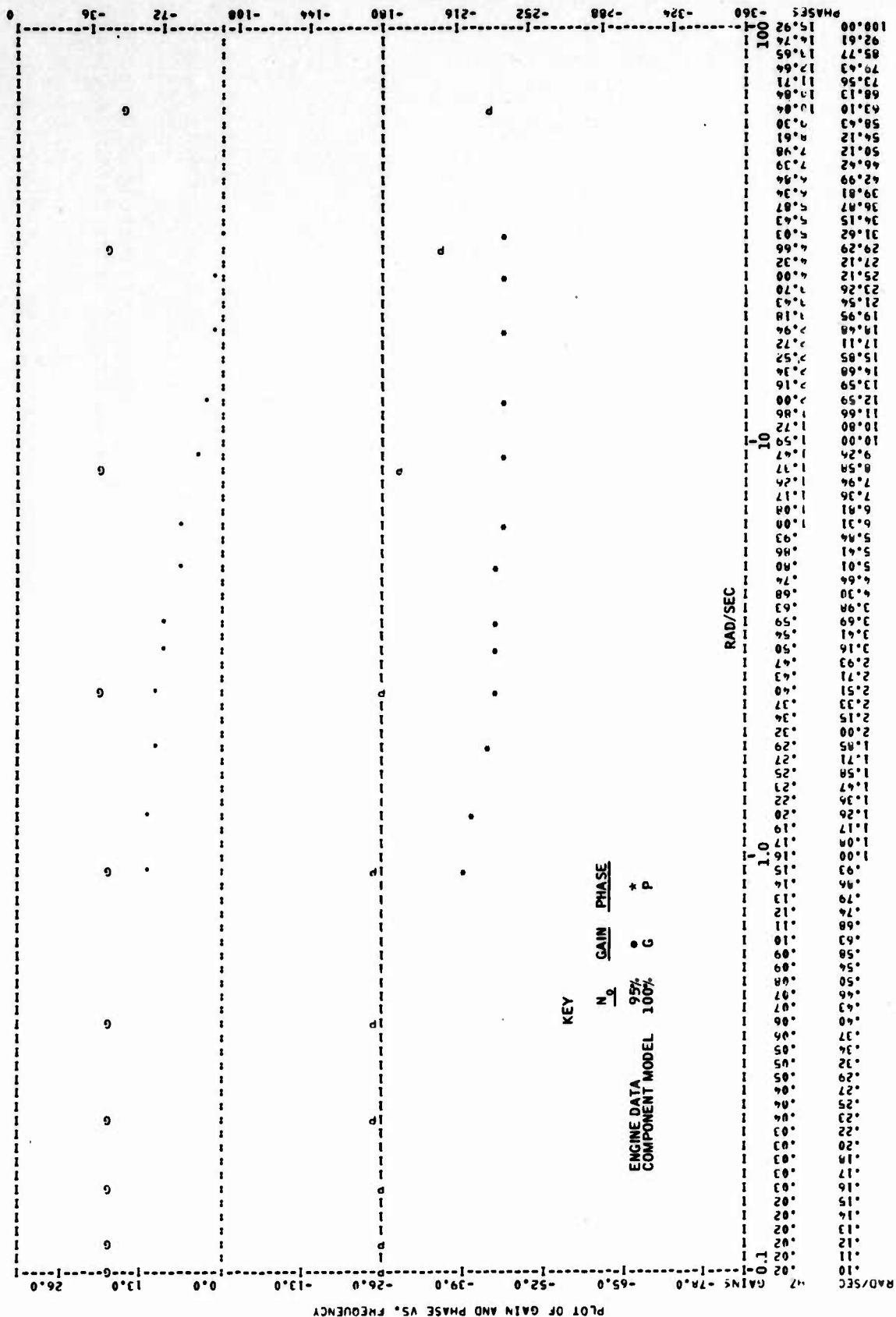
Figure 25. Compressor Discharge Pressure/Compressor Bleed, P_3/BLD
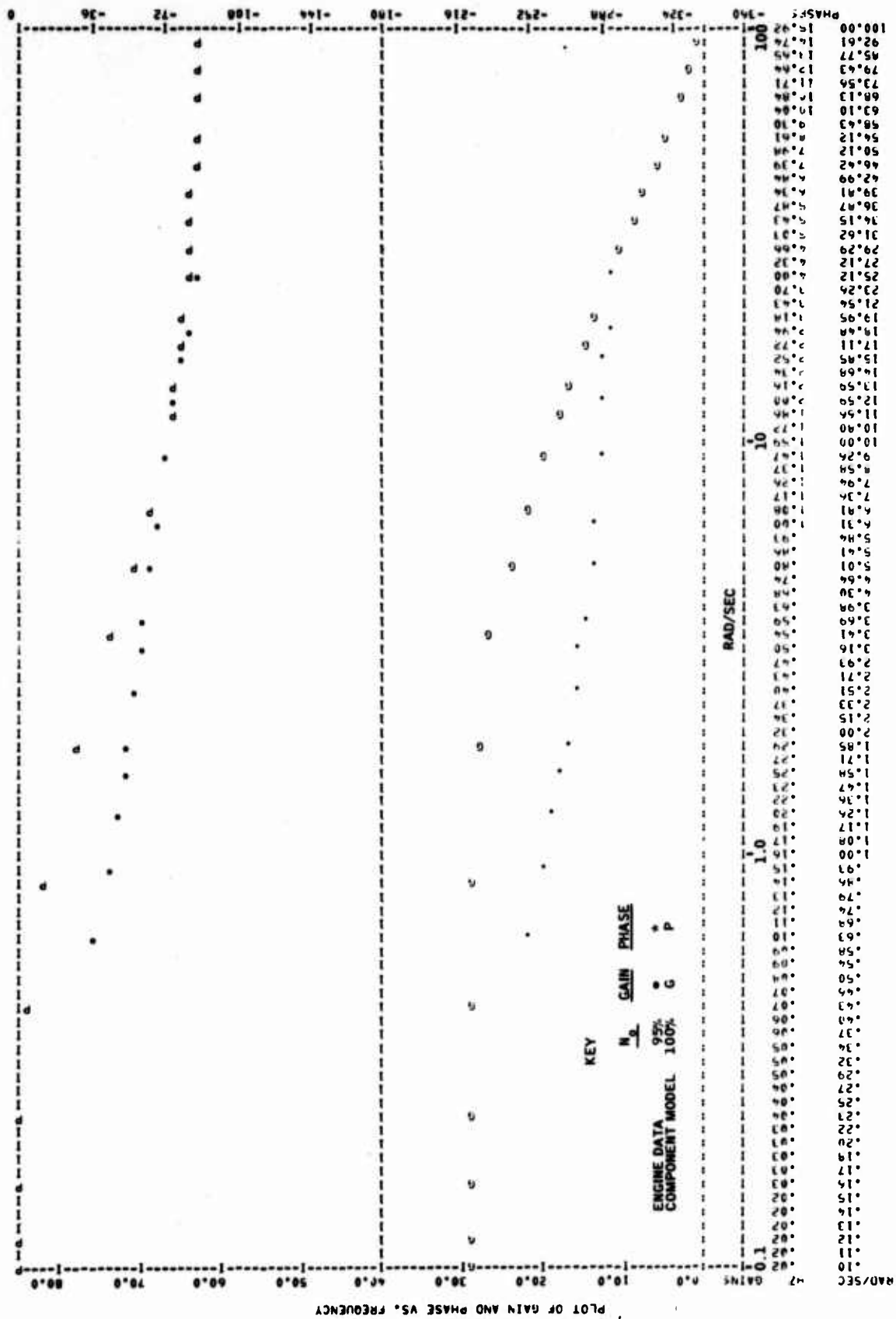
Figure 26. Turbine Discharge Temperature/Compressor Bleed, T_5/BLD
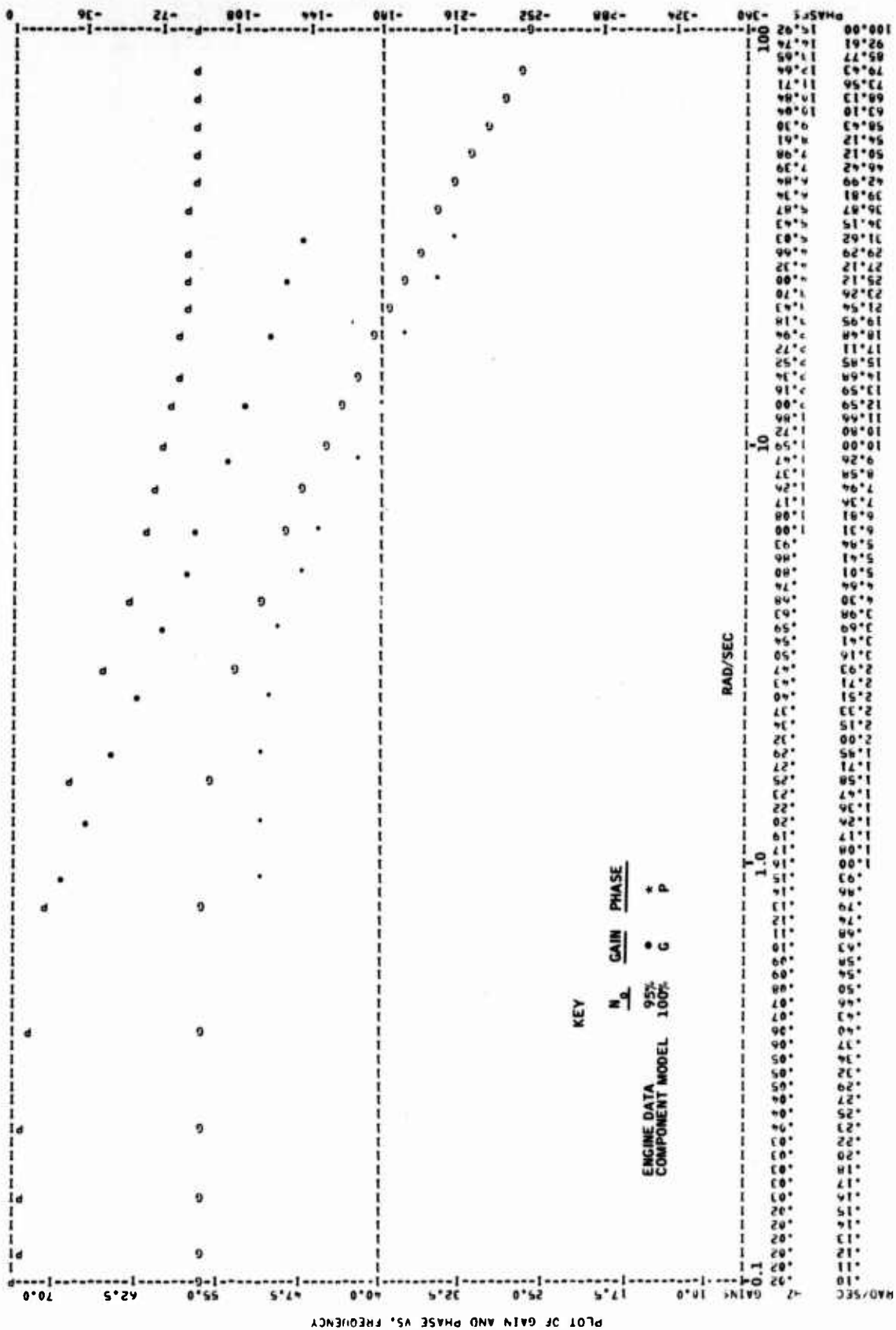
Figure 27. Spool Speed/Inlet Guide Vane, N/IGV
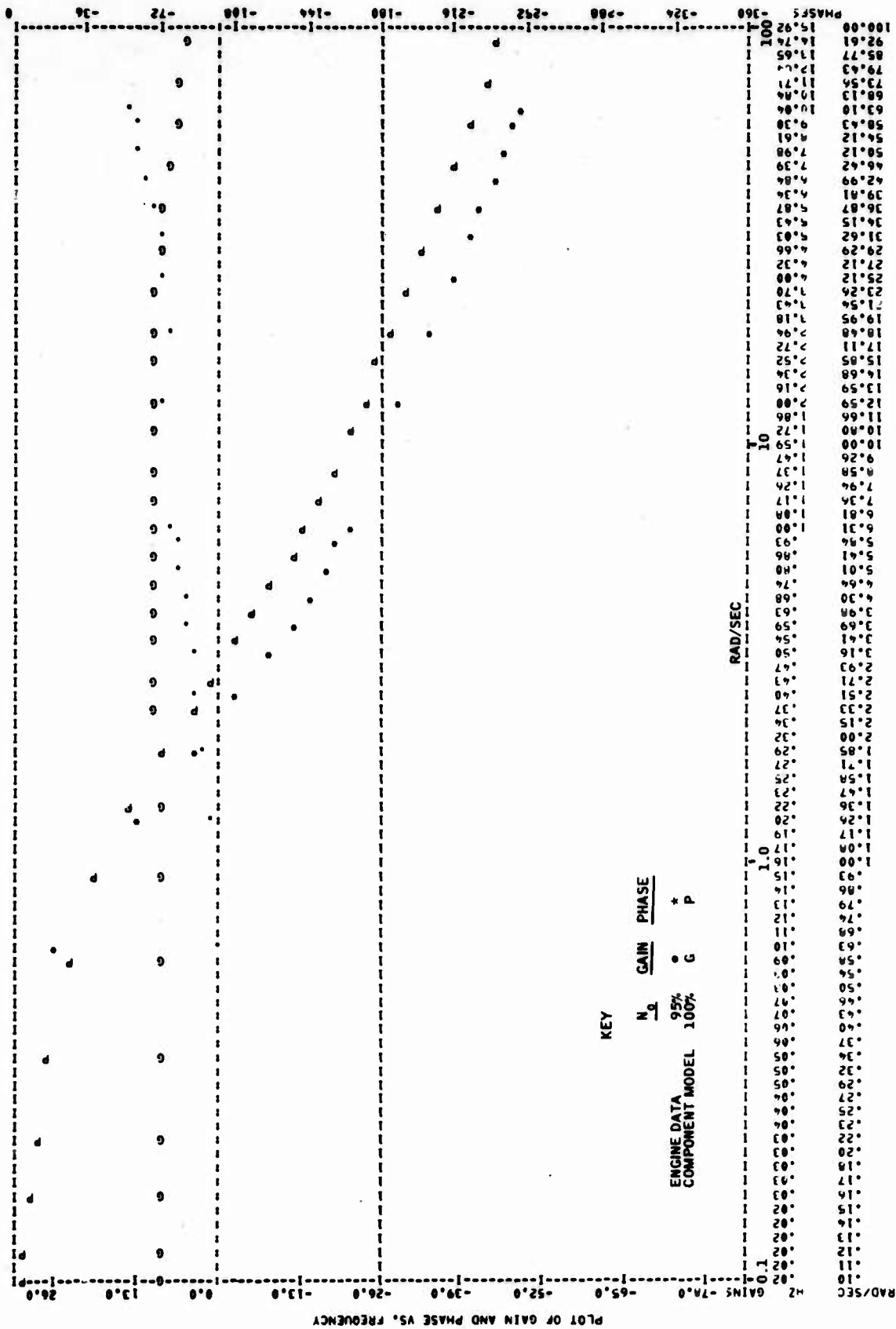
Figure 28. Compressor Discharge Pressure/Inlet Guide Vane, P_3/IGV
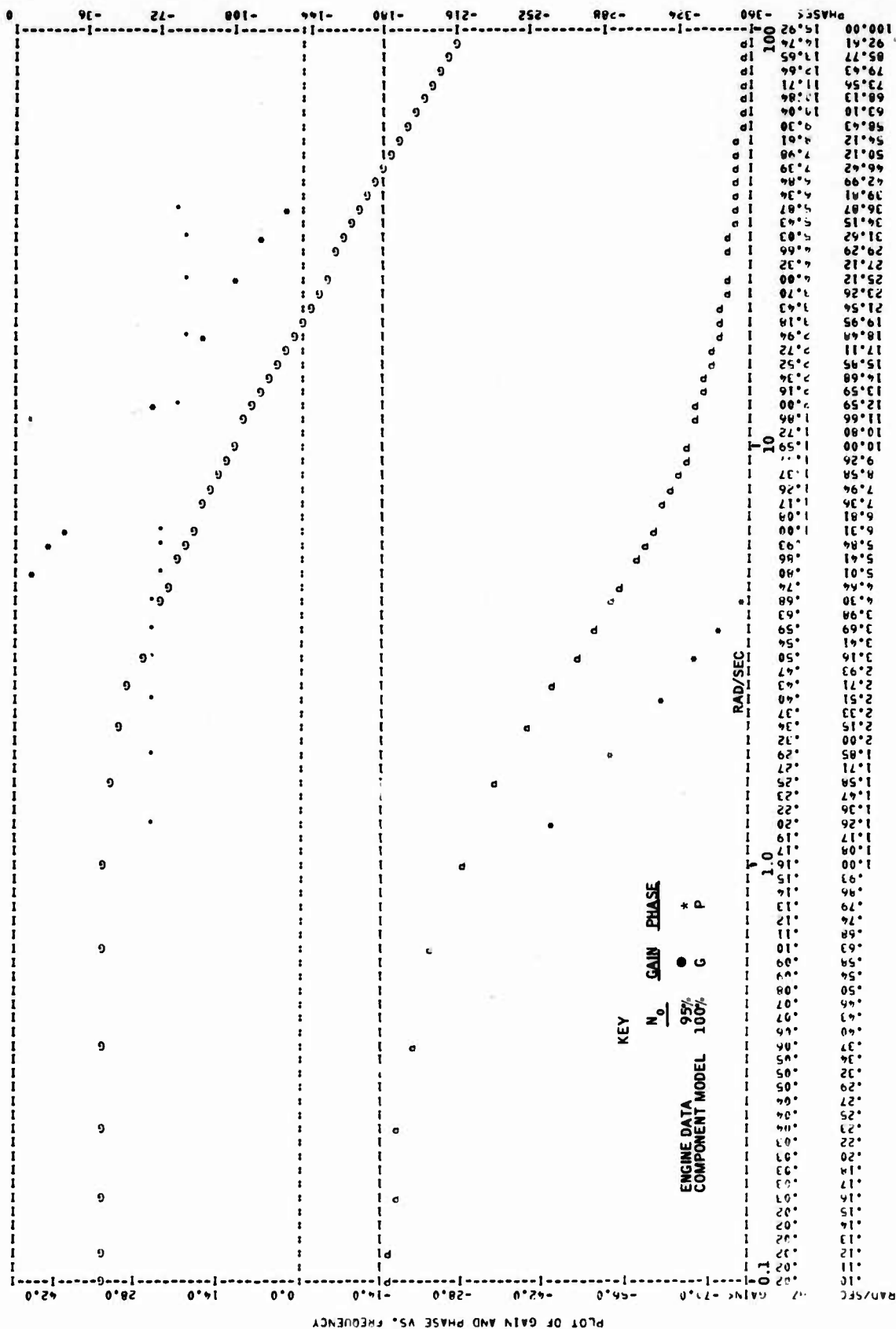
Figure 29. Turbine Discharge Temperature/Inlet Guide Vane, T_5/IGV

STATES (x_i)

$\underline{\text{N} \atop \text{TM}}$ } ENGINE DYNAMICS

$\left.\begin{matrix} \text{W}_f \\ \text{A}_8 \\ \text{IGV} \\ \text{BLD} \end{matrix}\right\}$ ACTUATOR DYNAMICS

$\left.\begin{matrix} \text{P}_3 \\ \text{P}_5 \\ \text{T}_5 \end{matrix}\right\}$ SENSOR DYNAMICS

CONTROLS (u_i)

$\underline{\begin{matrix} u_f \\ u_{A_8} \\ u_{IGV} \\ u_{BLD} \end{matrix}}$

RESPONSES (r_i)

$\underline{\begin{matrix} \text{N} \\ \text{P}_3 \\ \text{P}_5 \\ \text{T}_5 \end{matrix}}$

Figure 30. Linearized Component Model

Table 1. Steady-State Data--Engine Test

Response	Units	Operating Point, N/N_{max}		
		70 Percent	85 Percent	95 Percent
W_f	lb/hr	630.0	910.0	1504.0
A_8	in^2	162.0	158.0	115.0
IGV	Nondimensional	0.943	0.600	0.049
BLD	Nondimensional	0.983	0.638	0.115
N	rpm	11,319.0	13,976.0	15,279.0
P_3	psi	34.4	53.2	74.8
P_5	psi	15.8	18.0	24.1
$\Delta P/P_3$	psi/psi	0.125	0.152	0.161
T_4	°R	1331.0	1377.0	1632.0
T_5	°R	990.0	957.0	1141.0
ΔP_{fn}	psi	135.6	146.8	198.2

Table 2. Steady-State Data--Component Model

Response	Units	Operating Point, N/N_{max}		
		70 Percent	85 Percent	100 Percent
W_f	lb/hr	738.0	1052.0	2927.0
A_8	in^2	132.0	162.0	91.5
IGV	Nondimensional	1.0	0.619	0
BLD	Nondimensional	1.0	0.724	0
N	rpm	11,550.0	14,025.0	16,500.0
P_3	psi	39.9	60.4	101.5
P_5	psi	17.2	20.3	36.6
T_4	°R	1426.0	1498.0	2216.0
T_5	°R	1194.0	1179.0	1796.0

Table 3. Steady-State Data--APL Analog Model

Response	Units	Operating Point, N/N_{max}		
		70 Percent	85 Percent	95 Percent
W_f	lb/hr	852.0	1319.0	1857.0
A_8	in^2	156.5	156.5	142.0
N	rpm	11,598.0	14,066.0	15,660.0
P_3	psi	39.8	59.3	79.3
P_5	psi	27.8	28.4	20.9
$\Delta P/P_3$	psi/psi	0.125	0.152	0.171
T_4	°R	1447.0	1540.0	1725.0
T_5	°R	1167.0	1129.0	1180.0

SECTION III
MULTIVARIABLE DYNAMIC ENGINE MODEL

INTRODUCTION

Complete transfer function models corresponding to the Bode frequency response data obtained from the APL J85 engine are presented and discussed in this section. Consistency and physical significance of the models are analyzed in the following paragraphs. The results demonstrate that multivariable dynamic engine models can be successfully identified from experimental frequency response measurements.

Transfer function models were identified from the Bode frequency response plots with a computer algorithm called TFNS. The algorithm is programmed to calculate the transfer function which best approximates the experimental frequency response measurements. Polynomials in the transfer function are computed iteratively so that the square of the difference between the experimental frequency response and frequency response of the transfer function approximation is minimized. That is, if the experimental frequency response is denoted by $G(j\omega)$ and the frequency response of the transfer function approximation is denoted by $G_a(j\omega)$, the computer algorithm calculates the polynomials in $G_a(j\omega)$ so that the following error is minimized:

$$E \triangleq \int_{-\infty}^{\infty} |G(j\omega) - G_a(j\omega)|^2 \, d\omega$$

A detailed discussion of the TFNS program is included in Appendix B. The transfer function models identified with the TFNS program are listed in Tables 4 through 23. Models are presented for three engine speed operating points, N/N_{max} = 70 percent, 85 percent, and 95 percent. The transfer

61

functions included in these data are listed below in the same order in which they are discussed in the subsections that follow. Actuator inputs and sensor measurements represented in these transfer functions are described : Section II.

	Ref. Table	Transfer Function
Actuator transfer functions	4	Fuel flow/fuel command, W_f/u_{W_f}
	5	Exhaust area/exhaust area command, A_8/u_{A_8}
	6	Compressor bleed/compressor bleed command, BLD/u_{BLD}
	7	Inlet guide vane/inlet guide vane command, IGV/u_{IGV}
Fuel flow transfer functions	8	Spool speed/fuel flow, N/W_f
	9	Compressor discharge pressure/fuel flow, P_3/W_f
	10	Turbine discharge pressure/fuel flow, P_5/W_f
	11	Mach number sensor/fuel flow, $\frac{\Delta P}{P_3}/W_f$
	12	Turbine discharge temperature/fuel flow, T_5/W_f
Exhaust area transfer functions	13	Spool speed/exhaust area, N/A_8
	14	Compressor discharge pressure/exhaust area, P_3/A_8
	15	Turbine discharge pressure/exhaust area, P_5/A_8
	16	Mach number sensor/exhaust area, $\frac{\Delta P}{P_3}/A_8$
	17	Turbine discharge temperature/exhaust area, T_5/A_8

62

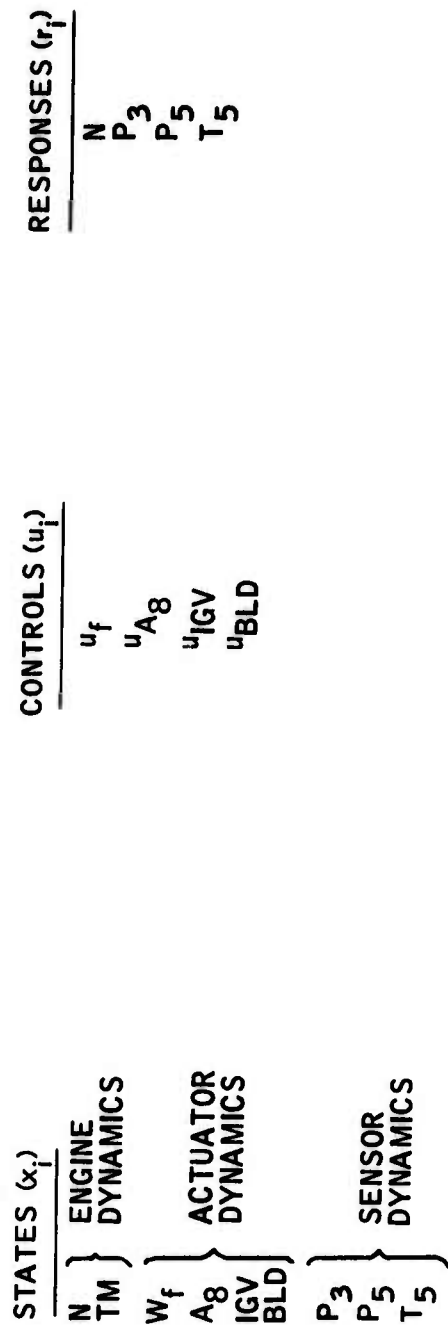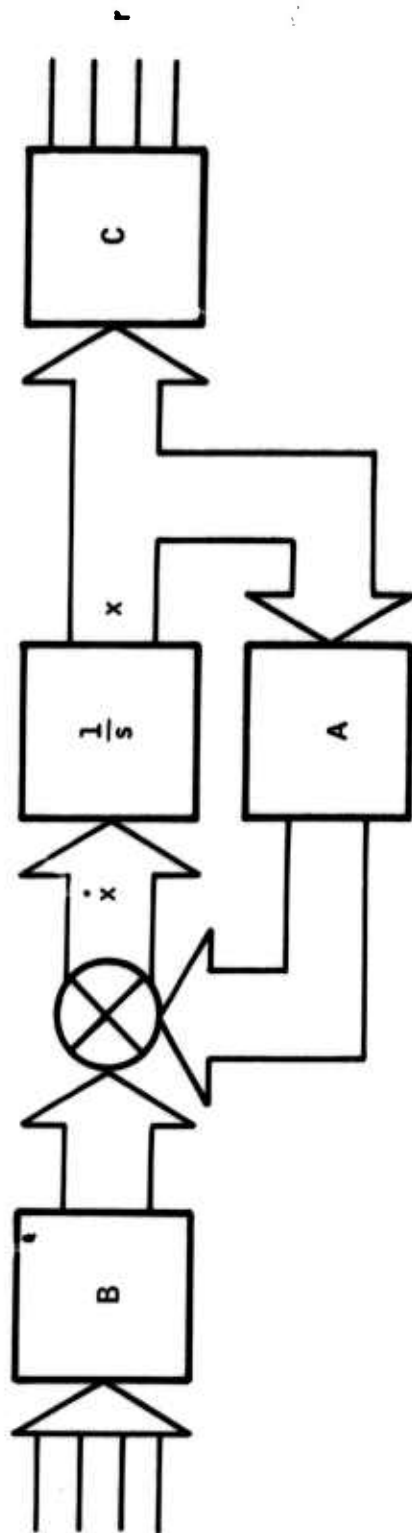|	Ref. Table	Transfer Function
Compressor bleed transfer functions	18	Spool speed/compressor bleed, N/BLD
	19	Compressor discharge/compressor bleed, P_3/BLD
	20	Turbine discharge temperature/compressor bleed, T_5/BLD
Inlet guide vane transfer functions	21	Spool speed/inlet guide vane, N/IGV
	22	Compressor discharge pressure/inlet guide vane, P_3/IGV
	23	Turbine discharge temperature/inlet guide vane, T_5/IGV

The quality of these transfer function models is summarized in the following statements:

- Engine dynamics in the 0. 05 to 100-Hz frequency range are identified in the models.

- Consistency is demonstrated between corresponding transfer functions at different operating points.

- Consistency is demonstrated between different transfer functions at the same operating point.

These statements are briefly discussed in the following paragraphs.

The transfer functions presented in Tables 4 through 23 contain a comprehensive, accurate description of the J85 engine. All significant actuator dynamics and gas dynamics in the frequency range 0. 05 to 100 Hz are accurately represented in the data. In the past it has beenpossible to experimentally measure engine dynamics only over a very limited frequency range due

63

to the difficulty in computing accurate amplitude and phase shift information from noisy sensor signals. This difficulty was circumvented with the BAFCO two-channel servoanalyzer which is unique in its ability to accurately identify frequency response data from noisy signals.

Examination of corresponding transfer functions at different operating points shows the results to be consistent with respect to the relative positions of the poles and zeros. As an example, consider the transfer function models of T_5/A_8 at the three operating points, N/N_{max} = 70 percent, 85 percent, and 95 percent. These three transfer functions are all first over second order. Poles and zeros in the transfer functions are listed below:

$$T_5/A_8 \text{ Transfer Function Models}$$

Association	N/N_{max} = 70%	85%	95%
Zeros (rad/sec)	-8.75	-13.4	-42.4
Poles (rad/sec)	-0.361	-1.01	-1.42
	-3.67	-8.14	-13.0

The data clearly show the location of the poles and zeros to shift consistently between operating points. That is, the poles and zeros for the N/N_{max} = 70 percent operating point are all located at lower frequencies than the corresponding poles and zeros for the 85 percent operating point. Similarly, the poles and zeros for the 85 percent operating point are all located at lower frequencies than the corresponding poles and zeros for the 95 percent operating point. This shows consistency with the physics of turbine engines.

Consistency between different transfer functions at the same operating point is also exhibited by the data. Dynamic states are properly identified in several transfer functions. For example, consider the three transfer functions N/W_f, N/A_8, and P_3/A_8 for the N/N_{max} = 95 percent operating point. The poles in these transfer functions are listed below:

64

Comparison of Transfer Function Models for
N/N_{max} = 95 Percent

Association	N/W_f	N/A_8	P_3/A_8
Poles (rad/sec)	-2.86	-3.38	-3.41
	-76.7	-53.9	-45.8
	-260.0	---	---

These data show a pole located at approximately -3.0 radians per second common to all three transfer functions. Another pole located at about -50 radians per second is common to both the N/A_8 and P_3/A_8 transfer functions. Possibly the pole located at -76.7 radians per second in the N/W_f transfer function also corresponds to the -50 radians per second pole identified in the other two transfer functions. Some thermodynamic states should appear in several output responses in this way.

In many cases the state variables identified in the transfer function models can easily be interpreted in terms of physical engine parameters. The most obvious of these relationships are summarized below:

- Spool inertia shows up in all the transfer functions.

- A time delay has been identified in the P_3/W_f, P_5/W_f, and $\frac{\Delta P}{P_3}/W_f$ transfer functions.

- T_5 thermocouple time constants are contained in the T_5 response.

- Tailpipe gas dynamics show up in the fuel flow respones, as well as in some of the other responses.

All of the transfer functions contain a low-frequency pole between about 0.7 and 3.5 radians per second which is associated with spool inertia. Approximate time constants are identified below for each of the three operating points modeled:

65

Spool Inertia Time Constants in Seconds

Association	N/N_{max} = 70%	85%	95%
Time constant	1.2	0.55	0.36
Range of data	1.4 to 0.5	0.85 to 0.27	0.65 to 0.20

These data were computed by averaging the results for each operating point.

The P_3/W_f, P_5/W_f and $\frac{\Delta P}{P_3}/W_f$ transfer functions contain Pade approximations corresponding to a time delay of between 11 and 15 milliseconds. Although this time delay is believed to be associated with the fuel combustion process, the specific physical interpretation of the delay is not clear at this time. This delay is considerably larger than the combustion time delay predicted by existing engine models. The time delay data are summarized below:

Combustion Time Delay in Seconds

Association	N/N_{max} = 70%	85%	95%
Delay time	0.015	0.014	0.011

Identification of these time delays from the transfer function data is discussed later in this section under the heading "Engine Transfer Functions for Fuel Flow."

The T_5 transfer functions contain a set of poles in the 0.35 to 1.90-radian per second frequency range which represents T_5 thermocouple dynamics. Approximate time constants are identified below for each of the three operating points modeled:

66

T_5 Thermocouple Time Constants in Seconds

Association	N/N_{max} = 70%	85%	95%
Time constant	2.71	1.21	0.60
Range of data	2.53 to 2.85	0.87 to 2.52	0.53 to 0.70

These data were computed by averaging the results for each operating point.

The fuel flow transfer functions also contain a consistent set of poles which represent the fundamental resonance in the engine tailpipe. The resonance is characterized by a natural frequency of between 35 and 50 radians per second with a damping coefficient around 0.2.

ACTUATOR TRANSFER FUNCTIONS

Transfer function models corresponding to the four engine actuators are presented in Tables 4 through 7. Poles and zeros for the fuel valve are identified out to about 50 Hz. The geometry actuators, exhaust area, compressor bleeds, and inlet guide vanes are lower bandwidth than the fuel valve and, consequently, the poles and zeros for these actuators are identified only out to about 10 Hz.

Comparison of corresponding actuator transfer functions at different operating points shows that the actuators respond more quickly at spool speeds near maximum than they do at lower speeds (i.e., the natural frequencies of the actuators increase with increasing spool speed). This behavior is related to the hydromechanical design of the actuators. The actuators respond faster at higher spool speeds because the hydraulic pressure power source increases with spool speed.

Transfer function models of the fuel valve at the three operating points tested are listed in Table 4. Both the 95 percent and 85 percent N/N_{max} models contain six orders of numerator and denominator dynamics; the 70 percent N/N_{max} model contains five orders of numerator and demoninator dynamics. Poles associated with the models are identified below.

$$W_f/u_f \text{ Dynamics}$$

Association	N/N_{max} = 70%		85%		95%	
	Frequency	Damping	Frequency	Damping	Frequency	Damping
Tailpipe dynamics	34.2	0.502	44.9	0.206	49.4	0.242
Actuator dynamics	148.0	0.208	137.0	0.145	134.0	0.172
	-156.0	---	239.0	0.179	248.0	0.172

These models contain representations of tailpipe resonance and actuator dynamics. Ideally, the models would only contain actuator dynamics, but because fuel flow was obtained by measuring the pressure differential across the fuel nozzle, $(\Delta P_{fuel\ nozzle} \triangleq P_{fuel\ nozzle} - P_3)$, these models contain dynamics identified with the P_3 response in addition to actuator dynamics. A detailed analysis of the effect of P_3 dynamics on the measurement of fuel flow is included in Appendix A.

Resonance in the tailpipe section is represented by a complex pole with natural frequency around 40 radians per second and a damping ratio of 0.25. The natural frequency of the pole is seen to increase with increasing spool speed because the velocity of the airflow in the tailpipe increases with spool speed. Similar representations of tailpipe dynamics are included in the P_3/W_f, P_5/W_f, and $\frac{\Delta P}{P_3}/W_f$ models discussed in the following subsection.

Except for the 70 percent model, fuel valve actuator dynamics are represented as a pair of complex poles, one with a natural frequency of 140 radians

68

per second and a damping ratio of 0.18, and the other with a natural frequency of 240 radians per second and a damping ratio of 0.175. This representation of actuator dynamics agrees with the results obtained from bench tests of the fuel valve which also showed the valve to be a fourth-order device characterized by two complex poles, one with a natural frequency of 20 Hz and a damping ratio of 0.20, and the other with a natural frequency of 30 Hz and a damping ratio of 0.80.

Exhaust actuator models are listed in Table 5. These models show the exhaust actuator to be a second-order device with a natural frequency around 33 radians per second and a damping ratio of about 0.40. The natural frequency increases with increasing spool speed from 27.2 radians per second at the 70 percent N/N_{max} operating point to 38.2 radians per second at the 95 percent N/N_{max} operating point.

Transfer function models of the compressor bleeds and inlet guide vane actuators presented in Tables 6 and 7 show both of these actuators to be essentially first-order devices. Time constants for the actuators are summarized below.

Bleed and IGV Time Constants in Seconds

Association	N/N_{max} = 70%	85%	95%
Compressor bleed time constant	0.032	0.029	0.028
Inlet guide vane time constant	---	0.066	0.050

No data are presented for the inlet guide vanes at N/N_{max} = 70 percent because the IGV actuator has little effect on engine responses at this speed. The time constants listed above show the BLD and IGV actuators to be much faster than expected; the ELD actuator was previously modeled with a time constant of 0.5 second and the IGV actuator was previously modeled with a time constant of 0.2 second.

ENGINE TRANSFER FUNCTIONS FOR FUEL FLOW

Transfer function models of spool speed N, compressor discharge pressure, P_3, turbine discharge pressure, P_5, Mach number sensor, $\Delta P/P_3$, and turbine discharge temperature, T_5, with respect to fuel flow, W_f, are presented in Tables 8 through 12. Engine dynamics in the 0.05 to 100-Hz frequency range are identified in the models, including representations of spool inertia, gas dynamics, sensor dynamics, and combustion time delay. Some of the important features of these models are summarized below and discussed in the following paragraphs:

- Spool inertia is consistently identified in the N/W_f, P_3/W_f, and $\frac{\Delta P}{P_3}/W_f$ transfer functions.

- Pade approximations to a combustion time delay are included in the P_3/W_f, P_5/W_f, and $\frac{\Delta P}{P_3}/W_f$ models.

- The T_5/W_f transfer functions contain T_5 thermocouple sensor dynamics.

- Tailpipe gas dynamics are identified in the N/W_f, P_3/W_f, P_5/W_f, and $\frac{\Delta P}{P_3}/W_f$ models.

Table 8 contains transfer function models of N/W_f for the three operating points tested, 70 percent, 85 percent, and 95 percent maximum spool speed. Two sets of poles are consistently identified in these models. The first set of poles occurs at relatively low frequency, around 2.0 radians per second, and is associated with spool inertia. The second set of poles which occurs at higher frequency, around 60 radians per second, and is associated with gas dynamics in the engine tailpipe. Locations of the poles for these three models are listed below:

N/W$_f$ Dynamics

Root Association	70%	85%	95%
Spool inertia	-0.714	-1.17	-2.86
Tailpipe dynamics	-42.8	-60.1	-76.7
	---	---	-260.0

Notice that the location of the poles varies consistent'y with spool speed. This result is predicted by engine thermodynamics.

Transfer function models of P_3/W_f are presented in Table 9. These models contain representations of spool inertia, gas dynamics, and combustion time delay. All three transfer functions contain seven poles. Associations with engine and sensor dynamics are outlined below:

P_3/W_f Dynamics

Association	70%		85%		95%	
	Frequency	Damping	Frequency	Damping	Frequency	Damping
Spool inertia	-0.800	---	-1.39	---	-2.83	---
Tailpipe dynamics	34.0	0.041	38.0	0.162	49.6	0.021
Combustion time delay	274.0	0.892	149.0	0.812	290.0	0.853
	479.0	0.328	423.0	0.133	542.0	0.039

The lowest-frequency pole at each operating point is associated with spool inertia. These roots agree with the spool inertia roots identified from the N/W_f transfer function models.

The second lowest-frequency pole at each operating point is a complex pair which is associated with gas dynamics in the engine tailpipe section. The resonant frequency increases with increasing spool speed because the air-flow velocity increases with increasing spool speed. A representation of

these dynamics (not as accurate) was also identified from the N/W_f transfer functions.

The two high-frequency complex pairs at each operating points are part of a Pade approximation of a time delay related to the combustion process. The Pade approximation is usually made up of two or more pairs of poles and zeros which have the same natural frequency and equal damping ratios with opposite algebraic signs. For example, consider the Pade approximation included in the 95 percent maximum spool speed P_3/W_f transfer function. In the frequency domain the Pade approximation is:

$$\frac{\left[\left(\frac{S}{282}\right)^2 + \frac{2(-0.754)S}{282} + 1\right]\left[\left(\frac{S}{528}\right)^2 + \frac{2(-0.056)S}{528} + 1\right]}{\left[\left(\frac{S}{290}\right)^2 + \frac{2(0.853)S}{290} + 1\right]\left[\left(\frac{S}{542}\right)^2 + \frac{2(0.039)S}{542} + 1\right]}$$

This approximation is composed of two pole-zero pairs. The zeros in each pair are roughly identical to the poles except for the algebraic sign on the damping term. This characteristic identifies the function as a Pade approximation to a time delay.

Similar Pade approximations are included in the P_3/W_f models at the other two operating points, 70 percent and 85 percent maximum spool speed. The delay times in seconds corresponding to these approximations are listed below:

Combustion Time Delays in Seconds

Association	70%	85%	95%
Delay time	0.015	0.014	0.011

Thus, the delay time decreases with increasing spool speed.

Transfer function models for P_5/W_f are presented in Table 10. Engine dynamics represented in these models are identified below:

P_5/W_f Dynamics

Association	70%		85%		95%	
	Frequency	Damping	Frequency	Damping	Frequency	Damping
Spool inertia	-1.52	---	-3.13	---	-8.82	---
Gas dynamics	43.7	0.291	44.7	0.239	45.7	0.268
	111.0	0.734	-81.7	---	123.0	0.866
	---	---	-130.0	---	---	---
Combustion time delay	314.0	0.335	-495.0	---	685.0	0.741
	---	---	574.0	0.310	---	---

The lowest-frequency pole at each operating point is believed to be associated with spool inertia, although the roots identified here are higher in frequency than the spool inertia roots identified in the N/W_f and P_3/W_f transfer functions.

The poles located in the intermediate frequency range, 50 to 130 radians per second, represent engine gas dynamics. Two resonance conditions are included in these models. The complex pair at about 45 radians per second with a damping ratio around 0.26 is identified with the fundamental resonance in the tailpipe section. The other complex pair at about 100 radians per second with a damping ratio around 0.80 represents either a secondary resonance in the tailpipe section or a resonance in a smaller volume in the engine such as the burner or compressor volume. It should be noted that the higher-frequency resonance is not accurately identified in the N/N_{max} = 85 percent model; it is represented by two real roots (natural frequencies of -81.7 and -130 radians per second) instead of by one complex pair. This inconsistency is apparently related to experimental error in the raw frequency data.

The high-frequency poles at each operating point are part of Pade approximations to combustions time delays. Although the poles and zeros associated with these Pade approximations are not identical to the poles and zeros associated with the Pade approximations identified in the P_3/W_f models, the time delays modeled are the same. Thus, at 70 percent maximum spool speed the delay is 0.015 second, at 85 percent the delay is 0.014 second, and at 95 percent the delay is 0.011 second.

Mach number sensor, $\frac{\Delta P}{P_3}/W_f$, transfer function models are listed in Table 11. The dynamic representations included in these models are similar to those included in the P_3/W_f and P_5/W_f models. Pole identifications are enumerated below:

$$\frac{\Delta P}{P_3}/W_f \text{ Dynamics}$$

Association	70%		85%		95%	
	Frequency	Damping	Frequency	Damping	Frequency	Damping
Spool inertia	- 0.716	---	- 1.49	---	- 3.50	---
Tailpipe dynamics	34.9	0.138	63.6	0.188	49.7	0.004
	- 58.4	---	- 31.2	---	- 60.4	---
Combustion time delay	171.0	0.567	180.0	0.541	240.0	0.414
	345.0	0.062	---	---	---	---

The lowest-frequency pole at each operating point is associated with spool inertia. These roots agree very well with the spool inertia roots identified from the N/W_f and P_3/W_f transfer function models.

The next two poles are associated with gas dynamics. Tailpipe dynamics are represented by the complex pair at about 50 radians per second with a damping ratio around 0.15. This representation roughly agrees with the

74

results presented for the N/W_f, P_3/W_f, and P_5/W_f transfer functions. A specific interpretation of the other pole is not clear.

The high-frequency poles are associated with the combustion time delay. These poles are part of Pade approximations equivalent to the approximations included in the P_3/W_f and P_5/W_f models. Thus, at 70 percent maximum spool speed the delay is 0.015 second, at 85 percent the delay is 0.014 second and at 95 percent the delay is 0.011 second.

Transfer function models for T_5/W_f are presented in Table 12. The dynamic states included in these models are identified below:

$$T_5/W_f \text{ Dynamics}$$

Association	70%		85%		95%	
	Frequency	Damping	Frequency	Damping	Frequency	Damping
T_5 sensor	-0.395	---	-0.749	---	---	---
Spool inertia	-2.98	---	-4.31	---	-6.19	---
Gas dynamics	-94.0	---	-214.0	---	-160.0	---
	---	---	-360.0	---	---	---

The lowest-frequency pole at each operating point in these models represents the response characteristic of the T_5 thermocouple sensor. This pole is missing from the 95 percent maximum spool speed model because frequency data were not obtained at a low enough frequency at this operating point to identify the root.

The next-lowest-frequency poles are associated with spool inertia. These poles are located at a higher frequency than the corresponding poles in the N/W_f, P_3/W_f, and $\frac{\Delta P}{P_3}/W_f$ models. This result is consistent with the spool inertia representation in the T_5/W_f model.

The high-frequency poles have not been identified specifically but are believed to be gas dynamics. It should be noted that the low-bandpass quality of the T_5 sensor reduces the signal-to-noise ratio at high frequency, increasing the identification error.

ENGINE TRANSFER FUNCTIONS FOR EXHAUST AREA

Transfer function models of spool speed, N, compressor discharge pressure, P_3, turbine discharge pressure, P_5, Mach number sensor, $\Delta P/P_3$, and turbine discharge temperature, T_5, with respect to exhaust area, A_8, are presented in Tables 13 through 17. Representations of spool inertia, gas dynamics, and T_5 sensor dynamics in the 0.5 to 10-Hz frequency range are included in the models. Important features of the models are:

- Consistency between the exhaust area transfer functions and the fuel flow transfer functions is demonstrated.

- Spool inertia is consistently identified in the N/A_8, P_3/A_8, and $\frac{\Delta P}{P_3}/A_8$ transfer functions.

- The T_5/A_8 models include the T_5 thermocouple sensor dynamics.

Transfer function models of N/A_8 are presented in Table 13. Spool speed is modeled by two lags in series, one with a break frequency around 2.0 Hz and the other with a break frequency around 10 Hz. The first of these two lags represents spool inertia. Specific location of the roots associated with this lag are listed below:

Poles Associated with Spool Inertia

Model	70%	85%	95%
N/A_8	-0.698	-2.68	-3.38
N/W_f	-0.714	-1.17	-2.86

76

Spool inertia roots identified from the N/W_f transfer functions discussed in the previous section are also shown in this table. Comparison of the spool inertia roots identified from the two models shows the results to be consistent. The models agree very well for the 70 percent and 95 percent maximum spool speed operating points. Agreement at the 85 percent operating point is not as good.

The second lag, with a break frequency at 54 radians per second, included in the 95 percent N/A_8 model represents gas dynamics in the engine tailpipe. This root is also identified in the 95 percent N/W_f model. Corresponding roots are not identified in the 70 percent and 85 percent N/A_8 models because the frequency data could not be analyzed at high frequencies.

Transfer function models of P_3/A_8 are presented in Table 14. These models contain representations of spool inertia which are consistent with the results presented in the N/A_8 models. The poles included in the P_3/A_8 transfer functions are identified below:

P_3/A_8 Dynamics

Association	70%	85%	95%
Spool inertia	-0.864	-2.59	-3.41
Tailpipe dynamics	---	-26.9	-45.8

The low-frequency poles at each operating point are identified with spool inertia. These roots agree with the corresponding roots identified in the N/A_8 models.

The higher-frequency poles included in the 85 percent and 95 percent maximum spool speed models are associated with engine gas dynamics in the tailpipe. A set of roots at about the same frequencies was also identified in the P_3/W_f models discussed in the previous section.

It should be noted that the time delays identified in the P_3/W_f models are not included in the P_3/A_8 models because the A_8 frequency test was only performed for frequencies below 10 Hz. In order to measure the time delays which are included in the W_f models, frequency response data must be measured in the 10 to 100-Hz frequency range.

P_5/A_8 transfer function models are identified in Table 15. Engine dynamics identified from these models are listed below:

$$P_5/A_8 \text{ Dynamics}$$

Association	70%	85%	95%
Spool inertia	---	-4.42	-5.28
Gas dynamics	-33.2	---	-97.2

The low-frequency poles identified at each operating point are associated with spool inertia. These poles do not agree with the spool inertia roots identified in the N/A_8 and P_3/A_8 models; the roots presented here are located at higher frequencies than the corresponding roots in the N/A_8 and P_3/A_8 models. This discrepancy was also observed in the comparison of spool inertia roots identified from the P_5/W_f, P_3/W_f, and N/W_f models.

The high-frequency poles included in the 70 percent and 95 percent P_5/A_8 models are associated with engine gas dynamics. Poles located at roughly the same frequency are also included in the P_5/W_f models.

Transfer function models of $(\Delta P/P_3)/A_8$ are listed in Table 16. These models contain representation of only one state, spool inertia. Locations of the poles in these models are listed below:

$$\frac{\Delta P}{P_3} / A_8 \text{ Dynamics}$$

Association	70%	85%	95%
Spool inertia	-1.98	-3.74	-4.90

These roots correspond more closely with spool inertia representations of the P_5/A_8 models than they do with the spool inertia representations included in the N/A_8 and P_3/A_8 models.

T_5/A_8 transfer function models are presented in Table 17. Consistent representation of spool inertia and T_5 thermocouple dynamics are contained in these models. Specific root locations are identified below:

$$T_5/A_8 \text{ Dynamics}$$

Association	70%	85%	95%
T_5 sensor	-0.361	-1.01	-1.42
Spool inertia	-3.67	-8.14	-13.0

The low-frequency roots are associated with the T_5 thermocouple sensor. Location of these poles agrees with the data from the T_5/W_f transfer function models.

The higher-frequency poles are identified as spool inertia. As was the case with the fuel flow data, the spool inertia roots are at considerably higher frequency in these models than in the N/A_8, P_3/A_8 or $\frac{\Delta P}{P_3}/A_8$ models. These roots are also larger than the spool inertia roots in the T_5/W_f models.

ENGINE TRANSFER FUNCTIONS FOR COMPRESSOR BLEED

Transfer function models of spool speed, N, compressor discharge pressure, P_3, and turbine discharge temperature T_5, with respect to compressor bleed, BLD, are presented in Tables 18, 19, and 20. Spool inertia, gas dynamics, and T_5 sensor dynamics in the frequency range 0.5 to 10 Hz are represented in the models. In general, the bleed models presented in this section are not as accurate as the fuel flow or exhaust area models presented in the previous sections due to the relative insensitivity of the measured variables to the bleed control. Important features of the bleed models are summarized below:

- Consistency with the fuel flow and exhaust area models is demonstrated.

- Consistent identification of spool inertia is included in the N/BLD and the P_3/BLD models.

- The T_5/BLD models contain T_5 sensor characteristics.

Transfer function models of N/BLD are presented in Table 18. These models contain representation of only one state, spool inertia. Location of the poles associated with this state are listed below:

Poles Associated With Spool Inertia

Model	70%	85%	95%
N/BLD	-0.936	-1.14	-1.53
N/W_f	-0.714	-1.17	-2.86
N/A_8	-0.698	-2.68	-3.38

Also listed in the table are spool inertia roots identified from the N/W_f and N/A_8 models. Comparison of the data in the table shows the N/BLD models to be consistent with the N/W_f and N/A_8 models. The models agree very

well at the 70 percent maximum spool speed operating point. At the 85 percent point the N/BLD and N/W_f model agree very well, but the root in the N/A_8 root is somewhat high. Model agreement is not as good at the 95 percent operating point; the roots differ by as much as 1.3 radians per second.

Models of P_3/BLD are presented in Table 19. Representations of both spool inertia and gas dynamics are included in these models. The poles are identified below:

$$P_3/BLD \text{ Dynamics}$$

Association	70%	85%	95%
Spool inertia	-1.06	-1.98	-1.96
Gas dynamics	-80.1	-40.1	-76.3

Neither spool inertia nor gas dynamics are represented as accurately in these data as in the data corresponding to the P_3/W_f and P_3/A_8 models. The spool inertia root associated with the 85 percent P_3/BLD model appears to be too large. This is also the case with the gas dynamics roots identified in the 70 percent and 95 percent models.

T_5/BLD transfer function models are listed in Table 20. The poles which have been identified in these models are listed below:

$$T_5/BLD \text{ Dynamics}$$

Association	70%	85%	95%
T_5 sensor	-0.351	-1.15	-1.88
	---	-159.0	-416.0

Thermocouple time constants identified in these models agree with the results presented for the T_5/W_f and T_5/A_8 transfer functions. The high-frequency root identified in the 85 percent and 95 percent models is probably incorrectly located.

ENGINE TRANSFER FUNCTIONS FOR INLET GUIDE VANE

Transfer function models of spool speed, N, compressor discharge pressure, P_3, and turbine discharge temperature T_5, with respect to inlet guide vane, IGV, are presented in Tables 21, 22, and 23. These models contain representations of spool inertia and T_5 thermocouple dynamics in the 0.5 to 10-Hz frequency range.

Models are presented for only the 85 percent and 95 percent maximum spool speed operating points. At the 70 percent operating point the effect of the IGV control on the engine is insignificant. IGV frequency response data was not measured at this operating point.

The IGV models presented here are not as accurate as the fuel flow and exhaust area models presented earlier in this section because the engine is not as sensitive to the IGV control as it is to the fuel flow and exhaust area controls. Thus, some of the poles identified in the IGV models are more subject to error due to the extremely low signal-to-noise ratio which characterizes the IGV frequency responses. Fortunately, the extraneous dynamics are easily identified by comparing the IGV models with the fuel flow, exhaust area, and compressor bleed models previously discussed.

The significant features of the IGV models are:

- Low-frequency dynamics (below 2.0 Hz) are consistently identified between the IGV models and the W_f, A_8, and BLD models.

- Spool inertia states are included in the N/IGV, P_3/IGV, and T_5/IGV models.

- The T_5/IGV models contain T_5 thermocouple dynamics.

-

82

Transfer function models of N/IGV are presented in Table 21. These models contain spool inertia dynamics which are consistent with the N/W_f, N/A_8, and N/BLD models. Spool inertia roots of all four models are listed below:

Poles Associated With Spool Inertia

Model	70%	85%	95%
N/IGV	---	-1.81	-2.70
N/W_f	-0.714	-1.17	-2.86
N/A_8	-0.698	-2.68	-3.38
N/BLD	-0.936	-1.14	-1.53

Agreement between the N/IGV models and the other three models is demonstrated.

The N/IGV model at the 95 percent maximum spool speed operating point also contains a second pole located at 19 radians per second. Comparison of this pole with the poles identified in the N/W_f, N/A_8, and N/BLD models suggests that the pole is incorrectly identified. A second pole does exist in the N/W_f and N/A_8 models for the 95 percent operating point, but it is at a higher frequency, around 60 radians per second.

Models of P_3/IGV are presented in Table 22. The only clearly identifiable dynamics in these models are the representations of spool inertia. All of the poles for these models are listed below:

P_3/IGV Dynamics

Association	85%	95%
Spool inertia	-2.01	-3.26
	-17.8	---
	-1570.0	-400.0

83

The poles associated with spool inertia agree very well with the spool inertia roots identified in the N/IGV models. This relationship is consistent with the results obtained for the fuel flow, exhaust area, and compressor bleed models.

The 85 percent maximum spool speed model also contains a second pole located at 17.8 radians per second. This pole is believed to be associated with tailpipe gas dynamics, although it is located at a lower frequency than the corresponding poles in the 85 percent P_3/W_f, P_3/A_8, and P_3/BLD models.

The high-frequency poles included in both the 85 percent and 95 percent maximum spool speed P_3/IGV models are extraneous. They are located at too high a frequency to be correctly measured on frequency responses in the 0.5 to 10-Hz frequency range.

T_5/IGV frequency response models are presented in Table 23. These models contain representations of spool inertia and T_5 thermocouple dynamics which agree with the results previously discussed for the T_5/W_f, T_5/A_8, and T_5/BLD models. In addition, the T_5/IGV models also contain a set of poles in the 3 to 9-Hz frequency range which is tentatively associated with gas dynamics. The poles included in these models are identified below:

T_5/IGV Dynamics

Association	85%	95%
T_5 thermocouple	-0.390	-1.90
Spool inertia	-4.59	-7.08
Gas dynamics	-17.9	-58.5

Table 4. Fuel Valve Transfer Functions

N/N_{max}	Fuel Nozzle Pressure/Fuel Flow Command, $\Delta P_{fn}/u_f$
70%	$$\frac{1.0\left[\left(\frac{S}{30.7}\right)^2 + \frac{2(0.107)S}{30.7} + 1\right]\left[\left(\frac{S}{208}\right)^2 + \frac{2(-0.259)S}{208} + 1\right]\left[\frac{S}{147} - 1\right]}{\left[\left(\frac{S}{34.2}\right)^2 + \frac{2(0.502)S}{34.1} + 1\right]\left[\left(\frac{S}{148}\right)^2 + \frac{2(0.208)S}{148} + 1\right]\left[\frac{S}{156} + 1\right]}$$
85%	$$\frac{1.0\left[\left(\frac{S}{42.3}\right)^2 + \frac{2(0.061)S}{42.3} + 1\right]\left[\left(\frac{S}{191}\right)^2 + \frac{2(-0.253)S}{191} + 1\right]\left[\left(\frac{S}{306}\right)^2 + \frac{2(-0.072)S}{306} + 1\right]}{\left[\left(\frac{S}{44.9}\right)^2 + \frac{2(0.206)S}{44.9} + 1\right]\left[\left(\frac{S}{137}\right)^2 + \frac{2(0.145)S}{137} + 1\right]\left[\left(\frac{S}{239}\right)^2 + \frac{2(0.179)S}{239} + 1\right]}$$
95%	$$\frac{1.0\left[\left(\frac{S}{49.8}\right)^2 + \frac{2(0.049)S}{49.8} + 1\right]\left[\left(\frac{S}{197}\right)^2 + \frac{2(-0.318)S}{197} + 1\right]\left[\left(\frac{S}{329}\right)^2 + \frac{2(-0.073)S}{329} + 1\right]}{\left[\left(\frac{S}{49.4}\right)^2 + \frac{2(0.242)S}{49.4} + 1\right]\left[\left(\frac{S}{134}\right)^2 + \frac{2(0.172)S}{134} + 1\right]\left[\left(\frac{S}{248}\right)^2 + \frac{2(0.172)S}{248} + 1\right]}$$

Table 5. Exhaust Actuator Transfer Functions

N/N_{max}	Exhaust Area/Exhaust Command, A_8/u_A
70%	$$\dfrac{1.0\left[\left(\dfrac{S}{50}\right)^2 + \dfrac{2(-0.284)S}{50} + 1\right]}{\left[\left(\dfrac{S}{27.2}\right)^2 + \dfrac{2(0.453)S}{27.2} + 1\right]}$$
85%	$$\dfrac{1.0\left[\left(\dfrac{S}{56.9}\right)^2 + \dfrac{2(-0.271)S}{56.9} + 1\right]}{\left[\left(\dfrac{S}{32.4}\right)^2 + \dfrac{2(0.402)S}{32.4} + 1\right]}$$
95%	$$\dfrac{1.0\left[\left(\dfrac{S}{59.7}\right)^2 + \dfrac{2(-0.303)S}{59.7} + 1\right]}{\left[\left(\dfrac{S}{38.2}\right)^2 + \dfrac{2(0.433)S}{38.2} + 1\right]}$$

Table 6. Bleed Actuator Transfer Functions

N/N_{max}	Bleed Position/Bleed Command, BLD/u_{BLD}
70%	$$\dfrac{1.0\left[\dfrac{S}{107} - 1\right]}{\left[\dfrac{S}{31.3} + 1\right]}$$
85%	$$\dfrac{1.0\left[\dfrac{S}{327} - 1\right]}{\left[\dfrac{S}{34.9} + 1\right]\left[\dfrac{S}{107} + 1\right]}$$
95%	$$\dfrac{1.0\left[\dfrac{S}{372} - 1\right]}{\left[\dfrac{S}{35.8} + 1\right]\left[\dfrac{S}{139} + 1\right]}$$

86

Table 7. Inlet Guide Vane Actuator Transfer Functions

N/N_{max}	IGV Position/IGV Command, IGV/u_{IGV}
85%	$\dfrac{1.0\left[\dfrac{S}{178} - 1\right]}{\left[\dfrac{S}{15.1} + 1\right]}$
95%	$\dfrac{1.0\left[\dfrac{S}{189} - 1\right]}{\left[\dfrac{S}{19.9} + 1\right]}$

Table 8. Fuel Flow Transfer Functions--
Spool Speed/Fuel Flow

N/N_{max}	Spool Speed/Fuel Flow, N/W_f
70%	$\dfrac{12.65\left[\dfrac{S}{148} - 1\right]}{\left[\dfrac{S}{0.714} + 1\right]\left[\dfrac{S}{42.8} + 1\right]}$
85%	$\dfrac{6.36\left[\dfrac{S}{82.3} - 1\right]}{\left[\dfrac{S}{1.17} + 1\right]\left[\dfrac{S}{60.1} + 1\right]}$
95%	$\dfrac{2.86\left[\dfrac{S}{192} - 1\right]}{\left[\dfrac{S}{2.86} + 1\right]\left[\dfrac{S}{76.7} + 1\right]\left[\dfrac{S}{260} + 1\right]}$

Table 9. Fuel Flow Transfer Functions--Compressor Discharge Pressure/Fuel Flow

N/N_{max}	Compressor Discharge Pressure/Fuel Flow, P_3/W_f
70%	$$\frac{0.0533\left[\frac{S}{6.37}+1\right]\left[\left(\frac{S}{34.3}\right)^2+\frac{2(0.017)S}{34.3}+1\right]\left[\left(\frac{S}{313}\right)^2+\frac{2(-0.804)S}{313}+1\right]\left[\left(\frac{S}{469}\right)^2+\frac{2(-0.310)S}{469}+1\right]}{\left[\frac{S}{0.800}+1\right]\left[\left(\frac{S}{34}\right)^2+\frac{2(0.041)S}{34}+1\right]\left[\left(\frac{S}{274}\right)^2+\frac{2(0.892)S}{274}+1\right]\left[\left(\frac{S}{479}\right)^2+\frac{2(0.328)S}{479}+1\right]}$$
85%	$$\frac{0.0514\left[\frac{S}{7.59}+1\right]\left[\left(\frac{S}{39.8}\right)^2+\frac{2(0.121)S}{39.8}+1\right]\left[\left(\frac{S}{365}\right)^2+\frac{2(-0.579)}{365}+1\right]}{\left[\frac{S}{1.39}+1\right]\left[\left(\frac{S}{38}\right)^2+\frac{2(0.162)S}{38}+1\right]\left[\left(\frac{S}{149}\right)^2+\frac{2(0.812)S}{149}+1\right]\left[\left(\frac{S}{423}\right)^2+\frac{2(0.133)S}{423}+1\right]}$$
95%	$$\frac{0.0308\left[\frac{S}{10.8}+1\right]\left[\left(\frac{S}{50.1}\right)^2+\frac{2(0.013)S}{50.1}+1\right]\left[\left(\frac{S}{282}\right)^2+\frac{2(-0.754)S}{282}+1\right]\left[\left(\frac{S}{528}\right)^2+\frac{2(-0.056)S}{528}+1\right]}{\left[\frac{S}{2.83}+1\right]\left[\left(\frac{S}{49.6}\right)^2+\frac{2(0.021)S}{49.6}+1\right]\left[\left(\frac{S}{290}\right)^2+\frac{2(0.853)S}{290}+1\right]\left[\left(\frac{S}{542}\right)^2+\frac{2(0.039)S}{542}+1\right]}$$

Table 10. Fuel Flow Transfer Functions--Turbine Discharge Pressure/Fuel Flow

N/N_{max}	Turbine Discharge Pressure/Fuel Flow, P_5/W_f
70%	$$\dfrac{0.00667\left[\dfrac{S}{6.25}+1\right]\left[\dfrac{S}{19.8}+1\right]\left[\left(\dfrac{S}{50.7}\right)^2+\dfrac{2(0.221)S}{50.7}+1\right]\left[\left(\dfrac{S}{287}\right)^2+\dfrac{2(-0.566)}{287}+1\right]\left[\dfrac{S}{674}-1\right]}{\left[\dfrac{S}{1.52}+1\right]\left[\left(\dfrac{S}{43.7}\right)^2+\dfrac{2(0.291)S}{43.7}+1\right]\left[\left(\dfrac{S}{111}\right)^2+\dfrac{2(0.734)S}{111}+1\right]\left[\left(\dfrac{S}{314}\right)^2+\dfrac{2(0.355)S}{314}+1\right]}$$
85%	$$\dfrac{0.00714\left[\dfrac{S}{14}+1\right]\left[\dfrac{S}{17.3}+1\right]\left[\left(\dfrac{S}{50.4}\right)^2+\dfrac{2(0.139)S}{50.4}+1\right]\left[\left(\dfrac{S}{254}\right)^2+\dfrac{2(0.793)S}{254}+1\right]\left[\left(\dfrac{S}{516}\right)^2+\dfrac{2(-0.227)S}{516}+1\right]}{\left[\dfrac{S}{3.13}+1\right]\left[\left(\dfrac{S}{44.7}\right)^2+\dfrac{2(0.239)S}{44.7}+1\right]\left[\dfrac{S}{81.7}+1\right]\left[\dfrac{S}{130}+1\right]\left[\dfrac{S}{495}+1\right]\left[\left(\dfrac{S}{574}\right)^2+\dfrac{2(0.310)S}{574}+1\right]}$$
95%	$$\dfrac{0.00833\left[\left(\dfrac{S}{25.2}\right)^2+\dfrac{2(0.953)S}{25.2}+1\right]\left[\left(\dfrac{S}{53}\right)^2+\dfrac{2(0.219)S}{53}+1\right]\left[\left(\dfrac{S}{258}\right)^2+\dfrac{2(-0.743)S}{258}+1\right]\left[\left(\dfrac{S}{565}\right)^2+\dfrac{2(-0.268)S}{565}+1\right]}{\left[\dfrac{S}{8.82}+1\right]\left[\left(\dfrac{S}{45.7}\right)^2+\dfrac{2(0.268)S}{45.7}+1\right]\left[\left(\dfrac{S}{123}\right)^2+\dfrac{2(0.866)S}{123}+1\right]\left[\left(\dfrac{S}{685}\right)^2+\dfrac{2(0.741)S}{685}+1\right]\left[\dfrac{S}{9707}+1\right]}$$

Table 11. Fuel Flow Transfer Functions--Mach No. Sensor/Fuel Flow

N/N_{max}	Mach Number Sensor/Fuel Flow, $\dfrac{\Delta P}{P_3}/W_f$
70%	$\dfrac{0.121E\text{-}3\left[\frac{S}{1.38}-1\right]\left[\left(\frac{S}{36.2}\right)^2+\frac{2(0.085)S}{36.2}+1\right]\left[\frac{S}{54.6}-1\right]\left[\left(\frac{S}{196}\right)^2+\frac{2(-0.578)S}{196}+1\right]\left[\left(\frac{S}{367}\right)^2+\frac{2(-0.056)S}{367}+1\right]}{\left[\frac{S}{0.716}+1\right]\left[\left(\frac{S}{34.9}\right)^2+\frac{2(0.138)S}{34.9}+1\right]\left[\frac{S}{58.4}+1\right]\left[\left(\frac{S}{171}\right)^2+\frac{2(0.567)S}{171}+1\right]\left[\left(\frac{S}{345}\right)^2+\frac{2(0.062)S}{345}+1\right]}$
85%	$\dfrac{0.408E\text{-}4\left[\left(\frac{S}{13.3}\right)^2+\frac{2(-0.786)S}{13.3}+1\right]\left[\left(\frac{S}{60.6}\right)^2+\frac{2(0.166)S}{60.6}+1\right]\left[\left(\frac{S}{223}\right)^2+\frac{2(-0.638)S}{223}+1\right]}{\left[\frac{S}{1.49}+1\right]\left[\left(\frac{S}{31.2}\right)^2+1\right]\left[\left(\frac{S}{63.6}\right)^2+\frac{2(0.188)S}{63.6}+1\right]\left[\left(\frac{S}{180}\right)^2+\frac{2(0.541)S}{180}+1\right]}$
95%	$\dfrac{0.835E\text{-}5\left[\frac{S}{4.32}-1\right]\left[\frac{S}{41.1}-1\right]\left[\left(\frac{S}{51}\right)^2+\frac{2(0.0045)S}{51}+1\right]\left[\left(\frac{S}{217}\right)^2+\frac{2(-0.450)S}{217}+1\right]}{\left[\frac{S}{3.50}+1\right]\left[\left(\frac{S}{49.7}\right)^2+\frac{2(0.0044)S}{49.7}+1\right]\left[\frac{S}{60.4}+1\right]\left[\left(\frac{S}{240}\right)^2+\frac{2(0.414)S}{240}+1\right]}$

Table 12. Fuel Flow Transfer Functions--Turbine Discharge Temperature/Fuel Flow

N/N_{max}	Turbine Discharge Temperature/Fuel Flow, T_5/W_f
70%	$$\dfrac{-0.328\left[\dfrac{S}{0.450}-1\right]\left[\dfrac{S}{122}-1\right]}{\left[\dfrac{S}{0.395}+1\right]\left[\dfrac{S}{2.98}+1\right]\left[\dfrac{S}{94.4}+1\right]}$$
85%	$$\dfrac{0.187\left[\dfrac{S}{0.074}+1\right]\left[\dfrac{S}{170}-1\right]\left[\left(\dfrac{S}{241}\right)^2+\dfrac{2(-0.279)S}{241}+1\right]}{\left[\dfrac{S}{0.749}+1\right]\left[\dfrac{S}{4.31}+1\right]\left[\dfrac{S}{214}+1\right]\left[\dfrac{S}{360}+1\right]}$$
95%	$$\dfrac{0.294\left[\left(\dfrac{S}{253}\right)^2+\dfrac{2(-0.773)S}{253}+1\right]}{\left[\dfrac{S}{6.19}+1\right]\left[\dfrac{S}{160}+1\right]}$$

Table 13. Exhaust Area Transfer Functions--Spool Speed/Exhaust Area

N/N_{max}	Spool Speed/Exhaust Area, N/A_8
70%	$$\dfrac{3.84}{\left[\dfrac{S}{0.698}+1\right]}$$
85%	$$\dfrac{2.99}{\left[\dfrac{S}{2.68}+1\right]}$$
95%	$$\dfrac{11.0}{\left[\dfrac{S}{3.381}+1\right]\left[\dfrac{S}{53.9}+1\right]}$$

Table 14. Exhaust Area Transfer Functions--Compressor Discharge Pressure/Exhaust Area

N/N_{max}	Compressor Discharge Pressure/Exhaust Area, P_3/A_8
70%	$$\dfrac{0.0601\left[\dfrac{S}{29.3}-1\right]}{\left[\dfrac{S}{0.864}+1\right]}$$
85%	$$\dfrac{0.0512\left[\dfrac{S}{13.9}+1\right]\left[\dfrac{S}{41.3}-1\right]}{\left[\dfrac{S}{2.59}+1\right]\left[\dfrac{S}{26.9}+1\right]}$$
95%	$$\dfrac{0.0445}{\left[\dfrac{S}{3.41}+1\right]\left[\dfrac{S}{45.8}+1\right]}$$

Table 15. Exhaust Area Transfer Functions--Turbine Discharge Pressure/Exhaust Area

N/N_{max}	Turbine Discharge Pressure/Exhaust Area, P_5/A_8
70%	$$\dfrac{-0.0175\left[\dfrac{S}{0.719}+1\right]\left[\dfrac{S}{24.5}+1\right]}{\left[\dfrac{S}{2.27}+1\right]\left[\dfrac{S}{33.2}+1\right]}$$
85%	$$\dfrac{-0.0363\left[\dfrac{S}{1.46}+1\right]}{\left[\dfrac{S}{4.42}+1\right]}$$
95%	$$\dfrac{-0.100\left[\dfrac{S}{0.591}+1\right]}{\left[\dfrac{S}{5.28}+1\right]\left[\dfrac{S}{97.2}+1\right]}$$

Table 16. Exhaust Area Transfer Functions--Mach No. Sensor/Exhaust Area

N/N_{max}	Mach Number Sensor/Exhaust Area, $\dfrac{\Delta P}{P_3}/A_8$
70%	$\dfrac{-0.455\text{E}{-}4\left[\dfrac{S}{4.76}-1\right]}{\left[\dfrac{S}{1.98}+1\right]}$
85%	$\dfrac{-0.471\text{E}{-}4\left[\dfrac{S}{7.19}-1\right]}{\left[\dfrac{S}{3.74}+1\right]}$
95%	$\dfrac{-0.116\text{E}{-}3\left[\dfrac{S}{30}-1\right]}{\left[\dfrac{S}{4.90}+1\right]}$

Table 17. Exhaust Area Transfer Functions--Turbine Discharge Temperature/Exhaust Area

N/N_{max}	Turbine Discharge Temperature/Exhaust Area, T_5/A_8
70%	$\dfrac{-0.954\left[\dfrac{S}{8.75}+1\right]}{\left[\dfrac{S}{0.361}+1\right]\left[\dfrac{S}{3.67}+1\right]}$
85%	$\dfrac{-1.78\left[\dfrac{S}{13.4}+1\right]}{\left[\dfrac{S}{1.01}+1\right]\left[\dfrac{S}{8.14}+1\right]}$
95%	$\dfrac{-5.10\left[\dfrac{S}{42.4}+1\right]}{\left[\dfrac{S}{1.42}+1\right]\left[\dfrac{S}{13}+1\right]}$

Table 18. Bleed Transfer Functions--Spool Speed/Bleed Position

N/N_{max}	Spool Speed/Bleed Position, N/BLD
70%	$\dfrac{-402\left[\dfrac{S}{3.34} - 1\right]}{\left[\dfrac{S}{0.936} + 1\right]}$
85%	$\dfrac{-505\left[\dfrac{S}{15.6} - 1\right]}{\left[\dfrac{S}{1.14} + 1\right]}$
95%	$\dfrac{134\left[\dfrac{S}{5.27} - 1\right]}{\left[\dfrac{S}{1.53} + 1\right]}$

Table 19. Bleed Transfer Functions--Compressor Discharge Pressure/Bleed Position

N/N_{max}	Compressor Discharge Pressure/Bleed Position, P_3/BLD
70%	$\dfrac{-4.63\left[\dfrac{S}{4.47} + 1\right]}{\left[\dfrac{S}{1.06} + 1\right]\left[\dfrac{S}{80.1} + 1\right]}$
85%	$\dfrac{-5.85\left[\dfrac{S}{5.94} + 1\right]\left[\dfrac{S}{81.6} + 1\right]}{\left[\dfrac{S}{1.98} + 1\right]\left[\dfrac{S}{40.1} + 1\right]}$
95%	$\dfrac{-4.54\left[\dfrac{S}{12} + 1\right]\left[\dfrac{S}{77.1} - 1\right]}{\left[\dfrac{S}{1.96} + 1\right]\left[\dfrac{S}{76.3} + 1\right]}$

Table 20. Bleed Transfer Functions--Turbine Discharge Temperature/Bleed Position

N/N_{max}	Turbine Discharge Temperature/Bleed Position, T_5/BLD
70%	$$\dfrac{83.4\left[\dfrac{S}{4.41}-1\right]}{\left[\dfrac{S}{0.351}+1\right]}$$
85%	$$\dfrac{60.3\left[\dfrac{S}{16.5}+1\right]\left[\dfrac{S}{26.7}-1\right]}{\left[\dfrac{S}{1.15}+1\right]\left[\dfrac{S}{159}+1\right]}$$
95%	$$\dfrac{19.1\left[\dfrac{S}{11.3}+1\right]\left[\dfrac{S}{13}-1\right]}{\left[\dfrac{S}{1.88}+1\right]\left[\dfrac{S}{416}+1\right]}$$

Table 21. Inlet Guide Vane Transfer Functions-- Spool Speed/IGV Position

N/N_{max}	Spool Speed/IGV Position, N/IGV
85%	$$\dfrac{457\left[\dfrac{S}{38.6}-1\right]}{\left[\dfrac{S}{1.81}+1\right]}$$
95%	$$\dfrac{631\left[\dfrac{S}{22.3}-1\right]\left[\dfrac{S}{27}+1\right]}{\left[\dfrac{S}{2.70}+1\right]\left[\dfrac{S}{19}+1\right]}$$

Table 22. Inlet Guide Vane Transfer Functions--Compressor Discharge Pressure/IGV Position

N/N_{max}	Compressor Discharge Pressure/IGV Position, P_3/IGV
85%	$$\dfrac{0.280\left[\dfrac{S}{0.079}-1\right]\left[\dfrac{S}{29.6}+1\right]\left[\dfrac{S}{48.1}-1\right]}{\left[\dfrac{S}{2.01}+1\right]\left[\dfrac{S}{17.8}+1\right]\left[\dfrac{S}{1570}+1\right]}$$
95%	$$\dfrac{0.886\left[\dfrac{S}{0.775}-1\right]\left[\dfrac{S}{31.4}-1\right]}{\left[\dfrac{S}{3.26}+1\right]\left[\dfrac{S}{400}+1\right]}$$

Table 23. Inlet Guide Vane Transfer Functions--Turbine Discharge Temperature/IGV Position

N/N_{max}	Turbine Discharge Temperature/IGV Position, T_5/IGV
85%	$$\dfrac{-18.3\left[\dfrac{S}{0.576}-1\right]\left[\dfrac{S}{6.61}-1\right]\left[\dfrac{S}{10.2}+1\right]}{\left[\dfrac{S}{0.390}+1\right]\left[\dfrac{S}{4.59}+1\right]\left[\dfrac{S}{17.9}+1\right]}$$
95%	$$\dfrac{-20.5\left[\dfrac{S}{1.93}-1\right]\left[\dfrac{S}{17.1}-1\right]\left[\dfrac{S}{36.9}+1\right]}{\left[\dfrac{S}{1.90}+1\right]\left[\dfrac{S}{7.08}+1\right]\left[\dfrac{S}{58.5}+1\right]}$$

APPENDIX A
DESCRIPTION OF INSTRUMENTATION

This appendix describes the equipment used to measure the frequency response of the engine. A block diagram of the experimental setup is shown in Figure A-1. The equipment includes engine sensors, interface electronics, an analog computer, an FM tape recorder, and a two-channel servoanalyzer.

The BAFCO servoanalyzer produces a sinusoidal test signal which drives the engine through one of the actuators. A system of actuator and engine sensors measures the responses of interest. Signals from the sensors are routed to their destinations through the interface electronics which serve as a link between the engine and the frequency analysis equipment. The sensor signals are also scaled in the interface electronics. All of the sensor signals are sent to the analog computer from the interface element. The DC portion of the signals is removed in the computer and the remaining AC component is amplified. The amplified AC components are relayed to the tape recorder where they are recorded along with three reference signals produced by the BAFCO servoanalyzer.

In addition to the signals which are recorded on tape, one input-output pair, spool speed/actuator command, is analyzed directly to monitor the frequency response test. These two signals are also recorded on tape to facilitate checking out the instrumentation in the tape playback mode. In the playback mode the BAFCO servoanalyzer is connected directly to the tape recorder so that the recorded signals can be analyzed one pair at a time. Instrumentation is discussed in more detail in the following paragraphs.

ENGINE ACTUATORS

All four engine actuators (fuel valve, exhaust area, compressor bleeds, and inlet guide vanes) are position control mechanisms of the type represented by the following simplified block diagram:

POSITION REQUEST → + Σ − → ACTUATOR → ACTUATOR POSITION
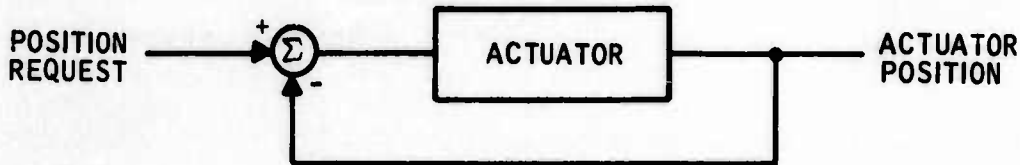
The actuators are open-loop devices with loops closed in the interface electronics (except exhaust area). Inputs to the actuators are position requests which are adjusted through the interface electronics. The DC content of the request signals is manually selected through four potentiometers (one for each actuator) located on the operator console. A summing junction is also provided so that a sinusoidal perturbation signal from the BAFCO servo-analyzer can be added directly to the DC position requests. The individual actuators are discussed in the following paragraphs.

Fuel Valve

A schematic diagram of the fuel system is shown in the upper half of Figure A-2. The system is represented by two components, a fuel valve and a fuel line which delivers fuel from the valve to the spray nozzles. Dynamic characteristics of these components are considered in the following paragraphs.

98

The fuel valve contains two stages, a metering valve and a bypass valve. Position feedback is provided around both stages. Valve characteristics established from bench tests of the actuator are identified as:

	Natural Frequency	Damping Ratio
Metering valve	30 Hz	0.80
Bypass valve	20 Hz	0.20

The fuel valve is connected to the engine with approximately 8 feet of fuel line varying in diameter from 0.5 inch to 0.75 inch. Fluid inertia and compressibility effects were analyzed to estimate the dynamic characteristics of this line. The results show that the fuel line does not contain any dynamics in the frequency range below 50 Hz.

Fuel flow dynamics are coupled to engine dynamics by the effect of P_3. In the experimental tests, fuel flow was obtained by measuring the pressure differential across the nozzle openings, since the bandwidth of the flowmeter was much less than the metering valve. Nozzle pressure differential is defined as

$$\Delta P_{fn} = P_{fn} - P_3 \tag{A-1}$$

where

ΔP_{fn} = Fuel nozzle pressure differential

P_{fn} = Pressure in the fuel line

P_3 = Compressor discharge pressure

Fuel line pressure was measured with a wall static pressure tap in the fuel line located about 6 inches downstream of the fuel valve. Compressor

discharge pressure was measured with a wall static tap located just aft of the compressor outlet guide vanes. These sensors are described in detail in the following sections. Neither sensor contains any dynamics in the frequency range below 100 Hz.

The outputs of the two sensors were algebraically combined in the APL analog computer to obtain ΔP_{fn}. Nozzle pressure differential is related to actual fuel flow by the relation

$$W_f = C_d A_N \sqrt{2\, g_c\, \rho\, \Delta P_{fn}} \tag{A-2}$$

where A_N is nozzle area, g_c is the gravitational constant (g_c / 32.2 ft/sec^2) and ρ is density of the fuel. The discharge coefficient, C_d, in this expression was determined from steady-state fuel-flow calibration data.

The dynamic characteristics of both the fuel valve and the fuel line were measured together in the frequency response tests. A block diagram of the procedure is shown in the lower half of Figure A-2.

Since P_3 was used in the fuel flow measurement, the transfer function models of the fuel system contain some engine dynamics in addition to actuator and line dynamics. The transfer function for the fuel system is

$$\frac{\Delta P_{fn}(s)}{u_f(s)} = \frac{N_1(s)[D_2(s)D_3(s) - N_2(s)N_3(s)]}{D_1(s)D_2(s)D_3(s)} \tag{A-3}$$

where

$N_1(s)$ represents the numerator dynamics of the fuel valve

$D_1(s)$ represents the denominator dynamics of the fuel valve

$N_2(s)$, $D_2(s)$ represent fuel line dynamics

$N_3(s)$, $D_3(s)$ represent engine dynamics in the P_3 response

Thus, the poles associated with the fuel system transfer function are the product of the poles associated with the three individual components: fuel valve, fuel line, and P_3 response. This explains why some engine dynamics appear in the fuel system transfer functions presented in Section III.

The fuel line dynamics are negligible below 50 Hz; therefore, the transfer functions are dominated by metering valve and engine dynamics:

$$\frac{\Delta P_{fn}(s)}{u_f(s)} = \frac{N_1(s)[D_3(s) - N_3(s)]}{D_1(s)D_3(s)} \tag{A-4}$$

if frequency (ω) $\leq$ 50 Hz.

Similarly, the transfer function models of engine responses with respect to fuel flow contain some fuel system dynamics in addition to engine dynamics. For example, the transfer function representation for P_3 is

$$\frac{P_3(s)}{\Delta P_{fn}(s)} = \frac{N_2(s)N_3(s)}{D_2(s)D_3(s) - N_2(s)N_3(s)} \tag{A-5}$$

Thus, fuel line dynamics described by $N_2(s)$ and $D_2(s)$ are included in this model. Even though the line dynamics can be neglected, the transfer function models obtained are still not the desired result: $N_3(s)/D_3(s)$. That is,

$$\frac{P_3(s)}{\Delta P_{fn}(s)} = \frac{N_3(s)}{D_3(s) - N_3(s)} \tag{A-6}$$

if $\omega \leq$ 50 Hz.

The poles associated with P_3 dynamics, $D_3(s)$, are shifted by the numerator dynamics, $N_3(s)$.

Although the individual transfer function models obtained, $\Delta P_{fn}/u_f$ and $P_3/\Delta P_{fn}$, do not have the desired form, the model for P_3/u_f obtained by multiplying $\Delta P_{fn}/u_f$ and $P_3/\Delta P_{fn}$ together is valid. That is,

$$\frac{P_3}{u_f} = \frac{P_3}{\Delta P_{fn}} \cdot \frac{\Delta P_{fn}}{u_f}$$

$$= \frac{N_2(s)N_3(s)}{D_2(s)D_3(s) - N_2(s)N_3(s)} \cdot \frac{N_1(s)[D_2(s)D_3(s) - N_2(s)N_3(s)]}{D_1(s)D_2(s)D_3(s)} \quad (A\text{-}7)$$

$$= \frac{N_1(s)N_2(s)N_3(s)}{D_1(s)D_2(s)D_3(s)}$$

It is this model, P_3/u_f, not the individual models, $P_3/\Delta P_{fn}$ and $\Delta P_{fn}/u_f$, which is used for controller synthesis. However, one should keep in mind that the engine responses to fuel flow have their high-frequency poles shifted by pressure dynamics.

Exhaust Actuator

The exhaust actuator is a mechanical clutch-brake device geared to the rotor shaft. The main body of the actuator is mounted on a pad near the front of the engine. A screw linkage connects the actuating mechanism with the nozzle apparatus at the rear of the engine.

Input to the actuator is requested nozzle area. A position feedback loop around the actuator is built into the hardware.

Nozzle area is measured by a linear potentiometer mounted on the actuator assembly which senses actuator movement. A steady-state calibration was made to convert the potentiometer readings in voltage to nozzle area units.

102

Compressor Bleed Actuator

The bleed actuator is a hydraulically powered valve which controls the amount of air vented out of the third, fourth, and fifth stages of the compressor. Pressurized fuel delivered by an auxiliary pump is used to drive the actuator.

Bleed area is measured by a linear potentiometer affixed to the actuator linkages. The potentiometer measures actuator movement. A steady-state calibration was performed to convert the potentiometer readings from voltage units to nondimensional units. In the latter system of units, 1 corresponds to fully open bleeds and 0 corresponds to closed bleeds.

Inlet Guide Vane Actuator

The IGV actuator is a hydraulic actuator which regulates the incidence angle of the compressor inlet guide vanes. Fluid pressure to drive the actuator is provided by the same pump which drives the bleed actuator.

IGV angle is measured by a linear potentiometer which measures actuator displacement. The potentiometer readings are converted to a nondimensional system of units, with 1 corresponding to the nominal low-speed IGV setting and 0 corresponding to the nominal high-speed IGV setting.

ENGINE SENSORS

Spool Speed Sensor

Spool speed was measured with an electronic sensor which measures elapsed time per revolution of the rotor shaft. The sensor is composed of two parts, a gear wheel with magnetic teeth and a 2.47-MHz oscillator. The gear wheel

is connected to the rotor shaft to turn at a fraction of the rotor speed. A magnetic pickoff attached to the engine and positioned over the gear wheel counts revolutions of the gear wheel by detecting magnetic teeth on the gear. Rotor speed is determined by counting the number of oscillator cycles per revolution of the gear wheel and performing the simple calculation:

$$N = \frac{1}{\text{oscillator cycles/revolution}} \times 2.47 \text{ MHz/sec} \times \text{gear ratio}$$

This sensor does not contain any dynamics in the frequency range tested, 0.04 to 100 Hz.

Compressor Discharge Pressure Sensor

A static pressure tap/pressure transducer sensor was used to measure compressor discharge pressure. The static tap is embedded in the wall of the engine about 2 inches behind the compressor outlet guide vanes. A piece of tubing 0.25-inch in diameter and about 4.5 inches long connects the tap to the pressure transducer. The fundamental resonance frequency of the connection line is about 650 Hz, and the response of the pressure transducer is flat to beyond 10,000 Hz.

Turbine Discharge Pressure Sensor

Turbine discharge pressure was measured with a system of five total pressure probes spread around the circumference of the engine behind the turbine outlet. Readings of the individual probes are averaged to determine the turbine discharge pressure. The five probes are connected to a 0.125-inch-diameter pressure manifold which encircles the engine and is connected to a pressure transducer. Thus, the lengths of the lines between the pressure

probes and the pressure transducer vary between 1 foot and 3 feet. The fundamental resonant frequency in the connection lines is estimated at 200 Hz. The response of the pressure transducer is flat to beyond 10,000 Hz.

Mach Number Sensor

A special sensor built by Bendix was used to measure $\dfrac{P_T - P_S}{P_T}$ at the compressor exit. The main body of the sensor is connected to static and total pressure taps located at the compressor exit by lines which are 0.25-inch in diameter and about a foot long. The resonant frequency of these lines is estimated at 400 Hz. A bench test of the sensor showed its response to be flat out to about 20 Hz.

Turbine Discharge Temperature Sensor

Turbine discharge temperature is measured by a system of 19 thermocouples spread around the circumference of the engine about 8 inches behind the turbine exit. The individual thermocouples are connected in parallel so that an average temperature reading is obtained.

Fuel Nozzle Pressure

A static pressure tap embedded in the wall of the line connecting the fuel valve with the fuel nozzles is used to measure fuel nozzle pressure. The tap is positioned about 6 inches downstream of the metering valve. A 4-inch length of 0.25-inch-diameter tubing connects the pressure tap with a pressure transducer. The fundamental resonance frequency of this tubing is well beyond the maximum frequency tested, 100 Hz. The frequency response of the transducer is flat to beyond 10,000 Hz.

INTERFACE ELECTRONICS

The interface electronics package serves as a link between the test instruments and the engine. The package consists mainly of amplifier circuits which perform two functions: (1) actuator commands from the test equipment are scaled to be compatible with the actuator hardware; and (2) sensor outputs from the engine are scaled to fall in the voltage range 0 to 5.0 volts. This equipment does not affect the measurement of engine dynamics in the frequency range tested, 0.04 to 100 Hz.

BAFCO SERVOANALYZER

A BAFCO servoanalyzer was used to measure the frequency responses of the engine. This instrument is capable of obtaining Bode frequency response plots (amplitude ratio and phase shift versus frequency) either directly from the engine or from tape-recorded data. Operation of the analyzer is described in the following paragraphs.

The normal or on-line operation of the servoanalyzer is shown in the upper half of Figure A-3. In this mode of operation the servoanalyzer measures the frequency response between a pair of engine sensor outputs, labelled $E_1(t)$ and $E_2(t)$. The servoanalyzer produces a sinusoidal test signal with time-dependent frequency (the frequency of the test signal is swept either linearly or logarithmically with time) which drives the engine through one of the actuators. Responses from the two sensors are fed into the servoanalyzer, where amplitude ratio, $\left| \dfrac{E_2}{E_1} \right|$, and phase shift, $\phi_2 - \phi_1$, of x - y plotters which record the data as a function of frequency.

In addition to on-line operation, the servoanalyzer can also be used to obtain Bode frequency data from tape-recorded signals. This operating mode is

called the tape mode and is shown in the lower half of Figure A-3. Operation in this mode is identical to on-line operation with the following exceptions:

- In the tape mode the signals to be analyzed, $E_1(t)$ and $E_2(t)$, are obtained from playback of the data tape instead of directly from the engine sensors.

- To maintain the precise relationship to the drive signal, three additional reference signals are needed to synchronize the BAFCO servoanalyzer computations. These three signals are recorded on the data tape at the same time as the sensor signals, $E_1(t)$ and $E_2(t)$, are recorded.

Both the on-line and tape modes were used to measure the engine frequency responses. During the actual engine tests, all sensor signals were recorded on magnetic tape, and, in addition, the signals from one sensor pair were analyzed on-line to monitor the results. Frequency responses from the other signals were obtained later by playing back the data tape with the analyzer operating in the tape mode.

The computations performed in the servoanalyzer are shown in the block diagram of Figure A-4. First, the fundamental components of the incoming sensor signals, $E_2(t)$ and $E_1(t)$, are identified by Fourier filters. These filters remove noise and harmonics from the sensor signals by dividing each signal into an in-phase component, I, and a quadrature (out-of-phase) component, Q. Then, a coordinate transformation is performed on the components to put them in a form better suited for computing the amplitude ratio and phase shift. Finally, the Bode plot parameters are computed in the amplitude ratio, $\left| \dfrac{E_2}{E_1} \right|$, and phase shift, $\phi_2 - \phi_1$, computer. A detailed description of these computations is included in the following paragraphs.

107

Ideally, the incoming sensor signals, $E_2(t)$ and $E_1(t)$, would both be sine waves at the test signal frequency, but phase shifted and of different amplitude. In this case, the Fourier filters shown in Figure A-4 would not be necessary, as the amplitude ratio and phase shift could be readily identified from the raw signals. However, in practice the sensor signals are rich in harmonic content and contain excessive noise which must be removed before the amplitude ratio and phase shift data can be identified. Therefore, the sensor signals are processed by Fourier filters which automatically reject harmonic components and noise from the signals.

A block diagram of a Fourier filter is shown in Figure A-5. The sensor signal is analyzed in the filter by multiplying it by a sine and cosine reference and integrating each product over a whole number of cycles. That is, the following integrals are computed:

$$\frac{1}{NT} \int_0^{NT} E(t) \sin \omega_1 r \, dt$$

$$\frac{1}{NT} \int_0^{NT} E(t) \cos \omega_1 t \, dt$$

where

    N = Number of cycles over which integration is performed (a whole number)

    T = Time per cycle = $2\pi/\omega_1$

    ω_1 = Test frequency in radians per second

It should be noted that the test signal is assumed to be maintained at a constant frequency in this development, whereas the frequency is actually time-dependent in practice.

The incoming sensor signal, $E(t)$, can be expanded in a Fourier series in the test frequency, ω_1, :

$$E(t) = A_0 + A_1 \sin \omega_1 t + \ldots A_n \sin n\omega_1 t$$

$$+ B_1 \cos \omega_1 t + \ldots B_n \cos n\omega_1 t \qquad \text{(A-8)}$$

$$+ \text{(noise)}$$

If we ignore the noise term in this expression and substitute the resulting $E(t)$ into the above integrals, we obtain:

$$\frac{1}{NT} \int_0^{NT} E(t) \sin \omega_1 t \, dt = A_1$$

$$\text{(A-9)}$$

$$\frac{1}{NT} \int_0^{NT} E(t) \cos \omega_1 t \, dt = B_1$$

since

$$\frac{1}{NT} \int_0^{NT} \sin \omega_1 t \cdot \sin n\omega_1 t \, dt = 1 \text{ for } n = 1$$
$$= 0 \text{ for } n \neq 1$$

$$\frac{1}{NT} \int_0^{NT} \cos \omega_1 t \cdot \cos n\omega_1 t \, dt = 1 \text{ for } n = 1$$
$$= 0 \text{ for } n \neq 1$$

$$\frac{1}{NT} \int_0^{NT} \sin \omega_1 t \cdot \cos n\omega_1 t \, dt = 0 \text{ for all } n$$

$$\frac{1}{NT} \int_0^{NT} \cos \omega_1 t \cdot \sin n\omega_1 t \, dt = 0 \text{ for all } n$$

Thus, the Fourier filter rejects the harmonic content of E(t) and identifies the fundamental components of the signal, A_1 and B_1. These constants are then multiplied by $\sin \omega_1 t$ and $\cos \omega_1 t$ to give the in-phase and quadrature components of E(t):

$$\text{In-phase} = A_1 \sin \omega_1 t$$
$$\text{Quadrature} = B_1 \cos \omega_1 t$$

An analysis of the noise rejection capability of the Fourier filter (presented in Reference 6) indicates that the filter also effectively removes noise from the sensor signal, E(t). The results presented in the reference show that noise at frequencies other than the test frequency, ω_1, is filter out, and the noise contribution which does get through the filter (noise at frequencies near ω_1) can be identified from visual inspection of the results.

To get the in-phase and quadrature components in a form better suited for the computation of amplitude ratio and phase shift, they are converted to

$$A_1 \sin \omega_1 t + B_1 \cos \omega_1 t = E \sin (\omega_1 T + \phi) \tag{A-10}$$

by the transformation

$$E = (A_1^2 + B_1^2)^{1/2}$$

$$\phi = \tan^{-1} \frac{B_1}{A_1}$$

Then, in the final step, the amplitude ratio, $\left|\dfrac{E_2}{E_1}\right|$, and phase shift, $\phi_2 - \phi_1$, between the Channel 2 signal, $E_2 \sin(\omega_1 t + \phi_2)$, and the Channel 1 signal, $E_1 \sin(\omega_1 t + \phi_1)$, are computed.

TAPE RECORDER - ANALOG COMPUTER

An Ampex tape recorder and the APL analog computer were used to record sensor signals during the engine frequency response tests. A block diagram of the sensor signal recording process is shown in Figure A-6. The analog computer was used to remove the DC bias on the sensor signals and to amplify the AC components before the signals were recorded on magnetic tape.

Thirteen signals were recorded on the data tape. They are identified below:

Channel	Description
1	DC level
2	Triangle wave } BAFCO servoanalyzer reference signals
3	Square wave
4	Actuator input (u_f, u_{A_8}, u_{BLD}, u_{IGV})
5	Actuator position (W_f, A_8, BLD, IGV)
6	Rotor speed (N)
7	Compressor discharge pressure (P_3)
8	Mach number sensor ($\Delta P/P_3$)
9	Turbine discharge pressure (P_5)
10	Burner temperature (T_4)
11	Blank

Channel	Description
12	Turbine discharge temperature (T_5)
13	Fuel nozzle pressure differential ($P_{fn} - P_3$)
14	Compressor pressure at bleed opening (P_{BLD})

Reference signals for tape playback were recorded on the first three channels. Sensor signals were recorded on the other 11 channels, except for Channel 11 which was left blank.

All of the record and reproduce amplifiers except for Channels 1, 2, and 3 were carefully calibrated for ±2.0 volts full scale before recording the data. The gain factors on Channels 1, 2, and 3 were adjusted according to the requirements of the BAFCO servoanalyzer.

In addition, the frequency response characteristics of the analog computer amplifiers and the tape recorder amplifiers were also measured before the engine tests were begun. It was determined that these components would not affect the engine frequency response data.
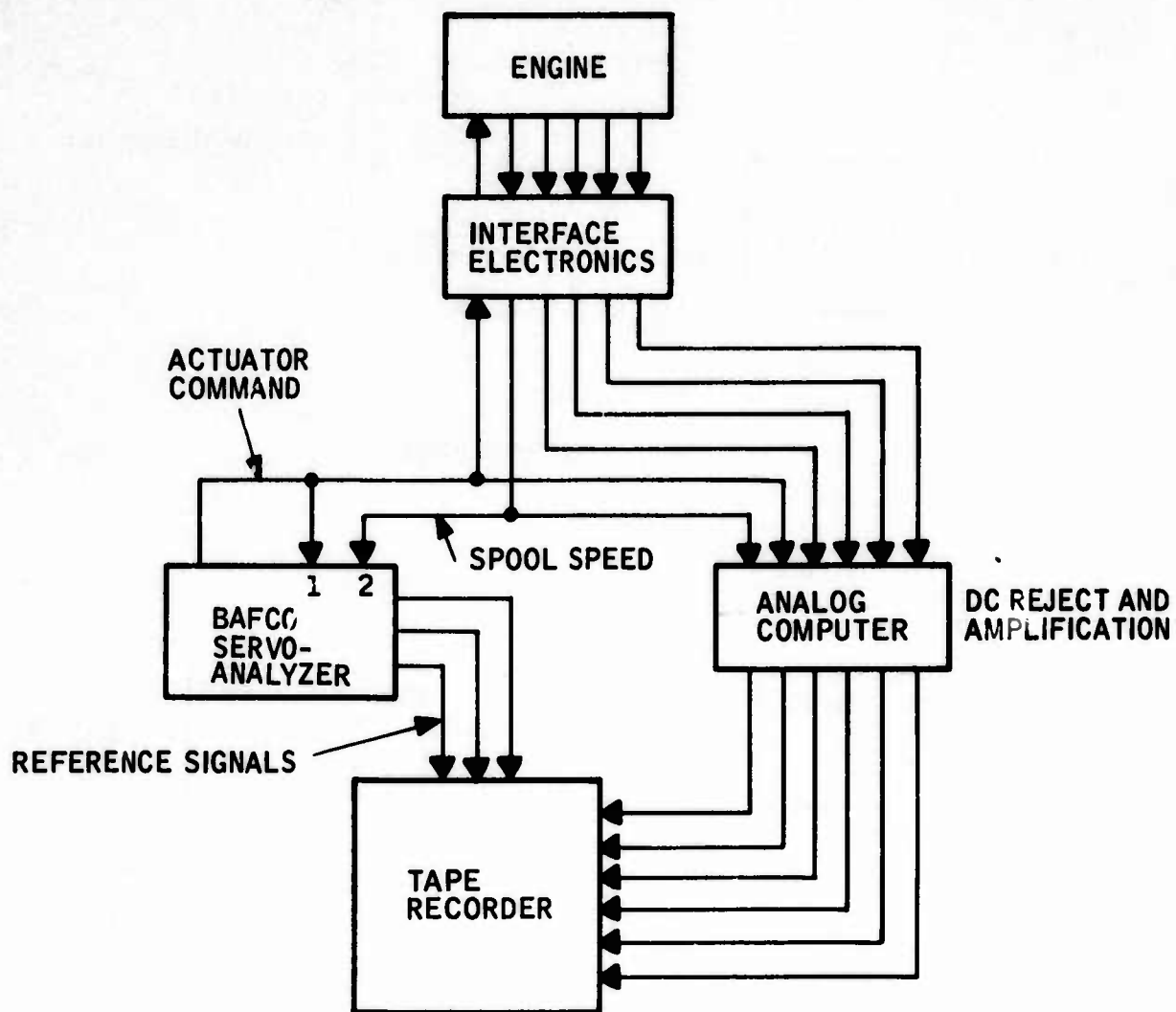
Figure A-1. Engine Test Configuration
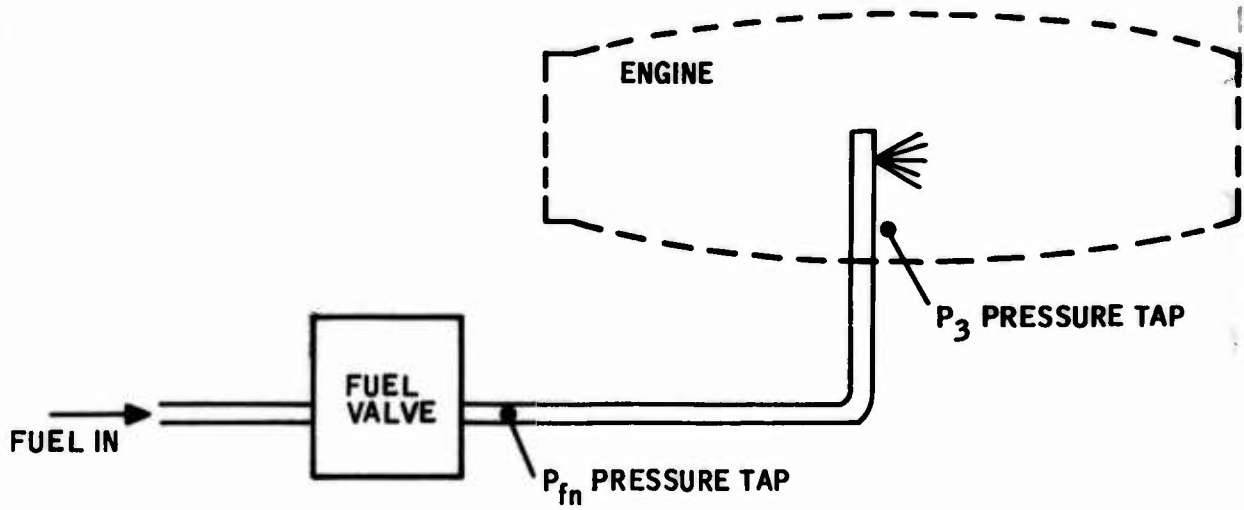
A. FUEL SYSTEM HARDWARE
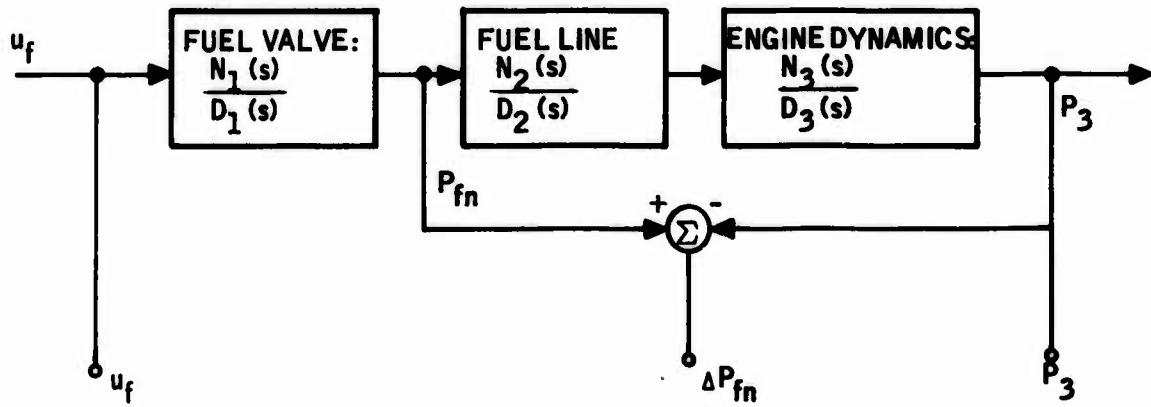
B. FUEL SYSTEM TRANSFER FUNCTION

Figure A-2. Fuel System Instrumentation

114
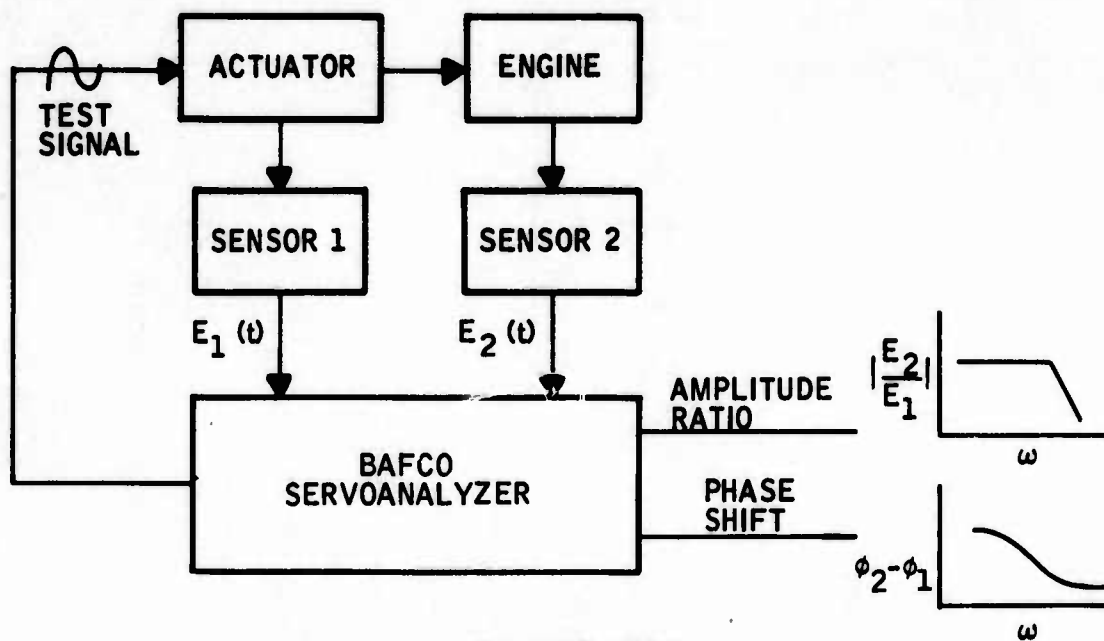
A. ON-LINE MODE
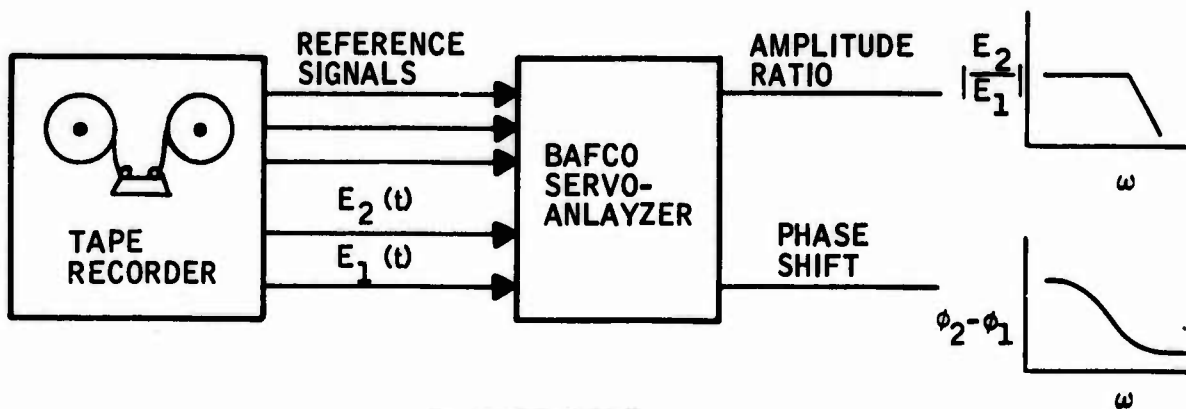
B. TAPE MODE

Figure A-3. Data Analysis

115
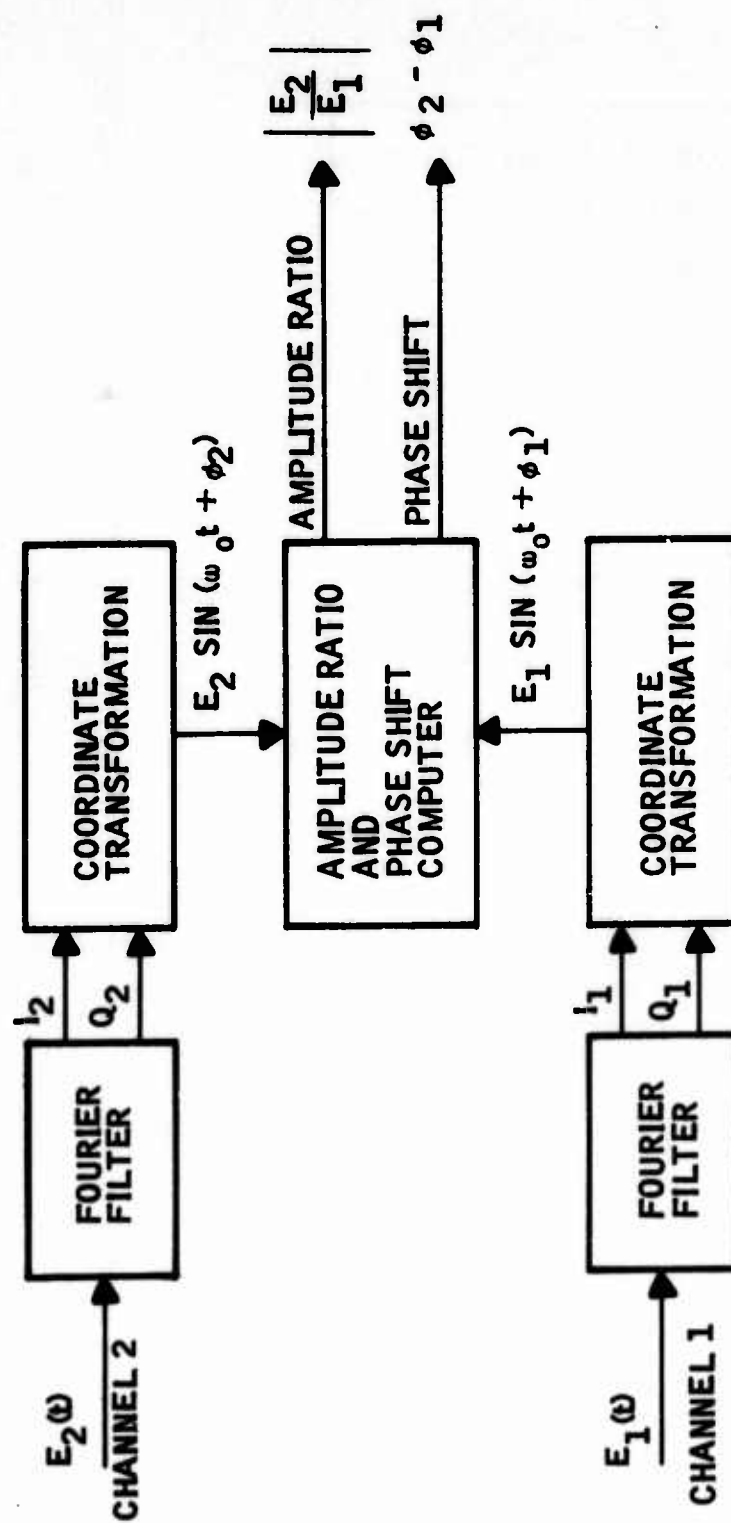
Figure A-4. BAFCO Servoanalyzer Block Diagram

116
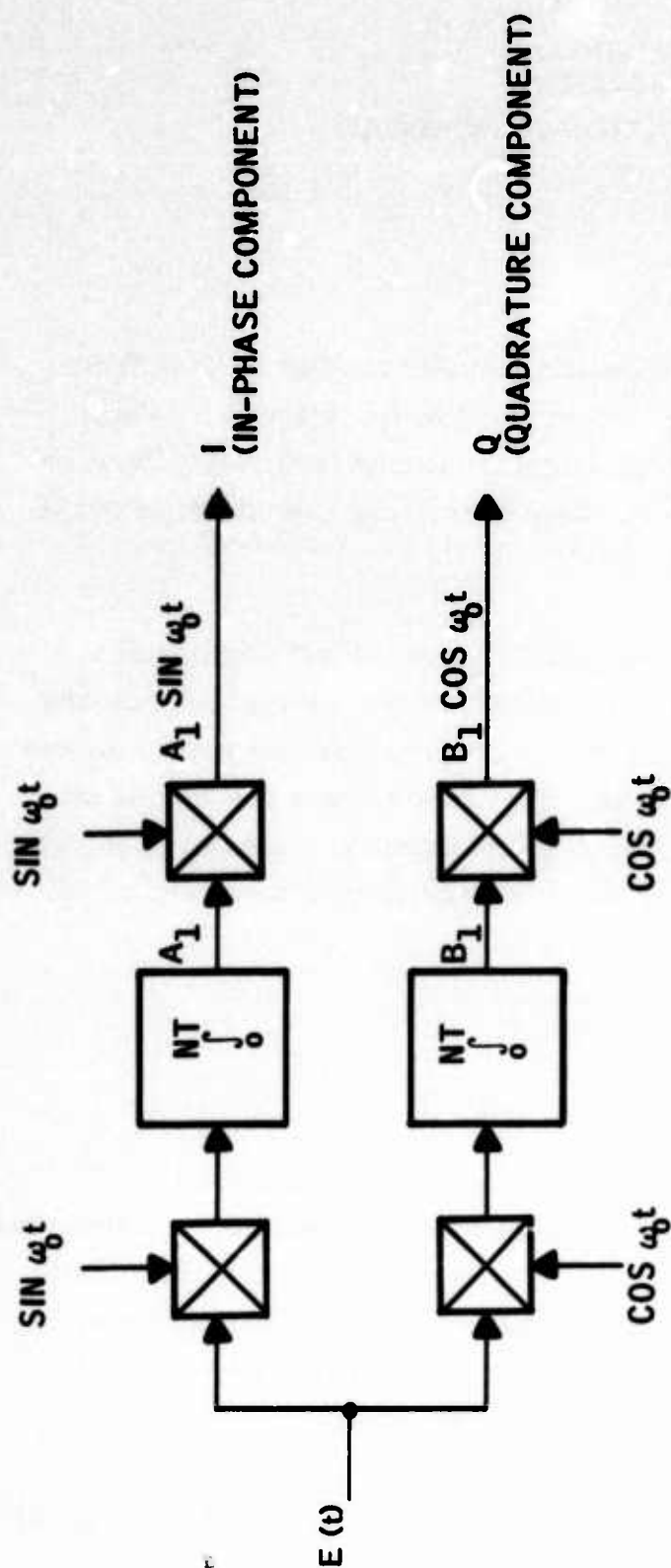
Figure A-5. Fourier Filter Block Diagram
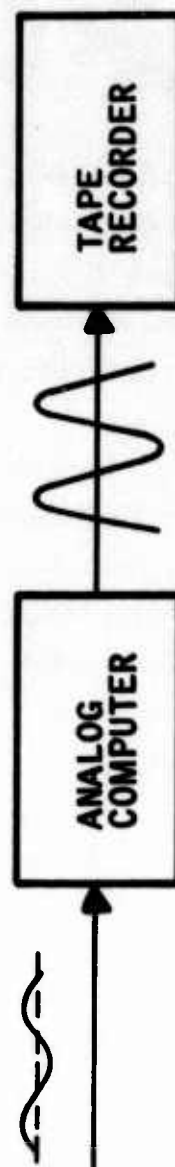
Figure A-6. Sensor Signal Recording Process

117

APPENDIX B
MODEL IDENTIFICATION PROCEDURE

INTRODUCTION

The computer program TFNS used to identify transfer function models from experimental frequency response data is discussed in this appendix. The principal topics discussed include a theoretical treatment of the identification procedure, a description of the algorithm flow chart, and a description of the input data cards used to run the program.

The algorithm presented is based on the identification method proposed by Yutaka Suzuki in Reference 7. Suzuki's method provides a systematic means of finding the transfer function model of lowest order which best approximates the experimental frequency response data. This method does not depend on knowledge of the order of the system; the transfer function of lowest possible order is automatically identified. Details of the method are discussed in the following section.

THEORY

Before beginning the actual theoretical discussion, the notation used in this section is introduced. The symbol $G(j\omega_i)$ is used to represent the experimental frequency response data. This information can be expressed in either of two ways: as real and imaginary components of the frequency response locus, or, alternatively, as amplitude ratio and phase shift data. The equivalence of these two representations is illustrated by Equation (B-1):

$$G(j\omega_i) = R_i + jI_i = A_i \cos \theta_i + jA_i \sin \theta_i \quad (i = 0, 1, \ldots r) \qquad (B-1)$$

118

where

R = Real part of frequency response

I = Imaginary part of frequency response

A = Amplitude ratio

θ = Phase shift

For convenience, the first notation, real and imaginary parts, is used throughout the appendix. The subscripts, i, on the variables indicate that the frequency data are discrete; i.e., the frequency data are composed of ordered pairs (R_i, I_i) measured at $(R + 1)$ different frequencies ω_i (i = 0, 1, ... r).

The transfer function model to be identified from the experimental data, $G(j\omega_i)$, is represented by the following rational function:

$$G_a(s) = \frac{N_a(s)}{D_a(s)} = \frac{b_0 + b_1 s + b_2 s^2 + \dots b_m s^m}{1 + a_1 s + a_2 s^2 + \dots a_n s^n} \tag{B-2}$$

where

m = Order of numerator polynomial, N_a

n = Order of denominator polynomial, D_a

The subscript, a, in this notation stands for "approximation." In general, the orders of the numerator, N_a, and the denominator, D_a, will not be equal, but all physical systems are characterized by the inequality, $n \geq m$.

The complex variable, s, has been used in Equation (B-2) to avoid confusion. Rewritten in terms of the variable, $j\omega$, the equation is:

119

$$G_a(j\omega) = \frac{N_a(j\omega)}{D_a(j\omega)} = \frac{(b_0 - b_2\omega^2 + \ldots) + j\omega(b_1 - b_3\omega^2 + \ldots)}{(1 - a_2\omega^2 + \ldots) + j\omega(a_1 - a_3\omega^2 + \ldots)} \qquad \text{(B-3)}$$

The objective of the identification procedure is to determine a transfer function, $G_a(j\omega)$, which accurately approximates the experimental data, $G(j\omega_i)$. This objective entails solving two separate problems. First, it is necessary to determine what order [values of the constants n and m in Equation (B-2)] the transfer function model must be to obtain a good approximation, and, secondly, once the order has been established, the unknown coefficients a_1, a_2, ... a_n, b_0, b_1, ... b_m must be calculated by some technique.

The identification method suggested by Suzuki contains a systematic approach for solving both of these problems simultaneously. The procedure is composed of two iteration loops: the outer loop addresses the problem of finding the order of the model (n and m), whereas the coefficients a_1, a_2, ... a_n, b_0, b_1, ... b_m are calculated in the inner loop.

To start the procedure, the user makes an initial guess for the variables n and m, called n_0 and m_0. Then the coefficients a_1, a_2, ... a_{n_0}, b_0, b_1, ... b_{m_0} corresponding to the transfer function model of order n_0, m_0 are calculated in the inner iteration loop. Once these parameters have been found, the frequency response of the model, $G_a(j\omega)$, is compared with the experimental data, $G(j\omega_i)$. If the difference is small, the calculation is stopped. However, if the difference is large (indicating that the model is not a very good approximation to the experimental data), the procedure is not stopped. Instead, the order of the transfer function model is increased by 1 ($n_1 = n_0 + 1$, $m_1 = m_0 + 1$) and the search for the coefficients a_1, a_2, ... a_{n_0}, a_{n_1}, b_0, b_1, ... b_{m_0}, b_{m_1} is begun anew. Note that this time there are two additional coefficients, a_{n_1} and b_{m_1}, which must be found because the order of the transfer function model has been increased by 1. The procedure is repeated until a transfer function model of suitable accuracy has been obtained.

Since the order of the transfer function model is increased systematically in the outer iteration loop, the procedure results in the transfer function of lowest possible order being found. This is a highly desirable outcome, signifying that minimum complexity has been achieved.

The important calculations included in the two iteration loops are considered in the following paragraphs.

In the inner iteration loop the unknown parameters a_1, a_2, ... a_n, b_0, b_1, ... b_m in the approximation $G_a(j\omega)$ are calculated to minimize the following error:

$$E = \sum_{i=0}^{r} |G(j\omega_i) - G_a(j\omega_i)|^2 \, \Delta\omega_i \qquad \text{(B-4)}$$

This error is called the real error.

Several numerical techniques could be used to find the set of coefficients which minimize this error. However, most of the techniques require many iterations because of slow convergence in the vicinity of the extremum. To avoid this difficulty, the following method is used.

First, weighting functions, ϕ_i, are added to the error equation and the terms rearranged to give:

$$E_N = \sum_{i=0}^{r} \phi_i \, |D_a(j\omega_i) \, G(j\omega_i) - N_a(j\omega_i)|^2 \, \Delta\omega_i \qquad \text{(B-5)}$$

The set of parameters a_1, a_2, ... a_n, b_0, b_1, ... b_m which minimizes Equation (B-5) is determined by solving the system of first-order simultaneous equations derived by differentiating E with respect to each of the

121

unknown parameters and setting the result equal to zero. That is, the following system of equations is solved for a_1, a_2, ... a_n, b_0, b_1, ... b_m:

$$\frac{\partial E}{\partial a_1} = 0$$

$$\frac{\partial E}{\partial a_2} = 0$$

$$\vdots$$

$$\frac{\partial E}{\partial b_0} = 0$$

$$\frac{\partial E}{\partial b_1} = 0$$

$$\vdots$$

In matrix notation these equations can be expressed as:

$$Ap = c \qquad\qquad (B-6)$$

where

$$A = \begin{bmatrix}
\lambda_0 & 0 & -\lambda_2 & 0 & \cdots & T_1 & S_2 & -T_3 & \cdots \\
0 & \lambda_2 & 0 & -\lambda_4 & \cdots & -S_2 & T_3 & S_4 & \cdots \\
\lambda_2 & 0 & -\lambda_4 & 0 & \cdots & T_3 & S_4 & -T_5 & \cdots \\
0 & \lambda_4 & 0 & -\lambda_6 & \cdots & -S_4 & T_5 & S_6 & \cdots \\
\vdots & \vdots & \vdots & \vdots & & \vdots & \vdots & \vdots \\
T_1 & -S_2 & -T_3 & S_4 & \cdots & u_2 & 0 & u_4 & \cdots \\
S_2 & T_3 & -S_4 & -T_5 & \cdots & 0 & u_4 & 0 & \cdots \\
T_3 & -S_4 & -T_5 & S_6 & \cdots & u_4 & 0 & -u_6 & \cdots \\
\vdots & \vdots & \vdots & \vdots & & \vdots & \vdots & \vdots
\end{bmatrix}$$

$$p = \begin{bmatrix} b_0 \\ b_1 \\ b_2 \\ b_3 \\ \vdots \\ a_1 \\ a_2 \\ a_3 \\ \vdots \end{bmatrix} \quad \text{and} \quad c = \begin{bmatrix} S_0 \\ T_1 \\ S_2 \\ T_3 \\ \vdots \\ 0 \\ u_2 \\ 0 \\ \vdots \end{bmatrix}$$

$$\lambda_h = \sum_{i=0}^{r} \phi_i \omega_i^{\,h} \, \Delta\omega_i$$

$$S_h = \sum_{i=0}^{r} \phi_i \omega_i^{\,h} \, R_i \Delta\omega_i$$

$$T_h = \sum_{i=0}^{r} \phi_i \omega_i^{\,h} I_i \, \Delta\omega_i$$

$$u_h = \sum_{i=0}^{r} \phi_i \omega_i^{\,h} \, (R_i^{\,2} + I_i^{\,2}) \, \Delta\omega_i$$

$$(h = 0,\ 1,\ 2\ \dots)$$

These equations are derived in Reference 7. The unknown coefficients a_1, a_2, $\dots$ a_n, b_0, b_1, $\dots$ b_m are contained in the vector, p.

The weighting coefficients, ϕ_i, are chosen to be:

$$\phi_i = \frac{1}{|D_a(j\omega_i)|^2} \qquad (i = 1,\ 2,\ \dots\ r) \tag{B-7}$$

so that when they are substituted into the error equation E_N [Equation (B-5)], it reduces to E [defined in Equation (B-4)].

However, since $D_a(j\omega)$ is unknown until the system of equations, Ap = c, is solved, an iterative technique must be used to obtain ϕ_i which approximates $1/|D_a(j\omega_i)|^2$ as closely as possible. The following method is used:

$$\phi_i^{(k)} = \frac{1}{\left| D_a^{(k-1)}(j\omega_i) \right|^2} \tag{B-8}$$

123

Namely, at the kth iteration, $\phi_i^{(k)}$ is determined from the results of the $(k-1)^{th}$ iteration. By approximating ϕ_i in this manner, it gradually approaches $1/\left|D_a(j\omega_i)\right|^2$.

This iteration on ϕ_i forms the basis of the inner-loop iteration. Parameters $a_1^{(k-1)}, a_2^{(k-1)}, \ldots a_n^{(k-1)}, b_0^{(k-1)}, b_1^{(k-1)}, \ldots b_m^{(k-1)}$ obtained from the $(k-1)^{th}$ iteration are used to estimate the weighting coefficients, $\phi_i^{(k)}$, for the kth iteration. These coefficients are substituted into the system of equations, $Ap = c$ [Equation (B-6)], which is then solved for new estimates of the parameters $a_1^{(k)}, a_2^{(k)}, \ldots a_n^{(k)}, b_0^{(k)}, b_1^{(k)}, \ldots b_m^{(k)}$. This procedure continues until the weighting coefficients, ϕ_i, have converged to a limit.

Whether or not ϕ_i converges is a key point in this algorithm. Convergence of ϕ_i implies that a minimum of the error function, E, in Equation (B-5) has been found. If ϕ_i does not converge, the identification procedure will not work. Although a sufficiency condition for convergence of ϕ_i has not been discovered, in practice, convergence has been obtained in every case.

The normalized error criterion, E_ϕ,

$$E_\phi = \frac{1}{r+1} \sum_{i=0}^{r} \left| 1 - \frac{D_a^{(k)}(j\omega_i)}{D_a^{(k-1)}(j\omega_i)} \right| \tag{B-9}$$

referred to as the equation error, is introduced to monitor the convergence of ϕ_i. When the equation error, E_ϕ, becomes less than a prescribed error tolerance, c_ϕ, the inner-loop iteration is stopped, since this implies that ϕ_i has converged.

After convergence of ϕ_i has been obtained, the real error, E_N, defined in Equation (B-5) is computed in the outer iteration loop to ascertain the accuracy of the approximation, $G_a(j\omega)$. The value of E_N is compared with a prescribed error tolerance, c_N, to determine what action is to be taken.

124

If E_N is less than or equal to c_N, the algorithm is halted. This outcome indicates that a transfer function model of sufficient accuracy has been identified.

The other alternative, E_N greater than c_N, indicates that further computation is necessary. This outcome implies that the assumed order of the approximation is not large enough to accurately model the experimental frequency data. Therefore, in this case the orders of the numerator, $N_a(j\omega)$, and the denominator, $D_a(j\omega)$, of $G_a(j\omega)$ are increased by 1 and control is transferred back to the inner iteration loop. The procedure is repeated until a transfer function model with $E_N \leq c_N$ is identified.

PROCEDURE

A flow chart of the computer algorithm is presented in Figure B-1 and discussed in the following paragraphs.

First, the constants n and m, and the orders of $D_a(j\omega)$ and $N_a(j\omega)$ at the beginning of the computation, are read in. Although these constants can be set to 1 in any case, it is often possible to roughly estimate the order of $G_a(j\omega)$ from the experimental frequency response data. Needless computations are avoided by selecting reasonable values of n and m at the beginning. If the selected order is not high enough to approximate the experimental data, the computer algorithm will automatically increase the order. This is often the case.

Next, the equation error and real error tolerance parameters, c_ℓ and c_N, are read in. The constant c_ϕ determines how hard the computer must work to find a transfer function model of a given order. This constant controls the inner iteration loop in the program. When the weighting coefficients, ϕ_i, have converged to within the tolerance specified by c_ϕ, the inner-loop iteration is stopped and the accuracy of the transfer function model is checked. Experience indicates that a value of about 0.01 for c_ϕ will give good results.

The real error tolerance, c_N, determines how accurate the transfer function approximation, $G_a(j\omega)$, must be. This constant controls the outer iteration loop in the program. After the inner loop has converged, the integral square error, E_N, defined in Equation (B-5) is checked. If the error, E_N, is found to be less than c_N, the computation is stopped, since this implies that a good approximation has been obtained. However, if the error, E_N, is larger than c_N, a good approximation has not been obtained. In this case, the orders of $N_a(j\omega)$ and $D_a(j\omega)$ are increased by 1 and the computations are begun anew. It has been discovered that a value of about 0.01 for c_N will produce satisfactory results.

After the error tolerance constants c_ϕ and c_N have been read into the program, the experimental frequency response data, $G(j\omega_i)$, is read in. Provision has been made in the program to input this information as Bode gain and phase data, Nyquist polar data, or Nyquist rectangular data. The data is converted to rectangular coordinates for internal use in the program.

Next, the weighting coefficients ϕ_i are initialized to a value of 1 and the inner iteration loop counter k is set to 1.

Then, the coefficients in the matrix A and vector c of the equations Ap = c are calculated and the equations solved for the vector of unknowns, p.

Following this, the real error, E_N, given by the following expression:

$$E_N = \sum_{i=0}^{r} \phi_i \left| D_a(j\omega_i)\, G(j\omega_i) - N_a(j\omega_i) \right|^2 \Delta\omega_i$$

is calculated and the result stored for future comparison with the error tolerance parameter, c_N.

126

Then, the denominator polynomial, $D_a^{(k)}(j\omega_i)$, is evaluated at the ω_i ($i = 0$, 1, ... r) corresponding to the experimental frequency response data. These numbers $D_a(j\omega_i)$ will be used later on to update the estimates of ϕ_i if an additional inner loop iteration is necessary.

At this time the inner iteration loop counter k is checked to see if its value is 1. A value of 1 indicates that this is the first time through the inner iteration loop. If k equals 1, the next calculation cannot be performed, so control is transferred to the end of the inner iteration loop where the weighting coefficients ϕ_i are updated.

If k is not equal to 1, the equation error E_ϕ is computed as

$$E_\phi = \frac{1}{r+1} \sum_{i=0}^{r} \left| 1 - \frac{D_a^{(k)}(j\omega_i)}{D_a^{(k-1)}(j\omega_i)} \right|$$

and compared with the equation error tolerance parameter, c_ϕ. If E_ϕ is greater than the allowable tolerance, c_ϕ, the inner loop is not converged. In this case the weighting coefficients ϕ_i are updated according to the relation

$$\phi_i = \frac{1}{|D_a^{(k)}(j\omega_i)|^2}$$

and control is transferred back to the beginning of the inner iteration loop denoted Station 2 in the flow chart.

However, if E_ϕ is less than the tolerance, c_ϕ, the inner loop iteration on ϕ_i has converged and control is transferred to a check on the real error, E_N. E_N, which has been computed in a previous step, is compared with the real error tolerance parameter, c_N. If E_N is less than c_N, the computation is stopped, since this implies that the transfer function model obtained is a good

127

approximation of the experimental frequency response data. However, if E_N is greater than c_N, the approximation is not good enough. In this case, the orders of the numerator, $N_a(j\omega)$, and denominator, $D_a(j\omega)$, in the approximation $G_a(j\omega)$ are increased by 1 and control is transferred to the beginning of the outer iteration loop, Station 1 in the flow chart. The iteration procedure continues until an accurate transfer function approximation has been obtained.

TFNS PROGRAM

The identification algorithm discussed in the previous sections has been assembled into a Fortran program called TFNS. In addition to performing the calculations associated with the identification algorithm, the program also contains a section which computes the frequency response of the transfer function approximation. These data are crossplotted with the experimental frequency response data on a single Bode plot to permit rapid visual verification of the accuracy of the transfer function model obtained. A listing of the Transfer Function Identification Program is presented in Tables B-1 through B-12. The input data cards needed to run the program are identified below.

The input data deck consists of two groups of cards, a program control group and a frequency response group. Each group ends with a card with an asterisk (*) in Column 1. The cards in each group are identified below.

Program Control Group

These cards have a flag character in Column 1 and parameters in 10-character fields thereafter. These cards may be in any order, and there may be more than one of each type in the group. However, only data from the last card of a particular type in the group are considered in that run.

<u>Card With "C" in Column 1</u> -- This card inputs parameters pertaining to the linear least squares algorithm. If a fit is to be performed in a run, A "C" card must appear in the Program Control Group:

1) <u>Denominator Starting Order, Columns 2-10</u> -- Right-justified integer.

2) <u>Numerator Starting Order, Columns 11-20</u> -- Right-justified integer. Should be ≤ denominator starting order. The difference between numerator and denominator order is preserved as the orders are increased by the program for better fit.

3) <u>Equation Error Tolerance, Columns 21-30</u> -- Free-field floating-point. This determines how hard the computer should work for a fit at a particular order. Recommended value = 0.01, but can be tightened up to achieve lower-order fit.

4) <u>Real Error Tolerance, Columns 31-40</u> -- Free-field floating-point. When the computer has ground out a transfer function at a particular order which satisfies the equation error tolerance, it checks a discrete approximation of the integral squared error over the entire curve against the real error tolerance. If the real error tolerance is satisfied, the algorithm halts. If not, numerator and denominator orders are increased by 1.

5) <u>Frequency Scale Factor, Columns 41-50</u> -- Free-field floating-point. This is used to center the range of the logarithms of input frequencies around zero. If this scale factor is not used when input frequencies are greater than 10 radians or less than 0.01 radian, then ill-conditioning in the matrix used in the linear least squares algorithm will result. For example, if the lowest frequency is 1 radian and the highest is 100 radians, then a suitable scale factor would be 0.1.

6) **Term Rejection Criterion, Columns 51-60** -- Free-field floating-point. Sometimes the algorithm is forced to compute a higher-order numerator than is needed for a good fit. When this happens, it comp tes a polynomial coefficient which is very small. Inclusion of such a term causes ill-conditioning which affects the accuracy of the computation of the zeros. To prevent this, there is logic to zero-out high-order coefficients which are too small to affect the transfer function. If the numerator polynomial is represented as

$$a_0 + a_1 \cdot j\omega + a_2 (j\omega)^2 + \text{---} + a_m \cdot (j\omega)^m$$

and if there are r frequency data points, ω_i (i = 0, 1, ... r), then the term a_m is tested as follows. If

$$\frac{\sum\limits_{i=1}^{r} \left| a_m (j\omega_i)^m \right|}{m \sum\limits_{i=1}^{r} \sum\limits_{k=0}^{m} \left| a_k (j\omega_i)^k \right|}$$

is less than term rejection criterion, then reject a_m, and reduce numerator order by 1.

Card With "O" (the letter) in Column 1 -- This card controls the output Bode plot. It must be included if a Bode plot is desired for a run. The Bode plot always gives four decades:

1) **Number of Points/Decade, Columns 2-10** -- Right-justified integer.

2) **Number of Points Evaluated For Plot Routine, Columns 11-20** -- Right-justified integer must be ≥ number of points/decade.

3) **Plot Starting Frequency, Columns 21-30** -- Free-field floating-point.

4) **Gain Scale, Columns 31-40** -- Free-field floating-point:

   - If gain scale > 0, plot scale = ± (gain scale) db.

   - If gain scale > 0 or blank, plot scale chosen automatically from plot values.

Card With "Z" or "P" in Column 1 -- It may be desirable to neglect extraneous-looking poles or zeros when evaluating the computed transfer function for a plot. This is done with a root deletion card. The roots to be deleted are punched left-justified in A4 fields from left to right on the card. Each field begins with a Z or P, meaning zero or pole, followed immediately by a two-digit number corresponding to the number of the desired pole or zero indicated on the output of the previous run. For instance, if pole 3 and zero 2 from the previous run are to be deleted, then the card would appear as follows:

```
         P03    Z02
          ↑      ↑
Columns   1      5
```

The poles and zeros may be listed on the card in any order whatsoever, but the first blank A4 field terminates the scan of the card. Thus, up to 20 poles and zeros may be deleted in one run. Note also that if a number refers to a conjugate pair, both members of the pair are deleted, and the order of either the numerator or the denominator is reduced by 2 by such a deletion. The output of a deletion run will print "DEL" in the appropriate entry of the pole-zero listing. Also, deletions can be made on a fit run, if pole and zero numbers are known a priori.

131

End program control group with "*" card.

Frequency Response Cards

These cards have input data points on them, one per card. The cards must be in order of ascending frequency. The frequency can be in Hz or radians per second, and the units need not be consistent from one card to the next. However, they must still be in order, as if they were in consistent units. In other words, 10 radians must appear before 5 Hz.

These cards have a common format:

- **Column 1 - Data Type Flag:**

  - Blank = Bode
  - B   = Bode
  - P   = Nyquist polar
  - R   = Nyquist rectangular

- **Columns 15-29 - Frequency, Free-Field Floating-Point:**

  - If H in Column 15, frequency is in Hz.
  - If R in Column 15, frequency is in radians per second.

- **Default:** If blank or frequency entry starts in Column 15, frequency is in radians per second.

- **Columns 30-44 - Gain, Magnitude, or Real Part:** Free-field floating-point. Defaults vary according to Column 1 entry, but D in Column 30 indicates decibels, and M in column 30 indicates magnitude.

- Columns 45-59 - Phase, Angle, or Imaginary Part: Defaults vary according to Column 1 entry, but D in Column 45 indicates degrees, and R in Column 45 indicates radians.

Defaults Chart

Col. 1	Frequency Field	Part 1	Part 2
Blank	rad/sec	Gain (db)	Phase (deg)
B	rad/sec	Gain (db)	Phase (deg)
P	rad/sec	Magnitude	Angle (rad)
R	rad/sec	Real	Imaginary

As indicated, defaults on units in frequency, gain, phase, magnitude, or angle can be overridden by punching the appropriate character (H, R, D, M) in the first column of the appropriate field.

End frequency response data group with "*" card.

Figure B-1.   TFNS Flow Chart

134

③

CALCULATE REAL ERROR:

$$E_N = \sum_{i=0}^{r} \phi_i \left| D_a(jw)\, G(jw) - N_a(jw) \right|^2 \Delta\omega_i$$

CALCULATE AND STORE:

$$D_a^{(k)}(j\omega_i) \quad (i = 0, 1, \ldots r)$$

K = 1? →YES

NO

CALCULATE EQUATION ERROR:

$$E_\phi = \frac{1}{r+1} \sum_{i=0}^{r} \left| 1 - \frac{D_a^{(k)}(j\omega_i)}{D_a^{(k-1)}(j\omega_i)} \right|$$

$E_\phi \leq c_\phi$? →YES

NO

$E_N \leq c_N$? →YES→ STOP

NO

UPDATE WEIGHING COEFFICIENTS:

$$\phi_i = \frac{1}{\left| D_a^{(k)}(j\omega_i) \right|^2}$$

$$(i = 0, 1, \ldots r)$$

INCREASE ORDER
OF $G_a(j\omega)$:

$$n = n + 1$$
$$m = m + 1$$

②   ①
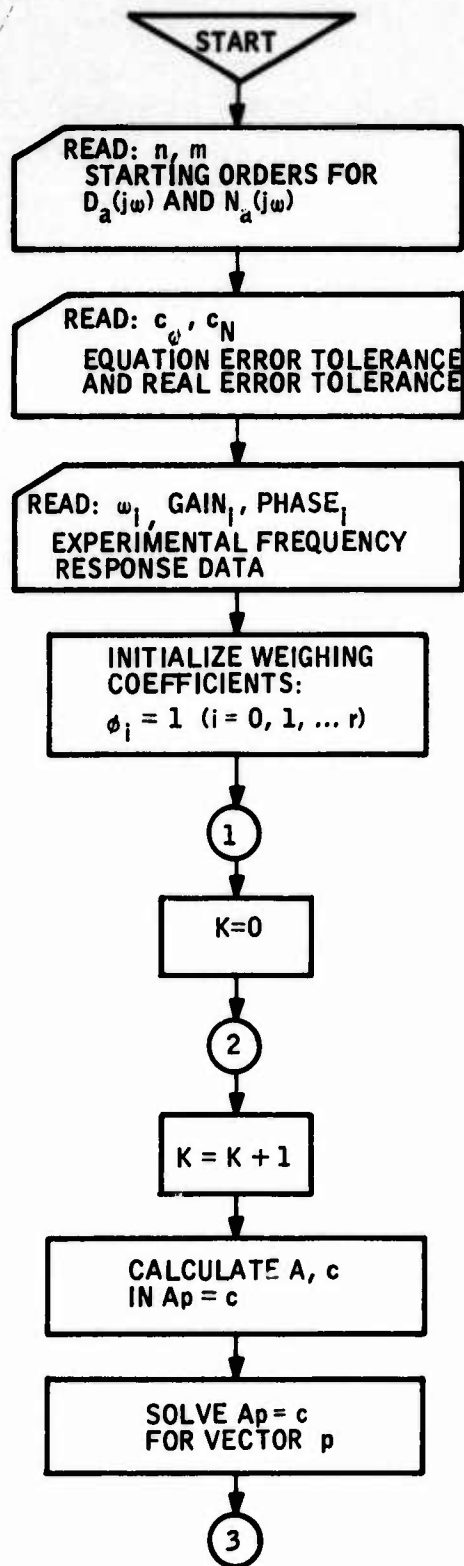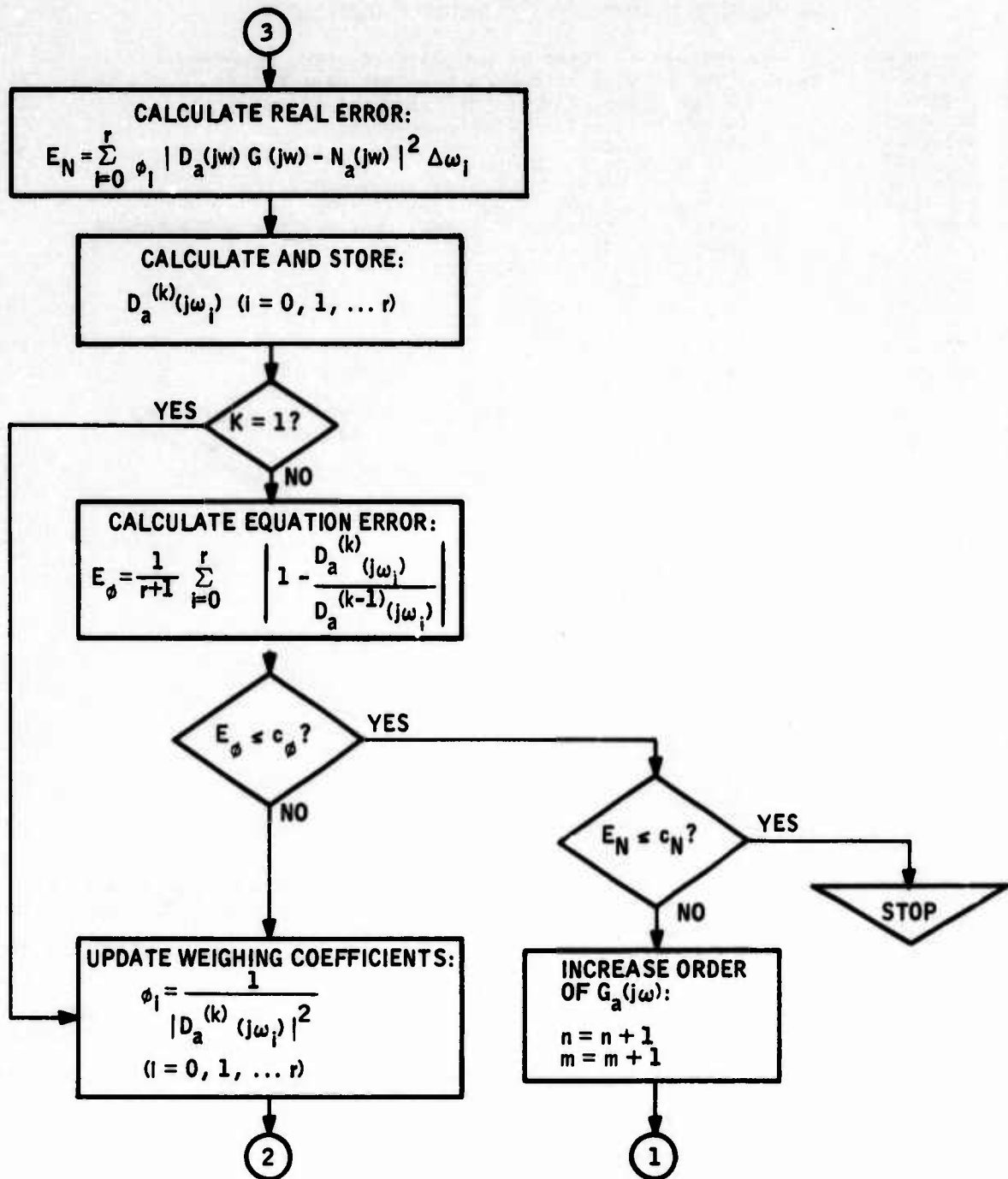
Figure B-1. TFNS Flow Chart (Concluded)

```
1    00000000   C.......PROGRAM TO IDENTIFY S-DOMAIN TRANSFER FUNCTION
2    00000001   C.......BEST FITTING FREQUENCY RESPONSE DATA POINTS
3    00000002           COMMON W(50),DELW(50),RESP(50),PHI(50),A(41,42)
4    00000003           COMMON S(43),T(43),U(43),LAMBDA(43)
5    00000004           COMMON/KLUGE/M                                         KLUGE
6    00000005           DIMENSION P(42),LORD(4)
7    00000006           DIMENSION FREQIN(100),PART1(100),PART2(100)
8    00000007           DIMENSION LIMAGE(20),JPT(20),JZT(20)
9    00000010           COMPLEX SA(50),TNUM,TDENOM,C1,FRAC,CPOLY,JW,TFN,CPOLYF
10   00000011           COMPLEX DA(50),DAOLD(50)
11   00000012           COMPLEX ZEROS(22),POLES(22)
12   00000013           COMPLEX RESP
13   00000014           REAL LAMBDA
14   00000015           INTEGER OTYPE
15   00000016           LOGICAL COMP,OUT
16   00000017           DATA NITER/100/
17   00000020           DATA NMAX/20/,MMAX/50/,NDEC/4/
18   00000021           DATA ICR/5/,LP/6/,LBODE/1HB/,LPOLAR/1HP/,LRECT/1HR/
19   00000022           DATA(LORD(I),I=1,4)/2HST,2HND,2HRD,2HTH/
20   00000023           DATA OTYPE/1HB/
21   00000024           DATA LCOMP/1HC/,LSTAR/1H*/,LBLANK/1H /,LOUT/1HO/
22   00000025           DATA LPOLE/1HP/,LZERO/1HZ/
23   00000026           CALL RESTART
24   00000027           DR=ATAN(1.0)/45.
25   00000030           RD=1./DR
26   00000031           PI=4.0*ATAN(1.0)
27   00000032   C...,...RERUN SENSE SWITCH
28   00000033   200     CALL SSWTCH(1,I1ON)
29   00000034           IF(I1ON.EQ.2)STOP
30   00000035           COMP=.FALSE.
31   00000036           OUT=.FALSE.
32   00000037           DO 91 I=1,20
33   00000040           JPT(I)=0
34   00000041           JZT(I)=0
35   00000042   91      CONTINUE
36   00000043           JPTP=0
37   00000044           JZTP=0
38   00000045   C.....READ IN PARAMETERS AND ROOTS TO BE DELETED
39   00000046   90      READ(ICR,1001)LIMAGE
40   00000047           DECODE(1,1002,LIMAGE)LFLAG
41   00000050   C.....READ IN STARTING DENOMINATOR ORDER,STARTING NUMERATOR ORDER,
42   00000051   C.....EQUATION ERROR TOLERANCE,REAL ERROR TOLERANCE,FREQUENCY SCALE
43   00000052   C.....FACTOR,TERM REJECTION CRITERION.
44   00000053           IF(LFLAG.EQ.LCOMP)DECODE(60,1000,LIMAGE)ND,NN,CS,CT,FSCALE,TOLMAG
45   00000054           COMP=COMP.OR.(LFLAG.EQ.LCOMP)
46   00000055           OUT=OUT.OR.(LFLAG.EQ.LOUT)
47   00000056   C.....READ IN NO. OF POINTS/DECADE,NUMBER OF POINTS,PLOT STARTING
48   00000057   C.....FREQUENCY,DESIRED GAIN SCALE. IF GAIN SCALE .LE.0. GAIN SCALE
49   00000060   C.....CHOSEN AUTOMATICALLY.
50   00000061           IF(LFLAG.EQ.LOUT)DECODE(40,1000,LIMAGE)NPDEC,NPOINTS,WLOW,GGAINX
51   00000062           IF(LFLAG.NE.LPOLE.AND.LFLAG.NE.LZERO)GO TO 92
52   00000063           DO 93 I=1,20
53   00000064           DECODE(3,1003,LIMAGE(I))LABEL,IPT
54   00000065           IF(LABEL.EQ.LBLANK)GO TO 92
55   00000066           IF(LABEL.NE.LPOLE)GO TO 94
56   00000067           JPTP=JPTP+1
57   00000070           JPT(JPTP)=IPT
58   00000071           GO TO 93
59   00000072   94      JZTP=JZTP+1
60   00000073           JZT(JZTP)=IPT
```

136

```
61  00000074   93      CONTINUE
62  00000075   92      IF(LFLAG.NE.LSTAR)GO TO 90
63  00000076        C.....SORT JPT AND JZT ARRAYS
64  00000077           IF(JPTP.LE.1)GO TO 80
65  00000100           JPTPM1=JPTP-1
66  00000101           DO 81 I=1,JPTPM1
67  00000102           IP1=I+1
68  00000103           DO 82 J=IP1,JPTP
69  00000104           IF(JPT(J).GE.JPT(I))GO TO 82
70  00000105           ITEMP=JPT(I)
71  00000106           JPT(I)=JPT(J)
72  00000107           JPT(J)=ITEMP
73  00000110   82      CONTINUE
74  00000111   81      CONTINUE
75  00000112   80      IF(JZTP.LE.1)GO TO 85
76  00000113           JZTPM1=JZTP-1
77  00000114           DO 83 I=1,JZTPM1
78  00000115           IP1=I+1
79  00000116           DO 84 J=IP1,JZTP
80  00000117           IF(JZT(J).GE.JZT(I))GO TO 84
81  00000120           ITEMP=JZT(I)
82  00000121           JZT(I)=JZT(J)
83  00000122           JZT(J)=ITEMP
84  00000123   84      CONTINUE
85  00000124   83      CONTINUE
86  00000125   85      CONTINUE
87  00000126           IF(.NOT.COMP)GO TO 100
88  00000127           WRITE(LP,2000)ND,NN,CS,CT,FSCALE,WLOW,NPDEC,NPOINTS,TOLMAG
89  00000130        C.....READ IN FREQUENCY RESPONSE DATA AND CONVERT FROM EXTERNAL
90  00000131        C.....TYPE TO INTERNAL TYPE(RECTANGULAR)
91  00000132           WRITE(LP,2001)
92  00000133           CALL CARDRD(ICR,LP,M,MMAX)
93  00000134           M=M-1
94  00000135        C.....SUBTRACT TIME DELAY FROM RAW DATA
95  00000136           IF(SENSE SWITCH 2) 55,56
96  00000137   55      WRITE(8,3000)
97  00000140           READ(8,3001) TDELAY
98  00000141           WRITE(LP,3002) TDELAY
99  00000142           DO 56 I=1,M
100 00000143           TEMPG = CABS(RESP(I))
101 00000144           TEMPP = ATAN2(AIMAG(RESP(I)),REAL(RESP(I)))*RD
102 00000145           TEMPP=TEMPP+W(I)*TDELAY*57.293
103 00000146           TEMPP=TEMPP*DR
104 00000147           RESP(I)=TEMPG*CMPLX(COS(TEMPP),SIN(TEMPP))
105 00000150   56      CONTINUE
106 00000151        C.....SCALE DOWN FREQUENCY
107 00000152           DO 60 I=1,M
108 00000153           W(I)=W(I)*FSCALE
109 00000154   60      CONTINUE
110 00000155        C.....INITIALIZE PHI,COMPUTE DELW,AND FIND DENOMINATOR OF REAL ERROR.
111 00000156           ERRORD=0.
112 00000157           PHI(1)=1.
113 00000160           DELW(1)=(W(1)+W(2))/2.
114 00000161           TEMP=CABS(RESP(1))
115 00000162           ERRORD=ERRORD+TEMP*TEMP*DELW(1)
116 00000163           MM1=M-1
117 00000164           DO 5 I=2,MM1
118 00000165           DELW(I)=(W(I+1)-W(I-1))/2.
119 00000166           PHI(I)=1.
120 00000167           TEMP=CABS(RESP(I))
121 00000170           ERRORD=ERRORD+TEMP*TEMP*DELW(I)
```

```
122   00000171     5        CONTINUE
123   00000172              PHI(M)=1.
124   00000173              DELW(M)=W(M)-W(M-1)
125   00000174              TEMP=CABS(RESP(M))
126   00000175              ERRORD=ERRORD+TEMP*TEMP*DELW(M)
127   00000176              IDAMAX=2*NMAX+1
128   00000177              C1=(1.,0.)
129   00000200              WRITE(LP,2013)
130   00000201     C.....BEGIN OUTER LOOP(INCREMENTING N)
131   00000202     6        K=0
132   00000203              NR=NN+ND+1
133   00000204              NC=NR+1
134   00000205              NDP1=ND+1
135   00000206              NP1=NN+1
136   00000207              NP2=NN+2
137   00000210     C.....BEGIN INNER LOOP(INCREMENTING K)
138   00000211     7        K=K+1
139   00000212              IF(K.GT.NITER)STOP 66666
140   00000213     C.....CALCULATE A-MATRIX AND C-VECTOR
141   00000214              CALL LDAC(M,ND,NN)
142   00000215     C.....SOLVE A*P=C FOR P
143   00000216              CALL TDINVR(ISOL,IDSOL,NR,-NC,A,IDAMAX,KWA,DET)
144   00000217              IF((ISOL+IDSOL).GT.2)STOP 77777
145   00000220              CALL MOVE(A(1,NC),P,NR,NP2)
146   00000221     C.....CALCULATE VALUE OF COMPUTED TRANSFER FUNCTION AT FREQUENCY
147   00000222     C.....DATA POINTS AND THEN EVALUATE ERROR FUNCTION.
148   00000223              EN=0.
149   00000224              DO 8 I=1,M
150   00000225              JW=CMPLX(0.,W(I))
151   00000226              TNUM=CPOLY(P(1),NP1,JW)
152   00000227              TDENOM=CPOLY(P(NP2),NDP1,JW)
153   00000230              DA(I)=TDENOM
154   00000231              GA(I)=TNUM/TDENOM
155   00000232              TEMP=CABS(RESP(I)-GA(I))
156   00000233              TEMP=TEMP*TEMP*DELW(I)
157   00000234              EN=EN+TEMP
158   00000235     8        CONTINUE
159   00000236              EN=EN/ERRORD
160   00000237              IF(K.EQ.1)GO TO 10
161   00000240     C.....CALCULATE APPROXIMATE EQUATION ERROR
162   00000241              EC=0.
163   00000242              DO 9 I=1,M
164   00000243              FRAC=DA(I)/DAOLD(I)
165   00000244              EC=EC+CABS(C1-FRAC)
166   00000245     9        CONTINUE
167   00000246              EC=EC/FLOAT(M)
168   00000247              WRITE(LP,2002)EN,K,ND,NN,EC
169   00000250              IF(EC.LE.CS)GO TO 11
170   00000251     C.....MOVE DA TO DAOLD AND CALCULATE PHI
171   00000252     10       DO 12 I=1,M
172   00000253              DAOLD(I)=DA(I)
173   00000254              TEMP=CABS(DAOLD(I))
174   00000255              PHI(I)=1./TEMP/TEMP
175   00000256     12       CONTINUE
176   00000257              GO TO 7
177   00000260     C.....CHECK FOR REAL ERROR CONVERGENCE AND IF MAX. ORDER REACHED.
178   00000261     11       IF(EN.LE.CT)GO TO 14
179   00000262              IF(ND.EQ.NMAX)GO TO 13
180   00000263              NN=NN+1
181   00000264              ND=ND+1
182   00000265              IF(ND.GT.(M+1))STOP 55555
```

138

```
182  00000266            GO TO 4
183  00000267     13     WRITE(LP,2003)ND,NN,FN
184  00000270     14     CONTINUE
185  00000271     C.....REDUCE ORDER OF NUMERATOR
186  00000272            WRITE(LP,2009)
187  00000273            NEND=NP1+NDP1
188  00000274            WRITE(LP,2005)(P(I),I=1,NP1)
189  00000275            WRITE(LP,2006)(P(I),I=NP2,NEND)
190  00000276            NNORD=NN
191  00000277            NDORD=ND
192  00000300            IF(TOLMAG.EQ.0.)GO TO 45
193  00000301            PMAG=0.
194  00000302            DO 41 I=1,M
195  00000303            JW=C1/CMPLX(0.,W(I))
196  00000304            DO 42 J=1,NP1
197  00000305            JW=JW*CMPLX(0.,W(I))
198  00000306            PMAG=PMAG+CABS(CMPLX(P(J),0.)*JW)
199  00000307     42     CONTINUE
200  00000310     41     CONTINUE
201  00000311            PMAG=PMAG/FLOAT(M)
202  00000312            DO 43 I=1,NP1
203  00000313            IR=NP1-I+1
204  00000314            TMAG=0.
205  00000315            DO 44 J=1,M
206  00000316            JW=CMPLX(0.,W(J))**(IR-1)
207  00000317            TMAG=TMAG+CABS(CMPLX(P(IR),0.)*JW)
208  00000320     44     CONTINUE
209  00000321            TMAG=TMAG/FLOAT(M)
210  00000322            RATIO=TMAG/PMAG
211  00000323            IF(RATIO.GE.TOLMAG)GO TO 46
212  00000324            P(IR)=0.
213  00000325            NNORD=NNORD-1
214  00000326     43     CONTINUE
215  00000327     46     CONTINUE
216  00000330     C.....PRINT SCALED TRANSFER FUNCTION AND DC GAIN
217  00000331            WRITE(LP,2004)
218  00000332            WRITE(LP,2005)(P(I),I=1,NP1)
219  00000333            WRITE(LP,2006)(P(I),I=NP2,NEND)
220  00000334     45     CONTINUE
221  00000335            DCGAIN=P(1)
222  00000336            WRITE(LP,2010)DCGAIN
223  00000337     C.....FIND ZEROS
224  00000340            CALL ROOT(P(1),NNORD,ZEROS,NZ,A,=LP)
225  00000341     C.....FIND POLES
226  00000342            CALL ROOT(P(NP2),NDORD,POLES,NP,A,=LP)
227  00000343     C.....UNSCALE TRANSFER FUNCTION AND FREQUENCY
228  00000344            TEMP=FSCALE
229  00000345            DO 61 I=2,NP1
230  00000346            P(I)=TEMP*P(I)
231  00000347            TEMP=TEMP*FSCALE
232  00000350     61     CONTINUE
233  00000351            NP3=NP2+1
234  00000352            TEMP=FSCALE
235  00000353            DO 63 I=NP3,NEND
236  00000354            P(I)=TEMP*P(I)
237  00000355            TEMP=TEMP*FSCALE
238  00000356     63     CONTINUE
239  00000357            DO 62 I=1,M
240  00000360            W(I)=W(I)/FSCALE
241  00000361     62     CONTINUE
242  00000362     C.....PRINT UNSCALED TRANSFER FUNCTION
```

139

```
244  00000363              WRITE(LP,2014)
245  00000364              WRITE(LP,2005)(P(I),I,1,NP1)
246  00000365              WRITE(LP,2006)(P(I),I,NP2,NEND)
247  00000366     100      CONTINUE
248  00000367     C.....PRINT UNSCALED ZEROS
249  00000370              IORD=NNORD
250  00000371              IF(NNORD.GT.4)IORD=4
251  00000372              WRITE(LP,2011)NNORD,LORD(IORD)
252  00000373              WRITE(LP,2015)
253  00000374              IPT=1
254  00000375              DO 70 I=1,NZ
255  00000376              IF(COMP)ZEROS(I)=ZEROS(I)/CMPLX(FSCALE,0.)
256  00000377              PREAL=REAL(ZEROS(I))
257  00000400              PIMAG=AIMAG(ZEROS(I))
258  00000401              IF(ABS(PIMAG).GT.1.0E-7)GO TO 71
259  00000402              WRITE(LP,2016)I,PREAL
260  00000403              GO TO 68
261  00000404     71       FREQ=CABS(ZEROS(I))
262  00000405              DAMP=-PREAL/FREQ
263  00000406              WRITE(LP,2016)I,PREAL,PIMAG,DAMP,FREQ
264  00000407     68       IF(JZT(IPT).NE.I)GO TO 70
265  00000410              WRITE(LP,2017)
266  00000411              IPT=IPT+1
267  00000412     70       CONTINUE
268  00000413     C.....PRINT UNSCALED POLES
269  00000414              IORD=NDORD
270  00000415              IF(NDORD.GT.4)IORD=4
271  00000416              WRITE(LP,2012)NDORD,LORD(IORD)
272  00000417              WRITE(LP,2015)
273  00000420              IPT=1
274  00000421              DO 72 I=1,NP
275  00000422              IF(COMP)POLES(I)=POLES(I)/CMPLX(FSCALE,0.)
276  00000423              PREAL=REAL(POLES(I))
277  00000424              PIMAG=AIMAG(POLES(I))
278  00000425              IF(ABS(PIMAG).GT.1.0E-7)GO TO 73
279  00000426              WRITE(LP,2016)I,PREAL
280  00000427              GO TO 69
281  00000430     73       FREQ=CABS(POLES(I))
282  00000431              DAMP=-PREAL/FREQ
283  00000432              WRITE(LP,2016)I,PREAL,PIMAG,DAMP,FREQ
284  00000433     69       IF(JDT(IPT).NE.I)GO TO 72
285  00000434              WRITE(LP,2017)
286  00000435              IPT=IPT+1
287  00000436     72       CONTINUE
288  00000437     C.....PRINT OUT FREQUENCY RESPONSE OF COMPUTED TRANSFER FUNCTION
289  00000440     C.....AT INPUT DATA POINTS
290  00000441              IF(.NOT.COMP)GO TO 101
291  00000442              WRITE(LP,2007)
292  00000443              DO 15 I=1,M
293  00000444              IF(OTYPE.EQ.LPOLAR)GO TO 20
294  00000445              IF(OTYPE.EQ.LRECT)GO TO 30
295  00000446              ARG1=20.*ALOG10(CABS(GA(I)))
296  00000447              ARG2=ATAN2(AIMAG(GA(I)),REAL(GA(I)))*RD
297  00000450              GO TO 40
298  00000451     20       ARG1=CABS(GA(I))
299  00000452              ARG2=ATAN2(AIMAG(GA(I)),REAL(GA(I)))*RD
300  00000453              GO TO 40
301  00000454     30       ARG1=REAL(GA(I))
302  00000455              ARG2=AIMAG(GA(I))
303  00000456     40       WRITE(LP,2008)W(I),ARG1,ARG2
304  00000457     15       CONTINUE
```

```
305  00000460   C......SET UP ARRAY OF FREQUENCY RESPONSE TO BE PLOTTED,
306  00000461   C......DELETING. DESIRED POLES AND ZEROS
307  00000462   101   CONTINUE
308  00000463         IF(.NOT.OUT)GO TO 51
309  00000464         WRITE(LP,2018)
310  00000465         EXPO=ALOG10(WLOW)
311  00000466         EINTVL=FLOAT(NDEC)/FLOAT(NPOINTS)
312  00000467         DO 50 I=1,NPOINTS
313  00000470         EXPO=EXPO+EINTVL
314  00000471         FREQIN(I)=10.**EXPO
315  00000472         FHZ=FREQIN(I)/2./PI
316  00000473         JW=CMPLX(0.,FREQIN(I))
317  00000474         TNUM=CPOLYF(JW,ZEROS,NZ,JZT)
318  00000475         TDENOM=CPOLYF(JW,POLES,NP,JPT)
319  00000476         TFN=DCGAIN*TNUM/TDENOM
320  00000477         PART1(I)=20.*ALOG10(CABS(TFN))
321  00000500         PART2(I)=ATAN2(AIMAG(TFN),REAL(TFN))*RD
322  00000501   C......ADD TIME DELAY BACK INTO DATA
323  00000502         IF(SENSE SWITCH 2) 57,58
324  00000503    57   PART2(I)=PART2(I)-FREQIN(I)*TDELAY*57.293
325  00000504    58   CONTINUE
326  00000505         WRITE(LP,2019)FREQIN(I),FHZ,PART1(I),PART2(I)
327  00000506    50   CONTINUE
328  00000507         ISC=0
329  00000510         IF(QGAINX.LE.0.)ISC=1
330  00000511    51   CONTINUE
331  00000512   C......ADD TIME DELAY BACK INTO RAW DATA
332  00000513         IF(SENSE SWITCH 2) 47,48
333  00000514    47   DO 48 I=1,M
334  00000515         TEMPG=CABS(RESP(I))
335  00000516         TEMPP=ATAN2(AIMAG(RESP(I)),REAL(RESP(I)))*RD
336  00000517         TEMPP=TEMPP-W(I)*TDELAY*57.293
337  00000520         TEMPP=TEMPP*DR
338  00000521         RESP(I)=TEMPG*CMPLX(COS(TEMPP),SIN(TEMPP))
339  00000522    48   CONTINUE
340  00000523         CALL BODPLT(FREQIN,PART1,PART2,I,I,WLOW,NDEC,NPDEC,LP,1HG,1HP,ISC,
341  00000524        *NPOINTS,ABS(QGAINX))
342  00000525         READ(ICR,2016) .
343  00000526         PAUSE
344  00000527         GO TO 200
345  00000530    1000 FORMAT(1X,I9,I10,4E10.3)
346  00000531    1001 FORMAT(20A4)
347  00000532    1002 FORMAT(A1)
348  00000533    1003 FORMAT(A1,I2)
349  00000534    2000 FORMAT(1H1,18HDENOMINATOR ORDER=,17X,I12/
350  00000535        21X,16HNUMERATOR ORDER=,19X,I12/
351  00000536        A1X,25HEQUATION ERROR TOLERANCE=,10X,E12.5/
352  00000537        B1X,21HREAL ERROR TOLERANCE=,14X,E12.5/
353  00000540        C1X,23HFREQUENCY SCALE FACTOR=,12X,E12.5/
354  00000541        D1X,29HBASE FREQUENCY FOR BODE PLOT=, 6X,E12.5/
355  00000542        E1X,28HPOINTS/DECADE FOR BODE PLOT=,7X,I12/
356  00000543        F1X,34HTOTAL POINTS PLOTTED ON BODE PLOT=,1X,I12/
357  00000544        G1X,25HTERM REJECTION CRITERION=,10X,E12.5//)
358  00000545    2001 FORMAT(1H0,38X,8HRAW DATA,40X,16HRECTANGULAR DATA/)
359  00000546    2002 FORMAT(10X,E12.5,2I10,3X,I2,4X,E12.5)
360  00000547    2003 FORMAT(1X,30(1H*),17HMAX ORDER REACHED,2I10,E12.5)
361  00000550    2004 FORMAT(1H0,20(1H*),35HTRUNCATED TRANSFER FUNCTION(SCALED))
362  00000551    2005 FORMAT(1H0,11HNUMERATOR==,2X,(6E15.5))
363  00000552    2006 FORMAT(1H0,13HDENOMINATOR==,(6E15.5))
364  00000553    2007 FORMAT(//1H0,20(1H*),24HFINAL FREQUENCY RESPONSE/)
365  00000554    2008 FORMAT(1X,E12.5,10X,2(1X,E12.5))
```

141

```
366   00000555   2009   FORMAT(1H1,20(1H*),34HCOMPUTED TRANSFER FUNCTION(SCALED))
367   00000556   2010   FORMAT(1H0,20(1H*),8HDC GAIN=,E12.5)
368   00000557   2011   FORMAT(1H1,20(1H*),9HROOTS OF ,I2,A2,17H ORDER NUMERATOR.)
369   00000560   2012   FORMAT(1H0,20(1H*),9HROOTS OF ,I2,A2,19H ORDER DENOMINATOR.)
370   00000561   2013   FORMAT(1H0,29X,17HITERATION HISTORY/
371   00000562          *14X,2HEN,15X,1HK,9X,1HN,14X,2HEC/)
372   00000563   2014   FORMAT(1H0,20(1H*),33HFINAL TRANSFER FUNCTION(UNSCALED))
373   00000564   2015   FORMAT(1H0,13X,4HREAL,8X,9HIMAGINARY,3X,7HDAMPING,5X,9HFREQUENCY/)
374   00000565   2016   FORMAT(5X,I2,5X,4(E12.5))
375   00000566   2017   FORMAT(1H+,7X,3HDEL)
376   00000567   2018   FORMAT(1H1,55X,21HPLOTTED OUTPUT VALUES/
377   00000570          A9X,13HFREQ(RAD/SEC),10X,8HFREQ(HZ),10X,8HGAIN(DB),10X,10HPHASE(DEG
378   00000571          B)/)
379   00000572   2019   FORMAT(4(10X,E12.5))
380   00000573   3000   FORMAT(2X,22HIMPUT TIME DELAY (SEC))
381   00000574   3001   FORMAT(E10.4)
382   00000575   3002   FORMAT(//,10X,15HTIME DELAY AT ,E10.4,9H  SECONDS,//)
383   00000576          END
```

Table B-2. Transfer Function Identification Program -- Subroutine Bode Plot

```
 1   00000000          SUBROUTINE BODPLT(FREQIN,GAININ,PHASIN,ICASE,MAXCASE,WLO,NDEC,
 2   00000001         $NPDEC,IW,LGAIN,LPHAS,NSCAL,NPOINT,SCGAIN)
 3   00000002          COMMON W(50),DELW(50),RESP(50),PHI(50),A(41,42)
 4   00000003          COMMON S(43),T(43),U(43),LAMBDA(43)
 5   00000004          COMMON/KLUGE/M                                            KLUGE
 6   00000005          DIMENSION IBUF(120)
 7   00000006          DIMENSION FREQIN(1),GAININ(MAXCASE,1),PHASIN(MAXCASE,1),IWORK(11),
 8   00000007         $PRINTS(11)
 9   00000010          REAL LENG
10   00000011          COMPLEX RESP                                             KLUGE
11   00000012          REAL LAMBDA
12   00000013          DATA IBLANK/4H    /,ISLASH/1H1/,II/4HI    /,IMINUS/4H-   /
13   00000014          DATA LSTAR/1H*/,LPLUS/1H+/                               KLUGE
14   00000015    C PLOTS GAIN AND PHASE (IN THE HORIZONTAL DIRECTION)           PLOT  30
15   00000016    C     VS. FREQUENCY (IN THE VERTICAL DIRECTION).               PLOT  40
16   00000017          RD=45./ATAN(1.0)                                        KLUGE
17   00000020          TWOPJ=8.*ATAN(1.0)
18   00000021          LENG=NPDEC
19   00000022    C NSCAL=0 SIGNIFIES THAT THE DEFAULT INPUT VALUES(-SCGAIN,+SCGAIN)
20   00000023    C                         ARE USED FOR THE GAIN SCALE,         PLOT  60
21   00000024    C NSCAL = 1 SIGNIFIES THAT THE GAIN SCALE IS ADJUSTED AUTOMATICALLY. PLOT  70
22   00000025          ILENG=NDEC*NPDEC+1
23   00000026          GGAINX=SCGAIN
24   00000027          IF(NSCAL.EQ.0)GOTO400
25   00000030    C SEARCH FOR THE MAXIMUM GAIN.                                 PLOT 290
26   00000031          GMAX=-1.0E+35
27   00000032          GMIN=1.0E+35
28   00000033          DO 360 IPOINT = 1, NPOINT                               PLOT 320
29   00000034          G = GAININ (ICASE,IPOINT)                               PLOT 330
30   00000035          IF (GMAX .LT. G)  GMAX = G                              PLOT 340
31   00000036          IF (GMIN .GT. G)  GMIN = G                              PLOT 350
32   00000037    360   CONTINUE                                                PLOT 360
33   00000040          ABSMIN = ABS (GMIN)                                     PLOT 370
34   00000041          IF (GMAX .LT. ABSMIN)  GMAX = ABSMIN                    PLOT 380
35   00000042          CALL SCAP (GMAX, GGAINX)                                PLOT 390
36   00000043    400   MGAINX = IFIX (GGAINX + 0.5)                            PLOT 400
37   00000044          GDIFF = GGAINX / 4.0                                    PLOT 410
38   00000045          GBOUND = 1.125 * GGAINX                                 PLOT 420
39   00000046    C PRINT HEADING.                                              PLOT 500
40   00000047          WRITE (IW, 520) LGAIN, LPHAS                            PLOT 510
41   00000050    520   FORMAT (1H1/37X,15H PLOT OF GAIN (,A1,13H) AND PHASE (,A1, PLOT 520
42   00000051         1   15H) VS. FREQUENCY/)                                 PLOT 530
43   00000052    C PRINT THE GAIN SCALE.                                       PLOT 540
44   00000053          DO 560 I = 1, 9                                         PLOT 550
45   00000054    560   PRINTS (I) = -GGAINX + GDIFF * FLOAT (I-1)              PLOT 560
46   00000055          WRITE (IW, 580) (PRINTS(I), I = 1, 9)                   PLOT 570
47   00000056    580   FORMAT(1X,7HRAD/SEC,4X,2HHZ,2X,6H GAIN:,9(F6.1,4X))     KLUGE
48   00000057          KPT=1                                                   PLOT 590
49   00000060          IPOINT = 1                                              PLOT 590
50   00000061          ILINE = 0                                              PLOT 600
51   00000062    610   ILINE = ILINE + 1                                      PLOT 610
52   00000063    C RESET IBUF TO ALL BLANKS.                                  PLOT 620
53   00000064          DO 640 I = 1, 120                                      PLOT 630
54   00000065    640   IBUF (I) = IBLANK                                      PLOT 640
55   00000066    C PRINT HORIZONTAL AXES.                                     PLOT 650
56   00000067          IF ((ILINE .NE. 1) .AND. (ILINE .NE. ILENG))  GO TO 750
57   00000070          DO 680 I = 20, 110                                     PLOT 670
58   00000071    680   IBUF (I) = IMINUS                                      PLOT 680
59   00000072    C PRINT TICK-MARKS.                                          PLOT 690
60   00000073          IF (ILINE.NE.1) GO TO 690
61   00000074          IC=15
62   00000075          ID=10
63   00000076    690   IF (ILINE.NE.ILENG) GO TO 700
64   00000077          IC=20
65   00000100          ID=9
66   00000101    700   DO 730 I = 1, 9
67   00000102    730   IBUF (IC + I * ID) = II                                PLOT 730
68   00000103    C PRINT THE VERTICAL AXES.                                   PLOT 740
69   00000104    750   IBUF(20)=II
70   00000105          IBUF(110)=II
71   00000106          IBUF (65) = ISLASH                                     PLOT 760
72   00000107    C CALCULATE THE LOGARITHM OF THE PLOTTED FREQUENCY.          PLOT 770
```

143

```
73  00000110        FREQLG=ALOG10(WLOW)+(FLOAT(ILINE-1))/LENG
74  00000111     C AVERAGE THE GAINS AND PHASES OF THE POINTS TO BE PLOTTED    PLOT 790
75  00000112     C   ON THIS ONE LINE.                                        PLOT 800
76  00000113        COUNT = 0.0                                               PLOT 810
77  00000114        GAIN = 0.0                                                PLOT 820
78  00000115        PHAS = - 180.0                                            PLOT 830
79  00000116        GAINSM = 0.0                                              PLOT 840
80  00000117        PHASSM = 0.0                                              PLOT 850
81  00000120    860 IF (IPOINT .GT. NPOINT)  GO TO 930
82  00000121        IF (ALOG10(FREQIN(IPOINT)) .GT. (FREQLG+.5/LENG))  GO TO 930  PLOT 870
83  00000122        GAINSM = GAINSM + GAININ (ICASE,IPOINT)                    PLOT 880
84  00000123        PHASSM = PHASSM + PHASIN (ICASE,IPOINT)                    PLOT 890
85  00000124        COUNT = COUNT + 1.0                                       PLOT 900
86  00000125        IPOINT = IPOINT + 1                                       PLOT 910
87  00000126        GO TO 860                                                 PLOT 920
88  00000127    930 IF (COUNT .EQ. 0.0)  GO TO 1150                           PLOT 930
89  00000130        GAIN = GAINSM / COUNT                                     PLOT 940
90  00000131        PHAS = PHASSM / COUNT                                     PLOT 950
91  00000132     C TEST WHETHER THE GAIN FALLS WITHIN THE BOUNDS (-45, +45).  PLOT 960
92  00000133        IF (GAIN .GE. (-QBOUND))  GO TO 1040                      PLOT 970
93  00000134        IC = 13                                                   PLOT 980
94  00000135    990 ENCODE(6,1000,IWORK(1))GAIN
95  00000136   1000 FORMAT(F6.2)
96  00000137        DECODE(6,1020,IWORK(1))IBUF(IC)
97  00000140   1020 FORMAT(6A1)
98  00000141        GO TO 1100                                               PLOT1030
99  00000142   1040 IF (GAIN .LE. QBOUND)  GO TO 1180                        PLOT1040
100 00000143        IC = 110                                                 PLOT1050
101 00000144        GO TO 990                                                PLOT1060
102 00000145     C PLOT THE GAIN.                                            PLOT1070
103 00000146   1080 IBUF(IFIX(45.*GAIN/QBOUND+65.5))=LGAIN
104 00000147     C TEST WHETHER THE PHASE FALLS WITHIN THE BOUNDS (-360, 0).  PLOT1090
105 00000150   1100 IF (PHAS .GE. (-360.))GO TO 1110
106 00000151        PHAS=PHAS+360.0
107 00000152        GO TO 1100
108 00000153   1110 IF(PHAS.LE.0.0)GO TO 1120
109 00000154        PHAS=PHAS-360.0
110 00000155        GO TO 1110
111 00000156     C PLOT THE PHASE.                                           PLOT1120
112 00000157   1120 IBUF (IFIX (0.25 * PHAS + 110.5)) = LPHAS                PLOT1130
113 00000160     C PLOT DATA POINTS
114 00000161        IF(KPT.GT.M)GO TO 1122                                   KLUGE
115 00000162   1123 IF(ABS(ALOG10(W(KPT))-FREQLG).GT.(.5/LENG))GO TO 1122    KLUGE
116 00000163        XGAIN=20.*ALOG10(CABS(RESP(KPT)))                        KLUGE
117 00000164        IBUF(IFIX(45.*XGAIN/QBOUND+65.5))=LSTAR                  KLUGE
118 00000165        XPHAS=ATAN2(AIMAG(RESP(KPT)),REAL(RESP(KPT)))*RD         KLUGE
119 00000166   1112 IF(XPHAS.GE.(-360.))GO TO 1113                          KLUGE
120 00000167        XPHAS=XPHAS+360.                                         KLUGE
121 00000170        GO TO 1112                                              KLUGE
122 00000171   1113 IF(XPHAS.LE.0.)GO TO 1121                               KLUGE
123 00000172        XPHAS=XPHAS-360.                                        KLUGE
124 00000173        GO TO 1113                                              KLUGE
125 00000174   1121 IBUF(IFIX(.25*XPHAS+110.5))=LPLUS
126 00000175        KPT=KPT+1
127 00000176        GO TO 1123                                              KLUGE
128 00000177   1122 CONTINUE                                                KLUGE
129 00000200     C PRINT THE LINE.                                          PLOT1140
130 00000201   1150 OMGA=10.**FREQLG
131 00000202        OMGAHZ=OMGA/TWOPI
132 00000203        WRITE(IW,1160)OMGA,OMGAHZ,(IBUF(I),I=20,118)
133 00000204   1160 FORMAT(1X,F7.2,1X,F7.2,3X,99A1)
134 00000205        IF (ILINE .LT. ILENG)  GO TO 610
135 00000206     C PRINT THE PHASE SCALE.                                   PLOT1180
136 00000207   1199 DO 1200  I = 1, 11                                      PLOT1190
137 00000210   1200 IWORK (I) = - 396 + 36 * I                              PLOT1200
138 00000211        WRITE (IW, 1220) (IWORK(I), I = 1, 11)                  PLOT1210
139 00000212   1220 FORMAT (7X,7H PHASE:,3X,11(I4,5X))                      PLOT1220
140 00000213        RETURN                                                  PLOT1230
141 00000214        END                                                     PLOT1240
```

Table B-3. Transfer Function Identification Program -- Subroutine Card Read

```
1   00000000            SUBROUTINE CARDRD(LUI,LUO,M,MMAX)
2   00000001      C.....SUBROUTINE TO READ FREQUENCY RESPONSE DATA OFF CARDS
3   00000002      C.....AND THE CONVERT DATA TO INTERNAL TYPE(RECTANGULAR)
4   00000003            COMMON W(50),DELW(50),RESP(50),PHI(50),A(41,42)
5   00000004            COMMON S(43),T(43),U(43),LAMBDA(43)
6   00000005            DIMENSION VALUE(3),LABEL(3),LIMAGE(20)
7   00000006            COMPLEX RESP
8   00000007            REAL LAMBDA
9   00000010            DATA LBODE/1HB/,LPOLAR/1HP/,LRECT/1HR/,LEND/1H*/,LHZ/1HH/
10  00000011            DATA LBLK/1H /,LDEG/1HD/,LRAD/1HR/,LDB/1HD/,LMAG/1HM/
11  00000012            PI=4.*ATAN(1.0)
12  00000013            DR=PI/4./45.
13  00000014            M=0
14  00000015        1   M=M+1
15  00000016            IF(M.GT.MMAX)GO TO 2
16  00000017            READ(LUI,1000)LIMAGE
17  00000020            DECODE(1,1001,LIMAGE(1))LIN
18  00000021            IF(LIN.EQ.LEND)RETURN
19  00000022            CALL STRING(LIMAGE,VALUE,LABEL)
20  00000023            W(M)=VALUE(1)
21  00000024            IF(LABEL(1).EQ.LHZ)W(M)=W(M)*2.*PI
22  00000025            IF(LIN.EQ.LPOLAR)GO TO 10
23  00000026            IF(LIN.EQ.LRECT)GO TO 20
24  00000027            BMAG=VALUE(2)
25  00000030            IF(LABEL(2).EQ.LBLK.OR.LABEL(2).EQ.LDB)BMAG=10.**(BMAG/20.)
26  00000031            BANG=VALUE(3)
27  00000032            IF(LABEL(3).EQ.LDEG.OR.LABEL(3).EQ.LBLK)BANG=BANG*DR
28  00000033            RESP(M)=BMAG*CMPLX(COS(BANG),SIN(BANG))
29  00000034            GO TO 30
30  00000035       10   CONTINUE
31  00000036            PMAG=VALUE(2)
32  00000037            IF(LABEL(2).EQ.LDB)PMAG=10.**(PMAG/20.)
33  00000040            PANG=VALUE(3)
34  00000041            IF(LABEL(3).EQ.LDEG.OR.LABEL(3).EQ.LBLK)PANG=PANG*DR
35  00000042            RESP(M)=PMAG*CMPLX(COS(PANG),SIN(PANG))
36  00000043            GO TO 30
37  00000044       20   RESP(M)=CMPLX(VALUE(2),VALUE(3))
38  00000045       30   IF(LUO.LT.0)GO TO 1
39  00000046            WRITE(LUO,2000)LIN,(LABEL(I),VALUE(I),I=1,3),W(M),RESP(M)
40  00000047            GO TO 1
41  00000050        2   IF(LIN.EQ.LEND)RETURN
42  00000051            READ(LUI,1000)LIMAGE
43  00000052            DECODE(1,1001,LIMAGE(1))LIN
44  00000053            IF(LIN.NE.LEND)WRITE(LUO,2001)LIMAGE
45  00000054            GO TO 2
46  00000055     1000   FORMAT(20A4)
47  00000056     1001   FORMAT(A1)
48  00000057     2000   FORMAT(1X,A1,3X,3(1X,A1,1X,E15.7),5X,1H*,5X,3(1X,E15.7))
49  00000060     2001   FORMAT(1X,11HEXTRA CARD=,20A4)
50  00000061            END
```

Table B-4. Transfer Function Identification Program -- Subroutine Change Signs

```
 1   00000000          SUBROUTINE CHS(ARR,N,IPAT)
 2   00000001          DIMENSION ARR(1)
 3   00000002   C.....SUBROUTINE TO CHANGE SIGNS IN PROPER PATTERNS
 4   00000003          IF(IPAT.EQ.1)RETURN
 5   00000004          IBEG=IPAT/4+1
 6   00000005          INCR=2-MOD(IPAT,2)
 7   00000006          DO 1 I=IBEG,N,INCR
 8   00000007        1 ARR(I)=-ARR(I)
 9   00000010          RETURN
10   00000011          END
```

Table B-5. Transfer Function Identification Program -- Subroutine Evaluate Complex Polynomial

```
 1   00000000          COMPLEX FUNCTION CPOLY(COEF,N,S)
 2   00000001          DIMENSION COEF(1)
 3   00000002          COMPLEX S
 4   00000003   C.....EVALUATE A COMPLEX POLYNOMIAL WITH REAL COEFFICIENTS
 5   00000004   C.....USING HORNERS RULE.
 6   00000005          CPOLY=CMPLX(COEF(N),0.)
 7   00000006          IF(N.EQ.1)RETURN
 8   00000007          NM1=N-1
 9   00000010          DO 1 I=1,NM1
10   00000011          IR=NM1-I+1
11   00000012          CPOLY=CPOLY*S+CMPLX(COEF(IR),0.)
12   00000013        1 CONTINUE
13   00000014          RETURN
14   00000015          END
```

Table B-6. Transfer Function Identification Program -- Subroutine Evaluate Factored Polynomial

```
 1   00000000          COMPLEX FUNCTION CPOLYF(JW,ROOTS,NORD,JRT)
 2   00000001   C.....EVALUATE A FACTORED POLYNOMIAL
 3   00000002          DIMENSION JRT(1)
 4   00000003          COMPLEX ROOTS(1),JW,JWSQ,PROD,FACT
 5   00000004          PROD=(1.,0.)
 6   00000005          IP=1
 7   00000006          JWSQ=JW*JW
 8   00000007          DO 1 I=1,NORD
 9   00000010          IF(I.EQ.JRT(IP))GO TO 2
10   00000011          IF(ABS(AIMAG(ROOTS(I))).LE.1.0E-07)GO TO 3
11   00000012          OMEG=CABS(ROOTS(I))
12   00000013          OMEGSQ=OMEG*OMEG
13   00000014          ZETA=REAL(ROOTS(I))/OMEG
14   00000015          FACT=JWSQ/OMEGSQ-JW*2.*ZETA/OMEG+(1.,0.)
15   00000016          GO TO 4
16   00000017        3 FACT=-JW/ROOTS(I)+(1.,0.)
17   00000020        4 PROD=PROD*FACT
18   00000021          GO TO 1
19   00000022        2 IP=IP+1
20   00000023        1 CONTINUE
21   00000024          CPOLYF=PROD
22   00000025          RETURN
23   00000026          END
```

146

```
 1  00000000          SUBROUTINE LDAC(M,ND,NN)
 2  00000001          COMMON W(50),DELW(50),RESP(50),PHI(50),A(41,42)
 3  00000002          COMMON S(43),T(43),U(43),LAMBDA(43)
 4  00000003          REAL LAMBDA
 5  00000004          COMPLEX RESP
 6  00000005          LOGICAL EVEN,ODD,LMB,SM,UM,TM
 7  00000006    C.....SUBROUTINE TO LOAD A-MATRIX AND C-VECTOR
 8  00000007          N=ND
 9  00000010          NP1=NN+1
10  00000011          NP2=NN+2
11  00000012          MSIZE=ND+NN+1
12  00000013          ILCOLM=MSIZE+1
13  00000014          MSP2=MSIZE+2
14  00000015          DO 1 I=1,MSP2
15  00000016    C.....FIRST,COMPUTE LAMBDA,S,T,U
16  00000017          EVEN=MOD(I,2).EQ.0
17  00000020          LAMBDA(I)=0.
18  00000021          S(I)=0.
19  00000022          T(I)=0.
20  00000023          U(I)=0.
21  00000024          DO 2 J=1,M
22  00000025          SQMAG=CABS(RESP(J))
23  00000026          SQMAG=SQMAG*SQMAG
24  00000027          TEMP=PHI(J)*DELW(J)*W(J)**(I-1)
25  00000030          IF(EVEN)T(I)=TEMP*AIMAG(RESP(J))+T(I)
26  00000031          IF(EVEN)GO TO 2
27  00000032          LAMBDA(I)=LAMBDA(I)+TEMP
28  00000033          S(I)=S(I)+TEMP*REAL(RESP(J))
29  00000034          U(I)=U(I)+TEMP*SQMAG
30  00000035        2 CONTINUE
31  00000036        1 CONTINUE
32  00000037    C.....FILL MAIN AND UPPER DIAGONAL OF A AND THEN TRANSPOSE
33  00000040          DO 4 I=1,MSIZE
34  00000041          DO 5 J=I,MSIZE
35  00000042          LMB=I.LE.NP1.AND.J.LE.NP1.AND.MOD(I+J,2).EQ.0
36  00000043          SM=I.LE.NP1.AND.J.GT.NP1.AND.MOD(I+(J-NP1),2).EQ.1
37  00000044          TM=I.LE.NP1.AND.J.GT.NP1.AND.MOD(I+(J-NP1),2).EQ.0
38  00000045          UM=I.GT.NP1.AND.J.GT.NP1.AND.MOD((I+J),2).EQ.0
39  00000046          A(I,J)=0.
40  00000047          IF(LMB)A(I,J)=LAMBDA(I+(J-1))
41  00000050          IF(UM)A(I,J)=U((I-NP1+2)+(J-NP1-1))
42  00000051          IF(SM)A(I,J)=S(I+(J-NP1))
43  00000052          IF(TM)A(I,J)=T(I+(J-NP1))
44  00000053          A(J,I)=A(I,J)
45  00000054        5 CONTINUE
46  00000055        4 CONTINUE
47  00000056    C.....CHANGE SIGNS IN PROPER PLACES
48  00000057    C.....FIRST PARTITION
49  00000060          DO 6 J=1,NP1
50  00000061          IPAT=MOD(J-1,4)+1
51  00000062          CALL CHS(A(1,J),NP1,IPAT)
52  00000063        6 CONTINUE
53  00000064    C.....SECOND PARTITION
54  00000065          DO 7 J=NP2,MSIZE
55  00000066          IPAT=MOD(J-NP1,2,4)+1
56  00000067          CALL CHS(A(1,J),NP1,IPAT)
57  00000070        7 CONTINUE
58  00000071    C.....THIRD PARTITION
59  00000072          DO 8 J=1,NP1
60  00000073          IPAT=MOD(J-1,4)+1
```

147

Table B-7. Transfer Function Identification Program -- Subroutine Load A-Matrix and C-Vector (Concluded)

```
61  00000074           CALL CHS(A(NP2,J),N,IPAT)
62  00000075        8 CONTINUE
63  00000076     C.....FOURTH PARTITION
64  00000077           DO 9 J=NP2,MSIZE
65  00000100           IPAT=MOD(J-NP1+2,4)+1
66  00000101           CALL CHS(A(NP2,J),N,IPAT)
67  00000102        9 CONTINUE
68  00000103     C.....LOAD C-VECTOR
69  00000104           DO 10 I=1,NP1
70  00000105           EVEN=MOD(I,2)+EQ+0
71  00000106           ODD=.NOT.EVEN
72  00000107           IF(ODD)A(I,ILCOLM)=S(I)
73  00000110           IF(EVEN)A(I,ILCOLM)=T(I)
74  00000111       10 CONTINUE
75  00000112           DO 11 I=NP2,MSIZE
76  00000113           EVEN=MOD(I-NP1,2)+EQ+0
77  00000114           ODD=.NOT.EVEN
78  00000115           IF(ODD)A(I,ILCOLM)=0.
79  00000116           IF(EVEN)A(I,ILCOLM)=U(I-NP1+1)
80  00000117       11 CONTINUE
81  00000120           RETURN
82  00000121           END
```

Table B-8. Transfer Function Identification Program -- Subroutine Move

```
 1  00000000           SUBROUTINE MOVE(AIN,AOUT,N,IBEGIN)
 2  00000001           DIMENSION AIN(1),AOUT(1)
 3  00000002           DO 1 I=1,N
 4  00000003           AOUT(I)=AIN(I)
 5  00000004        1 CONTINUE
 6  00000005     C.....INSERT 1. IN PROPER PLACE.
 7  00000006           IEND=N+1
 8  00000007           TEMP=1.
 9  00000010           DO 2 I=IBEGIN,IEND
10  00000011           TEMPB=AOUT(I)
11  00000012           AOUT(I)=TEMP
12  00000013           TEMP=TEMPB
13  00000014        2 CONTINUE
14  00000015           RETURN
15  00000016           END
```

148

Table B-9. Transfer Function Identification Program -- Subroutine Root

```
1    00000000          SUBROUTINE ROOT(P,NORD,ROOTS,NROOTS,SCR,LUO)
2    00000001          COMPLEX ROOTS(1)
3    00000002          DIMENSION P(1),SCR(NORD,1)
4    00000003          IF(NORD.GT.1)GO TO 10
5    00000004          ROOTS(1)=CMPLX(-P(1)/P(2),0.)
6    00000005          NROOTS=1
7    00000006          GO TO 5
8    00000007     10   NORDP1=NORD+1
9    00000010          NORDM1=NORD-1
10   00000011          DO 1 I=1,NORDM1
11   00000012          DO 1 J=1,NORD
12   00000013          SCR(I,J)=0.
13   00000014          IF(J.EQ.(I+1))SCR(I,J)=1.
14   00000015     1    CONTINUE
15   00000016          DO 2 I=1,NORD
16   00000017          SCR(NORD,I)=-P(I)/P(NORDP1)
17   00000020     2    CONTINUE
18   00000021          IF(NORD.LE.2)GO TO 11
19   00000022          CALL HESSEN(NORD,SCR,NORD)
20   00000023     11   CALL QRCALL(NORD,SCR,ROOTS,NROOTS,NORD)
21   00000024          NROOTS=NROOTS/2
22   00000025     5    IF(LUO.LT.0)RETURN
23   00000026          WRITE(LUO,2000)
24   00000027          DO 3 I=1,NROOTS
25   00000030          PREAL=REAL(ROOTS(I))
26   00000031          PIMAG=AIMAG(ROOTS(I))
27   00000032          IF(ABS(PIMAG).GT.1.0E-7)GO TO 4
28   00000033          WRITE(LUO,2001)PREAL
29   00000034          GO TO 3
30   00000035     4    FREQ=CABS(ROOTS(I))
31   00000036          DAMP=-PREAL/FREQ
32   00000037          WRITE(LUO,2001)PREAL,PIMAG,DAMP,FREQ
33   00000040     3    CONTINUE
34   00000041          RETURN
35   00000042     2000 FORMAT(1H0,13X,4HREAL,8X,9HIMAGINARY,3X,7HDAMPING,5X,9HFREQUENCY/)
36   00000043     2001 FORMAT(12X,4(E12.5))
37   00000044          END
```

Table B-10. Transfer Function Identification Program -- Subroutine Scale

```
1    00000000          SUBROUTINE SCAP (QMAX, QSCALX)              SCAP  10
2    00000001   C ESTABLISHES THE UPPER BOUND QSCALX OF THE SCALE. SCAP  20
3    00000002          DIMENSION SCALX(11)
4    00000003          DATA NSCALX/11/                            SCAP 160
5    00000004          DATA (SCALX(I),I=1,11)/1.,1.5,2.,2.5,3.,4.,5.,6.,7.,8.,9./
6    00000005          IF (QMAX .LE. 1.0)  GO TO 260              SCAP 180
7    00000006          FACT = 0.1                                 SCAP 190
8    00000007     200  FACT = 10.0 . FACT                         SCAP 200
9    00000010          DO 240  ISCALX = 1, NSCALX                 SCAP 210
10   00000011          QSCALX = FACT . SCALX (ISCALX)            SCAP 220
11   00000012          IF (QMAX .LE. QSCALX)  GO TO 360          SCAP 230
12   00000013     240  CONTINUE                                   SCAP 240
13   00000014          GO TO 200                                  SCAP 250
14   00000015     260  FACT = 1.0                                 SCAP 260
15   00000016          QNEW = 1.0                                 SCAP 270
16   00000017     280  FACT = 0.1 . FACT                         SCAP 280
17   00000020          DO 340  ISCALX = 1, NSCALX                 SCAP 290
18   00000021          ISCALY = NSCALX + 1 - ISCALX             SCAP 300
19   00000022          QSCALX = QNEW                              SCAP 310
20   00000023          QNEW = FACT . SCALX (ISCALY)             SCAP 320
21   00000024          IF (QMAX .GT. QNEW)  GO TO 360            SCAP 330
22   00000025     340  CONTINUE                                   SCAP 340
23   00000026          GO TO 280                                  SCAP 350
24   00000027     360  RETURN                                     SCAP 360
25   00000030          END                                        SCAP 370
```

149

Table B-11. Transfer Function Identification Program -- Subroutine Logical Function Search

```
1  00000000          LOGICAL FUNCTION SEARCH(LABEL,ACCEPT)
2  00000001          INTEGER ACCEPT(5)
3  00000002          DO 1 I=1,5
4  00000003          SEARCH=LABEL.EQ.ACCEPT(I)
5  00000004          IF(SEARCH)RETURN
6  00000005     1    CONTINUE
7  00000006          RETURN
8  00000007          END
```

Table B-12. Transfer Function Identification Program -- Subroutine String

```
1   00000000          SUBROUTINE STRING(LIMAGE,VALUE,LABEL)
2   00000001          DIMENSION ACCEPT(5),LABEL(3),LIMAGE(20)
3   00000002          DIMENSION VALUE(3)
4   00000003          INTEGER ACCEPT
5   00000004          LOGICAL FIND,SEARCH
6   00000005          DATA(ACCEPT(I),I=1,5)/1H ,1HD,1HR,1HM,1HH/,LBLK/1H /
7   00000006          DECODE(3,1000,LIMAGE(4))LABEL(1)
8   00000007          FIND=SEARCH(LABEL(1),ACCEPT)
9   00000010          IF(FIND)DECODE(17,3000,LIMAGE(4))VALUE(1)
10  00000011          IF(FIND)GO TO 1
11  00000012          LABEL(1)=LBLK
12  00000013          DECODE(17,3001,LIMAGE(4))VALUE(1)
13  00000014     1    DECODE(2,1001,LIMAGE(8))LABEL(2)
14  00000015          FIND=SEARCH(LABEL(2),ACCEPT)
15  00000016          IF(FIND)DECODE(16,3002,LIMAGE(8))VALUE(2)
16  00000017          IF(FIND)GO TO 2
17  00000020          LABEL(2)=LBLK
18  00000021          DECODE(16,3003,LIMAGE(8))VALUE(2)
19  00000022     2    DECODE(1,1002,LIMAGE(12))LABEL(3)
20  00000023          FIND=SEARCH(LABEL(3),ACCEPT)
21  00000024          IF(FIND)DECODE(15,3004,LIMAGE(12))VALUE(3)
22  00000025          IF(FIND)RETURN
23  00000026          LABEL(3)=LBLK
24  00000027          DECODE(15,3005,LIMAGE(12))VALUE(3)
25  00000030          RETURN
26  00000031   1000   FORMAT(2X,A1)
27  00000032   1001   FORMAT(1X,A1)
28  00000033   1002   FORMAT(A1)
29  00000034   3000   FORMAT(3X,E14.7)
30  00000035   3001   FORMAT(2X,E15.7)
31  00000036   3002   FORMAT(2X,E14.7)
32  00000037   3003   FORMAT(1X,E15.7)
33  00000040   3004   FORMAT(1X,E14.7)
34  00000041   3005   FORMAT(E15.7)
35  00000042          END
```

REFERENCES

1. Miller, N. E., "J85 Frequency Response Engine Tests," MR-12314, Honeywell Inc., Minneapolis, Minnesota, 13 November 1974.

2. Miller, N. E., "Comparison of J85 Engine Frequency Response Data with Component Model Frequency Response Data," MR-12315, Honeywell Inc., Minneapolis, Minnesota, 14 November 1974.

3. Miller, N. E., "J85 Analog Model Frequency Response Tests," MR-12322, Honeywell Inc., Minneapolis, Minnesota, 26 December 1974.

4. Volume I of this report.

5. Arnett, Samuel E., "Turbine Engine Control Synthesis," AFAPL-TR-74-113, Air Force Aero Propulsion Laboratory, Air Force Systems Command, Wright-Patterson Air Force Base, Ohio, December 1974.

6. Fuchs, Abraham M., "Two-Channel Frequency Response Analysis by Sweep Frequency Test Methods," Tech. Pub. No. 7172-1, Bafco, Inc., Warminster, Pennsylvania.

7. Suzuki, Yutaka, et al., "A Method to Find Transfer Functions from Frequency Response Data Based on Least Squares Principle," Technology Reports of Osaka University, Volume 21, March 1971.